# Hydrologic Control of Sliding Velocity in Two Alaskan Glaciers: Observation and Theory

Thesis by

Mark Allen Fahnestock

In Partial Fulfillment of the Requirements

for the Degree of

Doctor of Philosophy

California Institute of Technology

Pasadena, California

1991

(Defended May 29, 1991)

## Acknowledgments

This thesis is, in many respects, a direct result of the introduction to the Earth that was provided to me by my Father. From him I learned of the opportunities provided by a profession which deals in the questions posed by natural phenomena.

The investigations described in this document owe any clarity they possess to Barclay Kamb, whose contributions of discussion and patient criticism were invaluable. Discussions with Neil Humphrey and Hermann Engelhardt also contributed to the development of this work.

The observations reported from the two field projects represent the combined work of many people. I am indebted to: the field team on Variegated Glacier, which included Barclay Kamb, Andrea Donellan, Matthias Blume, and Bengt Magnuson; the Columbia Glacier drilling team, which included Hermann Engelhardt, Neil Humphrey, Barclay Kamb, Matthias Blume, and Mark Wumkes; and the members of Mark Meier's team, who spent long hours making detailed observations on Columbia - access to the data from their work is greatly appreciated.

Bob Krimmel kindly provided data from the USGS monitoring program on Columbia Glacier, as well as helpful discussions about the early work there.

Dan Stone responded quickly to my request for information about Kadin Lake.

Geoff Blake, Joe Kirschvink, Rob Clayton, and Ed Stolper generously provided access to computational resources.

I benefited from the help and support of quite a few friends while at Caltech. I must thank the residents of 109 S. Chester, and specifically Phil Ihinger, David Pickett, and Mike Wolf, for the numerous forays which characterized life at that house.

Pat, Maria, and David Pickett provided Sunday chili dinners during the final hectic weeks.

## Abstract

Short term variations in the velocities of glaciers reflect changes in the processes which determine sliding velocity. The role of water in these processes is considered for certain types of variable behavior observed on two glaciers in Alaska.

Pulses of increased velocity on Variegated Glacier (mini-surges) prior to its 1982-83 surge have been attributed to pulses of water at the glacier bed. Our field program in 1986 demonstrated that mini-surges still occurred following the surge; the propagation of two such disturbances over part of the upper reach of the glacier was documented. The mini-surges of 1986 had substantially lower peak velocities but only slightly lower propagation velocities than the pre-surge mini-surges. The first of the mini-surges observed in 1986 originated in the tributary, the second originated in the upper reach of the main glacier.

A model of the basal water system with pressure dependent conductivity and storage is developed to investigate the conditions necessary for propagation of a pulse of water. The response of this system to the introduction of a localized increase in input is followed with a finite difference formulation. The extra input of water produces a downglacier propagating front, which, for reasonable values of porosity and pre-event conditions, moves at speeds similar to those observed for mini-surges.

The relation between the non-linearity of the pressure dependence in this model and the shape and history of the propagating disturbances is investigated using conductivity relations which have linear, quadratic, and cubic dependence on pressure, and one with an inverse dependence on the effective pressure. The modeling indicates that a system with a non-linear change of conductivity in response to a change in water pressure (suggestive of a cavity system) is required to match the field observations.

The shapes of waves which propagate with unchanging form in this system can be found theoretically; the numerical model generates these waves when the input rate is

held constant. The constant form shapes are calculated for the conductivity relations mentioned above; for conductivities with higher-than-linear dependence on pressure the waves reach a plateau upglacier; the linear case increases without bound.

Modeling of a Röthlisberger tunnel system with the addition of a storage term indicates that such a system will propagate a disturbance, but will not match the abrupt rise times seen in boreholes as a mini-surge wave passes. The pressure dependent conductivity model does a better job of matching observations.

Columbia Glacier, a large tidewater glacier in southern Alaska, experiences noteworthy velocity fluctuations during the melt season in response to storms and increased ablation, and also displays a well developed diurnal cycle in velocity. A 1987 field project involving the University of Colorado, the USGS, and Caltech collected detailed time series of surface velocity, water input and discharge, and basal water pressure. These data show a complex pattern of behavior which is highly correlated with variations in hydrologic parameters. Basal water pressures near the floatation level are related to the rapid surface motion (4-8 m/d) of this glacier. A series of at least four velocity events accompanied elevated inputs of water to the glacier. These speed-ups did not have a strong coincident peak in basal water pressure, but were followed by an increase in outflow discharge from the glacier.

An estimate of the change in the volume of water stored in the glacier is made by relating input to the glacier (estimated from the filling rate of an ice-marginal lake and also from meteorological records) to discharge. This calculation shows that variations in velocity on time scales longer than one day can be explained by changes in the volume of water stored in or under the ice. The first velocity event was followed by a slowdown of the glacier which was coincident with a drop in stored water volume of about 0.1 $m^3/m^2$ averaged over the ice surface. The peak in velocity for the largest velocity event is accompanied by a large peak in stored water volume.

A model of the basal water system which consists of co-existing linked cavity and tunnel components is proposed to explain the melt season behavior of Columbia Glacier. In this hybrid cavity/tunnel system the distributed input of water reaches the bed and flows through the cavities to reach large tunnels which are responsible for the downglacier transport of water. The cavity part of this system is responsible for the correlation between stored water volume and velocity, while the tunnel system is responsible for the seasonal variation of velocity and the localized upwelling of water discharged from the terminus of the glacier.

A model based on a simple sliding law, an effective pressure distribution at the bed which is determined by the discharge through a tunnel system, and continuity for the ice is used to look at the role of effective pressure in the difference between winter and summer glacier-flow behavior. This model produces the late-melt-season pulse in velocity at the terminus which is related to an annual increase in calving rate. This may explain the previously discovered correlation between calving rate and outflow discharge, as well as the connection between the location of calving activity and the location of upwelling at the terminus.

The results of this work suggest that the complicated behavior of these glaciers can be understood at a simple level from the variations in hydrologic systems.

## Table of Contents

## List of Illustrations

# Chapter 1

## Introduction and Background

Variations in the velocity of glaciers reflect changes in the underlying causes for ice motion. This thesis considers the short term motion records of two glaciers in Alaska in an attempt to decipher the mechanisms behind the variations in their velocities. Field observations reveal complex patterns of behavior related to the interaction of the glaciers' hydrologic systems and the ice. The behavior observed in the field is here addressed with theoretical considerations and numerical techniques in order to improve our understanding of the processes involved.

Early work on glaciers concentrated on measuring the motion of the ice at the surface. Many ideas were advanced to explain the motion; these ideas have evolved into the commonly accepted combination of internal deformation, or flow, of the ice, and sliding of the glacier over its bed. The physics of ice deformation is understood as the creep of a polycrystalline solid. The nature of the process of basal sliding, which is not as amenable to direct observation or laboratory investigation, has not been as well documented.

An understanding of the processes which determine glacier motion is essential to any attempt to interpret the present or past motion of a glacier as an indication of its state of balance or reaction to climatic change. The role of glaciers in the water cycle and their interaction with the atmosphere is such that they must in some way reflect climatic conditions. The rate of flow, position of the terminus, or elevation of the boundary between zones of net gain and loss of ice should provide a measure of the state of balance of the processes which waste and replenish a glacier. The records provided by the deposits of past glaciers and ice sheets and by cores of ice from mountainous regions and high latitudes require an understanding of ice motion for their interpretation. Without a knowledge of the factors responsible for determining ice motion, any climatic

interpretation made from a body of ice, or the deposits left by one, is subject to uncertainty.

If the motion of a glacier were entirely due to internal deformation, it would be possible to make reasonable judgements about glacier behavior from information which is easily obtainable, such as ice thickness and surface slope measurements. The existence of a basal velocity boundary condition, with unknown dependence on these and other quantities, makes glacier behavior a subject worthy of further investigation.

As was noted by Paterson [1981], the inaccessible nature of basal sliding has led to the proliferation of theories concerned with the processes involved. The data to constrain these theories and to suggest new approaches cannot be gathered in a systematic fashion; as observations are made, the behavior of each glacier presents a new perspective on the problem.

Glaciers which have velocities that vary with time are promising candidates for investigations into the factors which control rates of motion. On these glaciers measurements of processes which also change with time, such as the rate of surface input of water, can be compared with velocity records to establish cause and effect relationships.

Conditions which could influence the rate of internal deformation in a glacier do not vary significantly on times scales shorter than a year. Large variations in velocity on time scales shorter than this must be due to rapidly changing factors; a recent focus on basal hydrology has documented that water and water pressure can play an important role in this variation.

Recent direct conformation [Engelhardt et al., 1990] of the importance of water in the sliding of Ice Stream B, West Antarctica, provides the strongest link yet between hydrologic control of sliding and the potential for significant influence on climate. The ice streams of the West Antarctic Ice Sheet carry most of the ice flux out of the ice sheet, and their stability is critical to its state of balance.

Several workers have observed velocity variations on a seasonal time scale. The lower reach of Unteraargletscher, Switzerland, was found to experience a rapid speedup and uplift at the beginning of the melt season and to maintain a high velocity through the summer [Iken et al., 1983]. In contrast, the lower Nisqually Glacier, Washington, was found to speed up gradually over the winter and early spring and to slow over the summer season [Hodge, 1974]. Work by the USGS has shown low average late summer and fall velocities over most of Columbia Glacier, Alaska, and high winter and spring velocities, but the pattern is reversed at the terminus, with the maximum speed there coming toward the end of the melt season [Meier and Post, 1987; Krimmel and Vaughn, 1987]. The three glaciers mentioned above cover a range from a small, steep alpine glacier to a large tidewater glacier. It would appear that seasonal variations in surface velocity are not confined to one size class of glacier and the variations are not necessarily similar from one glacier to the next.

Short term (several day long) velocity variations have been observed on at least two glaciers in the Alps and several in North America. Velocity pulses have been observed on Findelengletscher , Switzerland, and Variegated Glacier, Alaska [Iken, 1981; Kamb and Engelhardt, 1987]. The pulses on Variegated Glacier clearly propagated down the glacier. Short term velocity increases associated with increased water input from extra ablation or precipitation have been documented on Columbia Glacier [Walters and Dunlap, 1987]. Velocity variations can occur in cycles as short as half a day; an example is the semi-diurnal velocity fluctuations of Columbia Glacier [Walters and Dunlap, 1987].

All of these velocity variations are attributed to hydrologic influence on the sliding behavior of the glaciers in question. A detailed examination of the characteristics of some of these forms of velocity variation should yield some insight into the nature of the hydrologic systems in operation in these glaciers and the interactions between the hydrologic systems and the ice.

In the chapters which follow, I use measurements of the propagating velocity pulses of Variegated Glacier and the velocity variations of Columbia Glacier (Figure 1.1) to investigate the role of water in producing these variations.

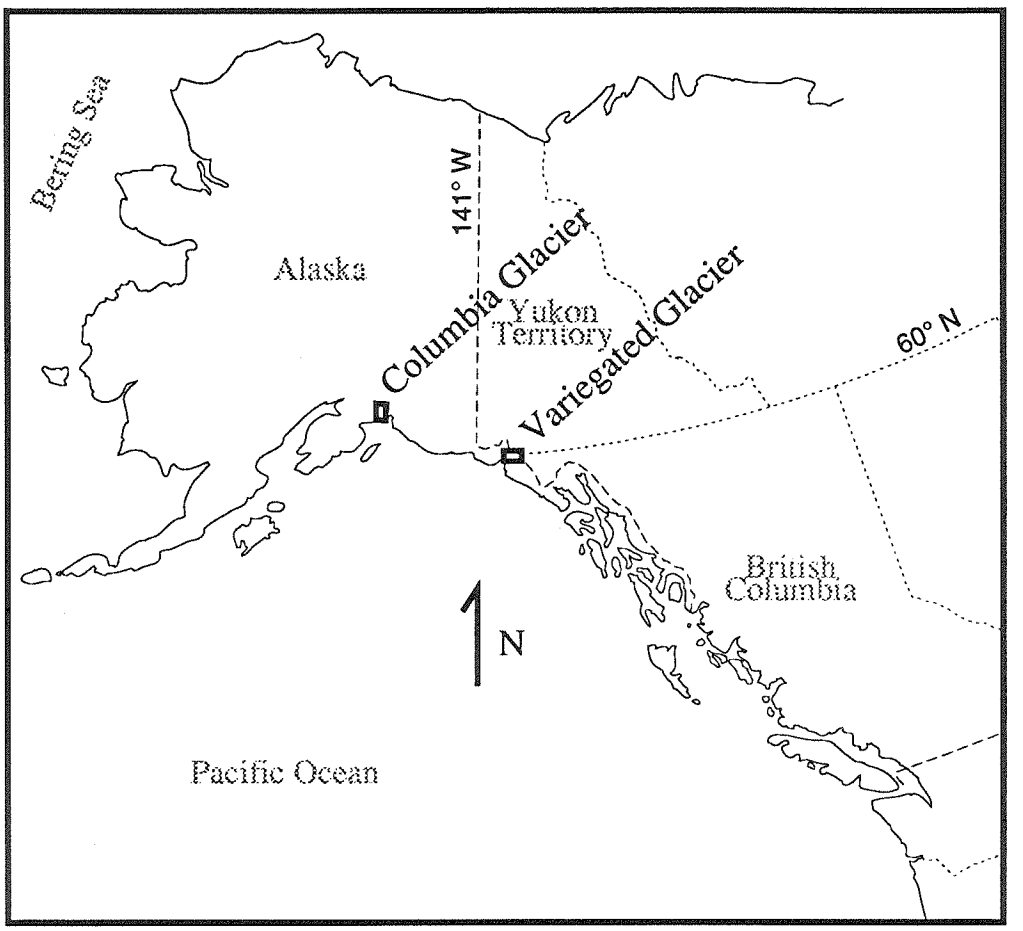


**Figure 1.1** Locations of Variegated Glacier and Columbia Glacier.

# Chapter 2

# Mini-Surges of Variegated Glacier

## Mini-Surges Before the 1982-83 Surge

Extensive study of Variegated Glacier, located in the St. Elias Range, southern Alaska, has revealed a complicated picture of surface velocity variations and changes in geometry [Kamb et al., 1985]. The most profound variations are the surges of this glacier, which occur on a twenty year cycle [Post, 1969]. The surge is a phenomenon which has been attributed to changes in ice geometry and basal hydrologic conditions [Kamb et al., 1985]. The surface velocity variations discussed in this chapter occur on shorter time scales and recur much more frequently than a surge. These variations are propagating pulses of increased velocity that occur during June and July in the mid to upper region of this glacier (Figure 2.1). The study of Variegated Glacier from 1975 up to the surge in 1982-1983, carried out by teams from the University of Washington, the University of Alaska, and the California Institute of Technology was responsible for the discovery and characterization of these disturbances. At the time it was hypothesized that the disturbances might be be characteristic of a glacier building up to surge [Kamb and Engelhardt, 1987].

Propagating velocity events of the kind observed on Variegated glacier cannot be explained by enhanced internal deformation. They have been explained as being the result of a traveling wave of increased basal sliding [Raymond and Malone, 1986; Kamb and Engelhardt, 1987]. The change at the base of the glacier which is responsible for this increase in sliding is related to some disturbance which is capable of propagating down the glacier.

The velocity events of Variegated Glacier are part of a package of co-propagating disturbances which has been given the name "mini-surge" by Kamb and Engelhardt [1987]; this terminology was also used by Raymond and Malone [1986], and Humphrey

et al. [1986], and so will be adopted here to refer to the particular events which occur on this glacier. It has yet to be determined whether these events are confined to surge type glaciers or if similar propagating events occur on glaciers which do not surge.

The most noticeable manifestation of a mini-surge is the pulse of increased surface velocity. The velocity pulse is accompanied by a large increase in basal water pressure [Kamb and Engelhardt, 1987], uplift of the ice surface [Kamb and Engelhardt, 1987], and a pulse in ice quake activity and longitudinal surface strain [Raymond and Malone, 1986]. The mini-surge moves downglacier with a propagation velocity of 200 - 600 meters per hour [Kamb and Engelhardt, 1987; Raymond and Malone, 1986]. A good record of these various effects is presented in Figure 2.2 (taken from Kamb and Engelhardt [1987, Figure 10]). In this figure the locations of the recording stations are given in the Km coordinate system of Figure 2.1 and the velocity data are plotted as bars representing the average velocity over the time intervals between distance measurements. The figure clearly shows the propagating character of the disturbances, with later arrivals at the downglacier observation points.

The phasing between the velocity wave and the wave of water pressure in the basal water system is best illustrated in the records from Km 6.4 and 6.5 (Figure 2.2 *a* and *c*). From these measurements it is apparent that the maximum velocity is nearly coincident with the peak in water pressure [Kamb and Engelhardt, 1987]. It is seen from Figure 2.2 that the maximum rate of surface uplift at Km 6.5 is also coincident with the peak in water level. Based on the data in Figure 2.2 and other similar observations, Kamb and Engelhardt [1987] have suggested that the uplift and increase in surface velocity are both due to increased cavitation at the glacier bed caused by the high basal water pressure.

The surface uplift is shown in Figure 2.3 (from Kamb and Engelhardt [1987, Figure 11]), which gives the elevation of a site on the ice for the entire 1980 summer season. The deviation from the smooth pre-mini-surge descent path is shown in this

figure as the deviation from the dashed line. While some part of the surface uplift from these events may be due to a traveling strain wave associated with the changes in velocity, Kamb and Engelhardt have argued that due to the phasing of the uplift rate, which peaks with the peak in velocity, the larger part must be due to basal cavitation.

The relation of the various disturbances to the velocity record is somewhat hindered by the poor time resolution of the surface velocity measurements. Measurement of the absolute motion of the glacier's surface is limited by the accuracy of surveying and electronic distance measuring equipment, which precludes obtaining accurate velocities from frequent measurements. Raymond and Malone used short base line wire strain gages to measure surface strain on the scale of 10 meters [Raymond and Malone, 1986]. Their technique does not suffer from a limited time resolution, but their measurements differ in some respects from the long baseline strain measurements made with surveying instruments, possibly because of the potentially large effect of local crevassing on the short-base-line strains.

Humphrey et al. [1986] documented several effects of mini-surges on the outlet stream of the glacier. It was found that each mini-surge was accompanied by a sharp spike in turbidity. Stacking of records for all of the mini-surges which occurred in a season suggested that the events may be followed by a several day long increase in discharge, which was interpreted to be due to the release of extra water from the basal water system.

The studies described briefly above attribute the traveling nature of mini-surge disturbances to propagation of a wave of increased water pressure (or volume) through the basal water system. It is the high water pressures in this wave which are thought to cause the increase in basal sliding responsible for the pulse in surface velocity [Kamb and Engelhardt, 1987].

## 1986 Field Work on Variegated Glacier

The preceding discussion is based on mini-surges which occurred in the upper glacier between Km 3 and Km 9 during the melt seasons of 1978-1981 [Kamb and Engelhardt, 1987; Raymond and Malone, 1986]. The connection between the surge cycle of Variegated Glacier and the occurrence of these mini-surges is not well understood. It was not known if mini-surges would continue to occur during the early part of the build up in the years following a surge. The potential for the continued occurrence of mini-surges was increased by the observation in 1983, 18 days after surge termination, of a mini-surge propagating down the glacier between Km 9 and Km 15 [Kamb et al, p. 473]. Three years after the surge, in the summer of 1986, a group from Caltech went back to investigate conditions on the glacier.

Our 1986 field program was designed to detect the occurrence of mini-surges and to document their propagation. Surface motion was measured at an array of surveying sites on the upper glacier and main tributary (Figure 2.4). The field crew of five made continuous measurements over the period June 22 to July 19 (Julian Days 172 - 200).

Surveying stations were set up on the ice at points B and T (Figure 2.4). A Lietz/Sokkisha Red 1A Electronic Distance Meter (EDM) was used at station B to determine the relative motions of a network of reflectors located both on the ice and on bedrock. At station T, near the glacier margin, a Wild T-2 theodolite was used to measure vertical angles to a nearby bedrock bench mark in order to observe uplift of the ice. At both sites benchmarks were constructed by setting 2.5 m long wooden poles in drill holes in the firn. The benchmarks were maintained by shoveling a thin layer of snow over the markers several times a day, to counteract the effects of surface melting.

The downglacier velocity of station B was determined by EDM measurements to reflector AL on bedrock. The relative velocities between station B and the reflectors F+7, F+2, and F-4 were also determined by EDM measurement from station B. The

absolute velocities of these reflectors were calculated by subtraction (in the case of F+2 and F-4) or addition (for F+7) of the relative velocity from (or to) the velocity of station B. The direct addition or subtraction of these records was possible (without geometric correction) because all of the sites in question are nearly collinear. The velocity is used in this calculation, rather than the distances measured, because the measurements were made at slightly different times; adding velocities provides a linear interpolation over the interval between measurements. In most cases the EDM shots from B to AL and the other reflectors were closely spaced in time, making errors from interpolation small and preventing the "contamination" problems [Kamb and Engelhardt, 1987, p. 31] which could otherwise arise from this technique. The motion of reflector G was determined using the motion of station B toward bedrock reflector SE and the relative motion between B and G. The velocity of station T was tracked with EDM measurements from T to bedrock reflector MCE over the interval July 10 to July 19 (Julian Days 191 - 200). The technique for calculating velocity presented here ignores an angular correction that depends on the directions of the actual surface motion vectors. The angular correction is less than 15 percent in the worst case (F-4); neglecting it results in the under-estimation of the true velocity. Reflectors F-4 and G were located in areas where the ice flow direction deviated the most from the line of site to station B; their velocities may be under-estimated as a result.

The random errors in the velocity data, which were collected with the same methods used by Kamb and Engelhardt, are estimated by them to be $\sim 0.1/\Delta t$ m/day, where $\Delta t$ is the time interval between surveys in hours [Kamb and Engelhardt, 1987, p. 30]. The surveying interval was 8-12 hours when mini-surges were not occurring, and was reduced to ~1.5 hours once the onset of a mini-surge was detected. This gives an estimated accuracy for the calculated velocities of 1 cm/day (non-mini-surge) and 7 cm/day during a mini-surge. The large probable error during a mini-surge does not

hinder data interpretation because the velocity during a mini-surge is high enough that the error remains a small percentage of the total.

Figure 2.5 shows the magnitudes of deviations from the mean velocity of station B over an 8 day interval (Julian Days 188 - 196) in 1986, plotted against the length of time between surveys. If the velocity of the station was constant over the interval the deviations would be a measure of the error in the data relative to the interval between surveys. If the velocity was variable during the interval, the deviations would over-estimate the error. The line in the figure is the estimated error of Kamb and Engelhardt. Although about one third of the deviations are greater than the estimate of Kamb and Engelhardt (possibly due to actual variation in the ice velocity), their curve provides a reasonable idea of the magnitude of the error in the velocity values.

The elevation of station T was measured by shooting vertical angles to bedrock marker NW, 260 m away. An estimate of the error involved in this measurement can be made from Figure 2.6, which shows the deviation from 360° of the sum of the forward and reverse angles from each survey. The line sketched in the figure indicates the trend of the deviation with time, which is assumed to be an instrumental drift. The scatter of the points around this line is taken as an indication of the error inherent in the measurement; the deviation is approximately ±0.005°, representing an error of ± 1.1 cm of elevation at 260 m.

## Results: Mini-Surges of 1986

The record of surface motion obtained at station B provides clear evidence for the occurrence of mini-surges during the 1986 season. The motion of station B toward reflector AL is shown for the entire season in Figure 2.7. The two prominent peaks in this record were produced by the passing of disturbances which have been designated mini-surges 86-1 and 86-2. The mini-surges occurred on July 2-3 (J.D.183-184) and July 17-18 (J.D.198-199). The effects of the mini-surges are also visible in Figure 2.8, which

shows the elevation of station T over the period of measurement. The mini-surges produced the deviations from the linear trend due to normal glacier flow in this figure. The peak in uplift during the first mini-surge was missed by the surveying, but the tail of the event can be seen.

From Figure 2.7 it can be seen that the mini-surges have maximum velocities 6 to 8 times higher than the 10-13 cm/day background velocity (average omitting large peaks) of this station.

The velocities at all sites during the two recorded mini-surges of the 1986 season are shown in detail in Figures 2.9 and 2.10. The reflector at F-4 was not put in place until day 188 and the EDM was not used at station T until day 192, so these sites do not appear in Figure 2.9.

The most striking thing about both events is the propagating nature of the disturbances. It is clear that the first mini-surge had the tributary as its source area while the second mini-surge came out of the upper part of the main glacier. Both the propagating nature of the disturbances and the varying source areas are features seen in previous years, but the data presented in Figures 2.9 and 2.10 are the clearest demonstrations of these features to date.

The sharp temporary drop in the velocity of station B during mini-surge 86-1 just after midnight on J.D. 184 (~184.05) is related to the opening of a 1.5 cm wide crevasse 2 m downglacier from the station. For comparison, the high velocity peak immediately before the drop was due to 3.9 cm of motion in 76 minutes. The drop in velocity had an effect on the record for F+2, which shows reverse motion over this interval, and the record for F+7, which shows a sharp temporary slowdown. The contamination of the velocity records for these two sites may be due to a transient in the motion of site B related to the opening of the crevasse; this would lead to a failure of the assumption of a constant velocity for station B over the intervals between the surveys to the different reflectors.

The propagation velocities of the two mini-surges in 1986 can be estimated from the velocity records in Figures 2.9 and 2.10. For the peak in velocity the speed of propagation for mini-surge 86-1 between G and F+7 is in the range 270±70 m/hr, while for mini-surge 86-2 between F-4 and F+7 it is in the range 220±80 m/hr. The range in these estimates comes from the uncertainty in the determination of the timing of the peaks due to the low time resolution of the surface velocity records. The propagation velocity of the onset (or sharp rise in velocity) can not be readily calculated for mini-surge 86-1 because of the long time elapsed between surveys in which it appears. The propagation velocity of the onset of mini-surge 86-2 is approximately double the peak velocity.

## Comparison With Mini-Surges Of Previous Years

The mini-surges of 1986 differ in several ways from those reported by Kamb and Engelhardt [1987]. The maximum velocities attained in the pre-surge mini-surges were in the range 150 - 250 cm/day with background velocities of 40 - 100 cm/day (a ratio of between 2.5 and 4), while the mini-surges of 1986 had peak velocities of 60 - 80 cm/day and background velocities of 10 - 20 cm/day (a ratio of between 4 and 6). The record of propagation obtained for the second mini-surge in 1986, which shows a clear sequence of progression through the upper glacier, is unlike any record obtained in previous seasons, when the mini-surges seemed to jump quickly through the region between F-4 and F+2 [Kamb, personal communication].

The ice in the middle and upper reaches of the glacier following the surge was on the order of 50 m thinner than it had been when the pre-surge mini-surges were recorded. This fact explains the lower background velocities and may play an important role in determining the peak speeds attained during the mini-surges.

The propagation speeds of the 1986 mini-surges are comparable with the speeds of propagation of peaks in flow velocity reported by Kamb and Engelhardt, although

perhaps 20-25% slower; this indicates that the differences in maximum flow velocity and background velocity do not seem to have a strong effect on the speed of propagation of a mini-surge.

The velocity records for mini-surge 86-1, which had its source in the tributary, are similar to the records for mini-surge 80-3, which also had its source in the tributary (see Kamb and Engelhardt [1987, Figure 7]). The peaks on the main glacier for these events tend to be more symmetric in the reach from Km 6.0 to Km 6.5 than similar peaks for events with source areas on the main glacier.

The velocity records for mini-surge 86-2 show an asymmetric pulse shape (fast rise, slow decline) similar to the events in earlier years (compare with Kamb and Engelhardt [1987, Figures 5 *a*, 7 *d* and *f*]). The pulse shape decays at sites downglacier. Near the source area there is a sharp rise at onset; farther downglacier a more gradual increase at onset is seen (compare Figure 2.10 sites F-4, F+2, B, and F+7). The pulse of increased velocity has a 12-24 hour duration in the 1986 mini-surges, which is within the range of what was observed for pre-surge mini-surges.

The uplift curve for station T in 1986 (Figure 2.8) can be compared with Kamb and Engelhardt's curve for station T in 1980 (Figure 2.3). The pre-event trend and peak in uplift for the first mini-surge in 1986 are not well documented. The second event in 1986 has about one half the maximum uplift of most of the events in 1980. The decay of the uplift from event 86-1 is similar in length (4 days) to that seen in events 80-3 and 80-4.

The detailed record of uplift and velocity for station T during mini-surge 86-2 is shown in Figure 2.11. The shape of the uplift peak is more symmetric than in previous years, but there is a fair scatter in the measurements (for example, the two points at day 199.6 were shot a few minutes apart). It seems clear from this record that the maximum rate of uplift corresponds with the maximum in velocity. This correspondence, as has already been mentioned, was also seen by Kamb and Engelhardt.

Mini-surge 86-1 is thought to be the first of the melt season, although data were only taken from June 22 onward; in several previous years the first event had already occurred by this date. If mini-surge 86-1 is the first event, it differs from the first events in 1979 and 1980 in that the background velocity only shows a slight increase following the event (compare Figure 2.7 with Kamb and Engelhardt [1987, Figures 2 and 3]). The interval between the two mini-surges in 1986 (15 days) is comparable to the intervals between the first two events in the years for which data are available (7-18 days from the years 1978 to 1981).

## Conclusions

The occurrence of mini-surges in 1986 and the similarities between these events and the pre-surge events suggest that mini-surges are characteristic features of the motion of Variegated Glacier throughout the build up to a surge. The basic features of propagation and downglacier degradation were maintained in spite of the drastic change in the geometry of the glacier caused by the 1982-83 surge. The clear propagation of event 86-2 through the upper glacier, which was not observed in previous years, may be a result of changes caused by the surge. The similarity of propagation velocities in 1986 and before the surge suggest that the basic propagating element in a mini-surge, the pulse of water, is still moving by the same basic mechanism.

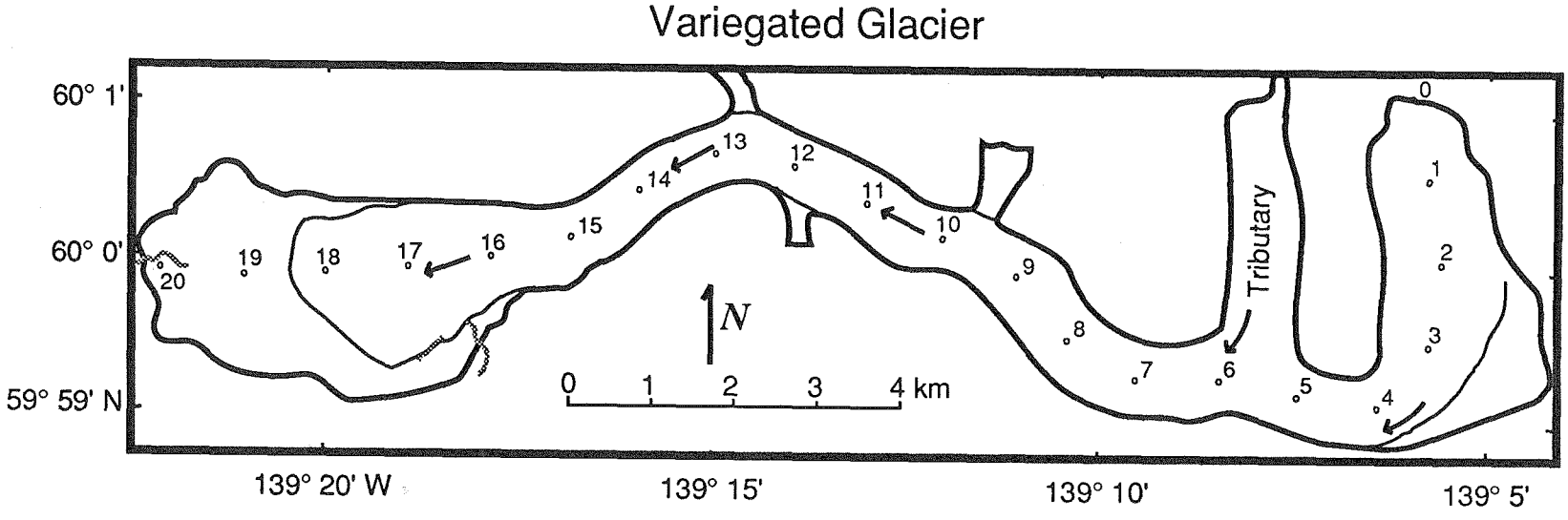


**Figure 2.1** Variegated Glacier, Alaska showing the centerline (Km) coordinate system of Raymond and Harrison used in the text and in Figure 2.2.

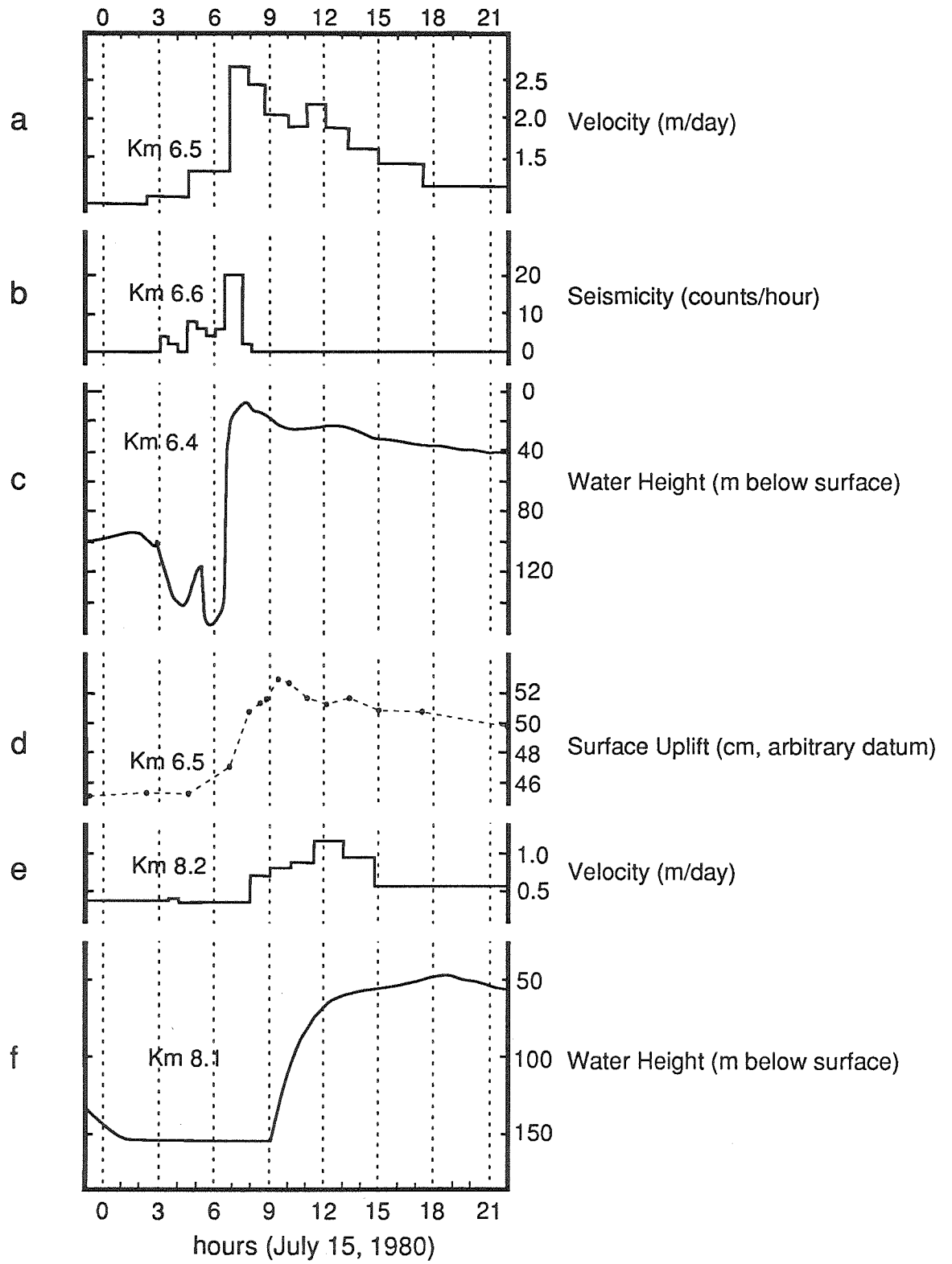


**Figure 2.2** Records of velocity, seismicity, and water pressure for mini-surge 80-5 (after Kamb and Engelhardt, 1987, Figure 10)

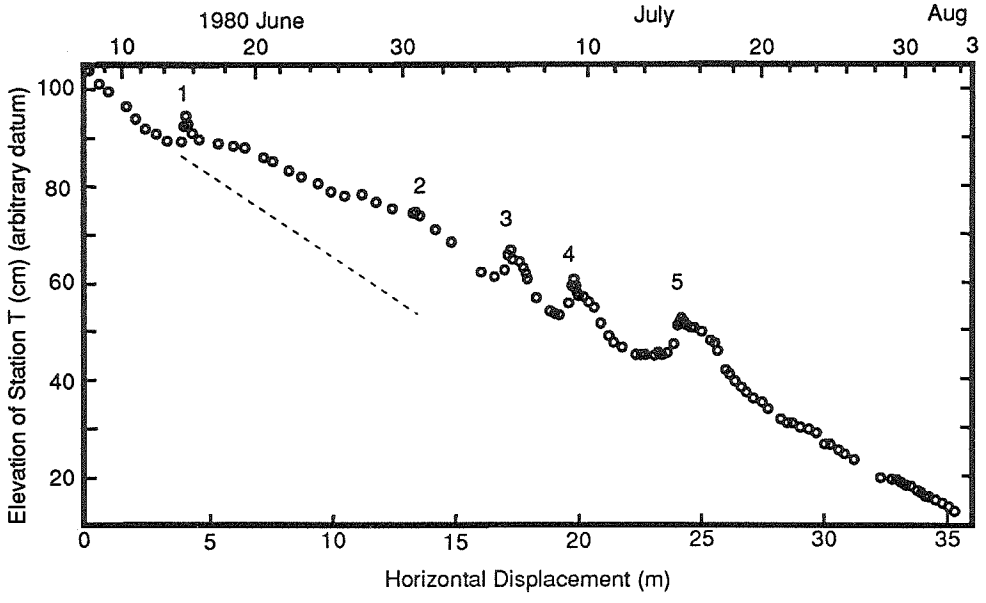


**Figure 2.3** Uplift of glacier surface during summer 1980. Mini-surges indicated by number. Line indicates pre-uplift trend. (after Kamb and Engelhardt, 1987 Figure 11).

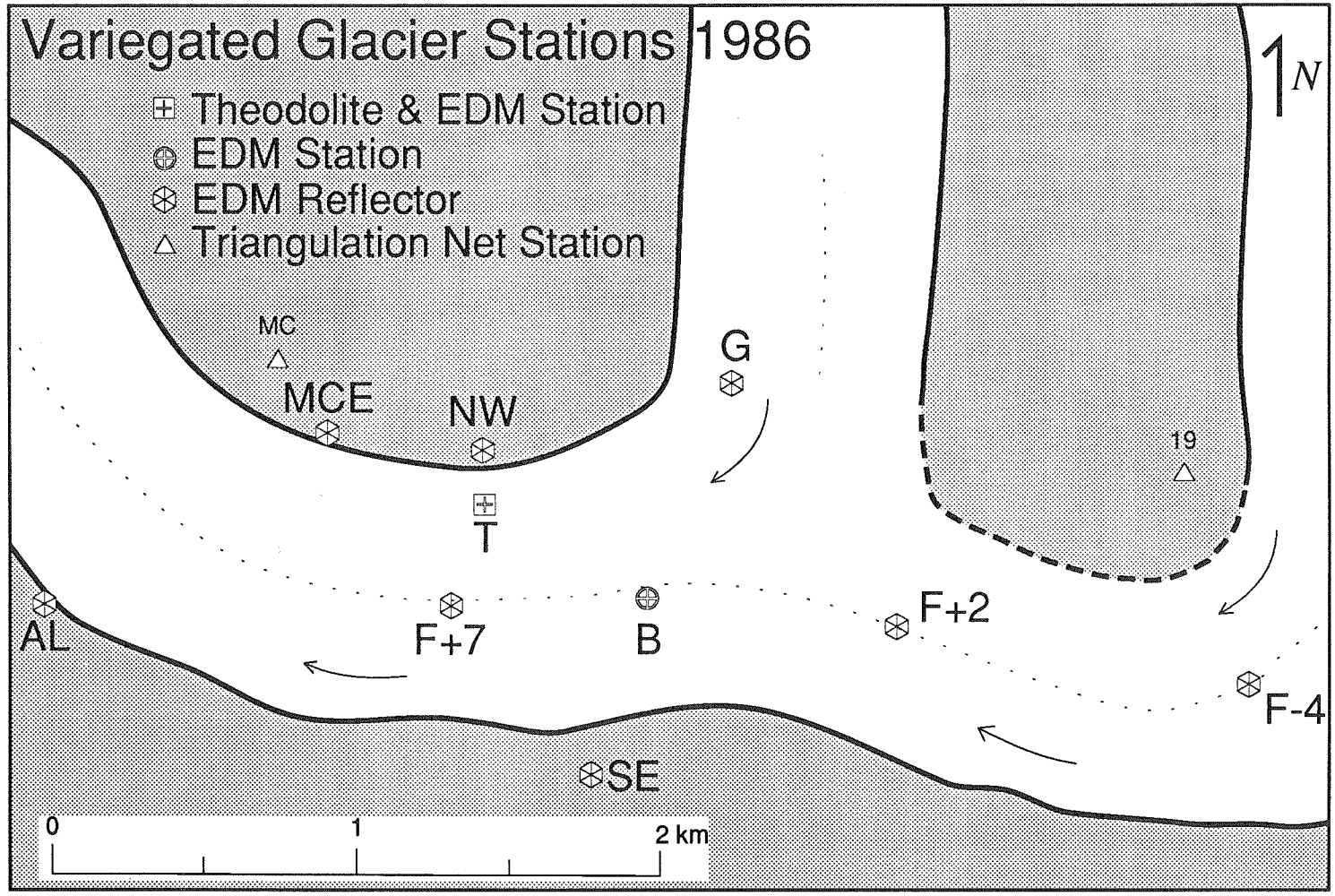


**Figure 2.4** 1986 Variegated Glacier surveying station and reflector locations

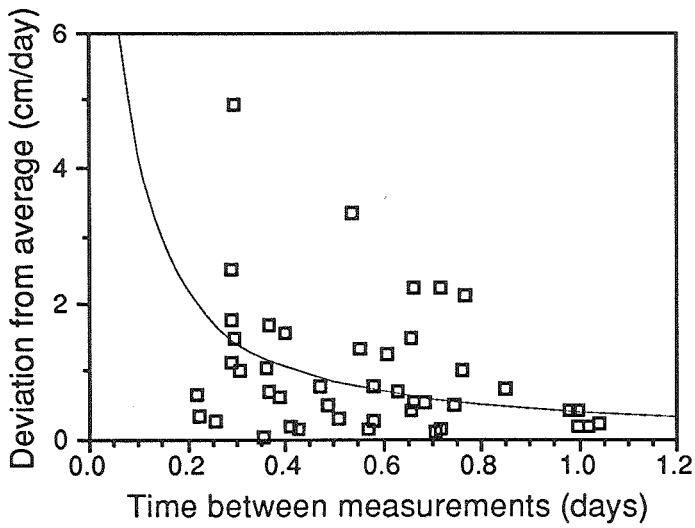


**Figure 2.5** Magnitude of deviation of B-AL velocities measured between days 188 and 196 (1986) from mean velocity over the same interval. Line is estimate of Kamb and Engelhardt discussed in text.

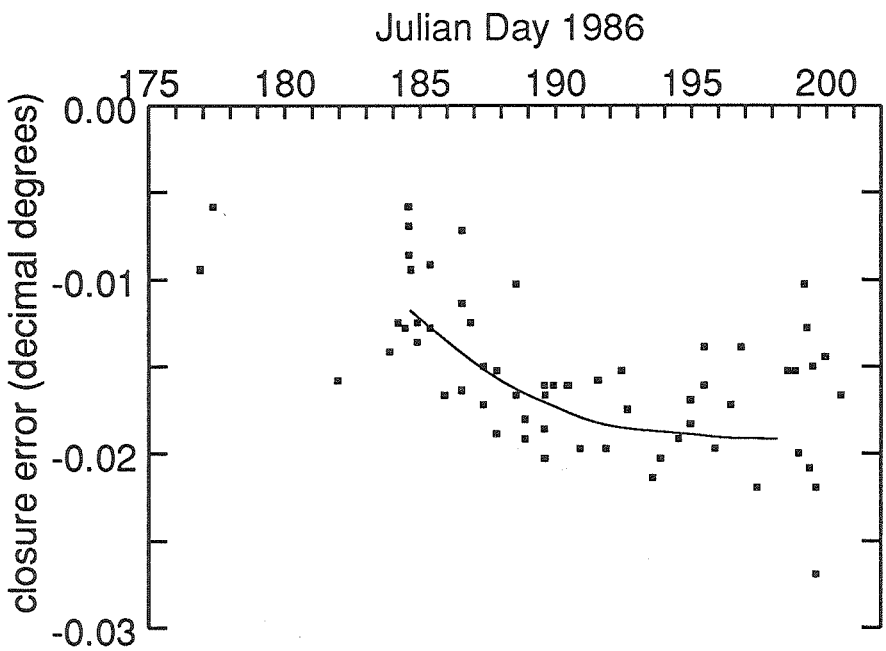


**Figure 2.6** Deviation of the sum of the forward and reverse angles from 360° for theodolite surveys from station T to NW. Plotted in decimal degrees. The reference line in the figure is a hand drawn trend representing instrument drift. The scatter around this line is ~±0.005°, representing an error in surveyed elevation of ±0.011 m.

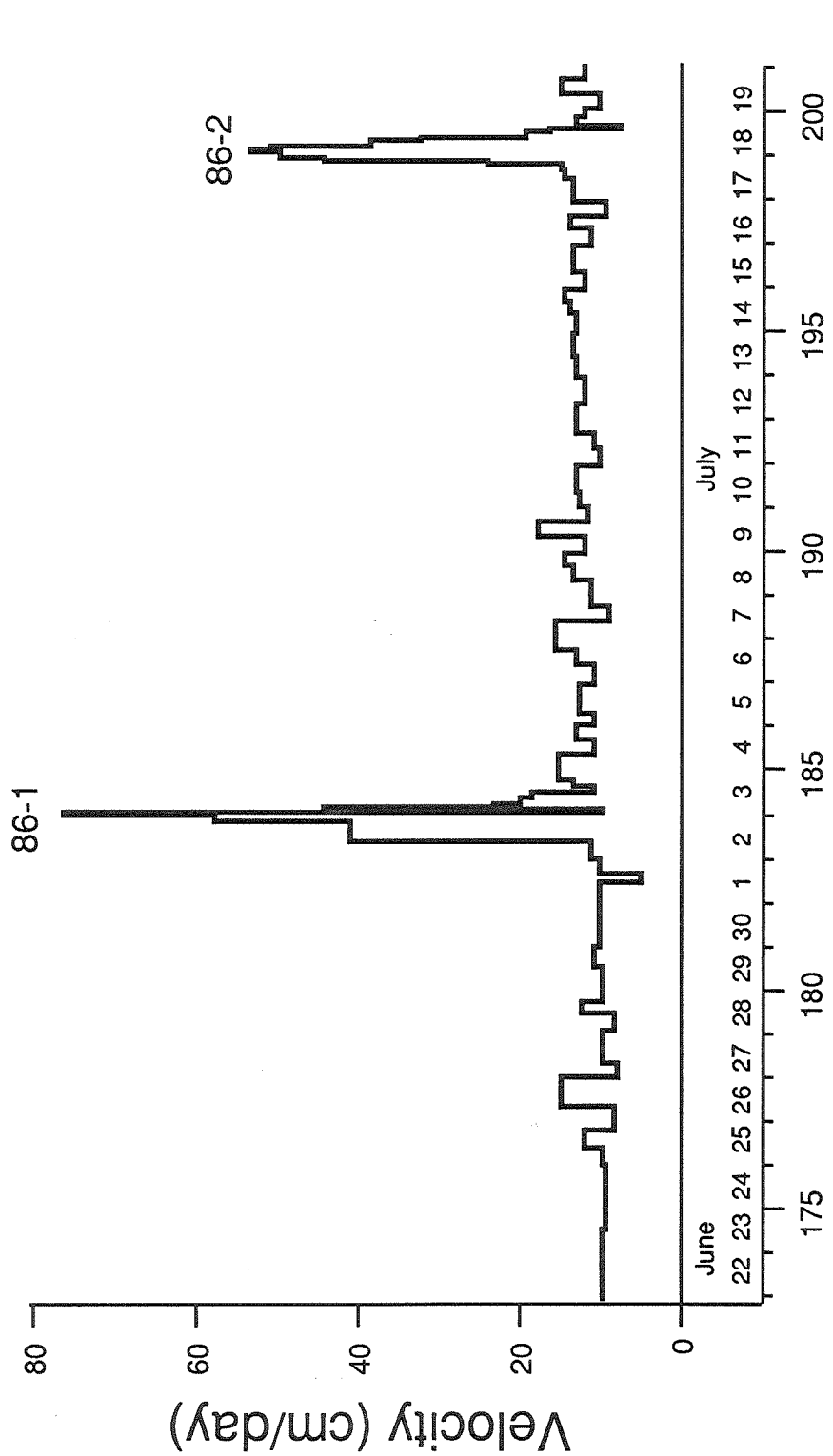


**Figure 2.7** Velocity of Station B toward reflector AL. Numbers designate mini-surges.

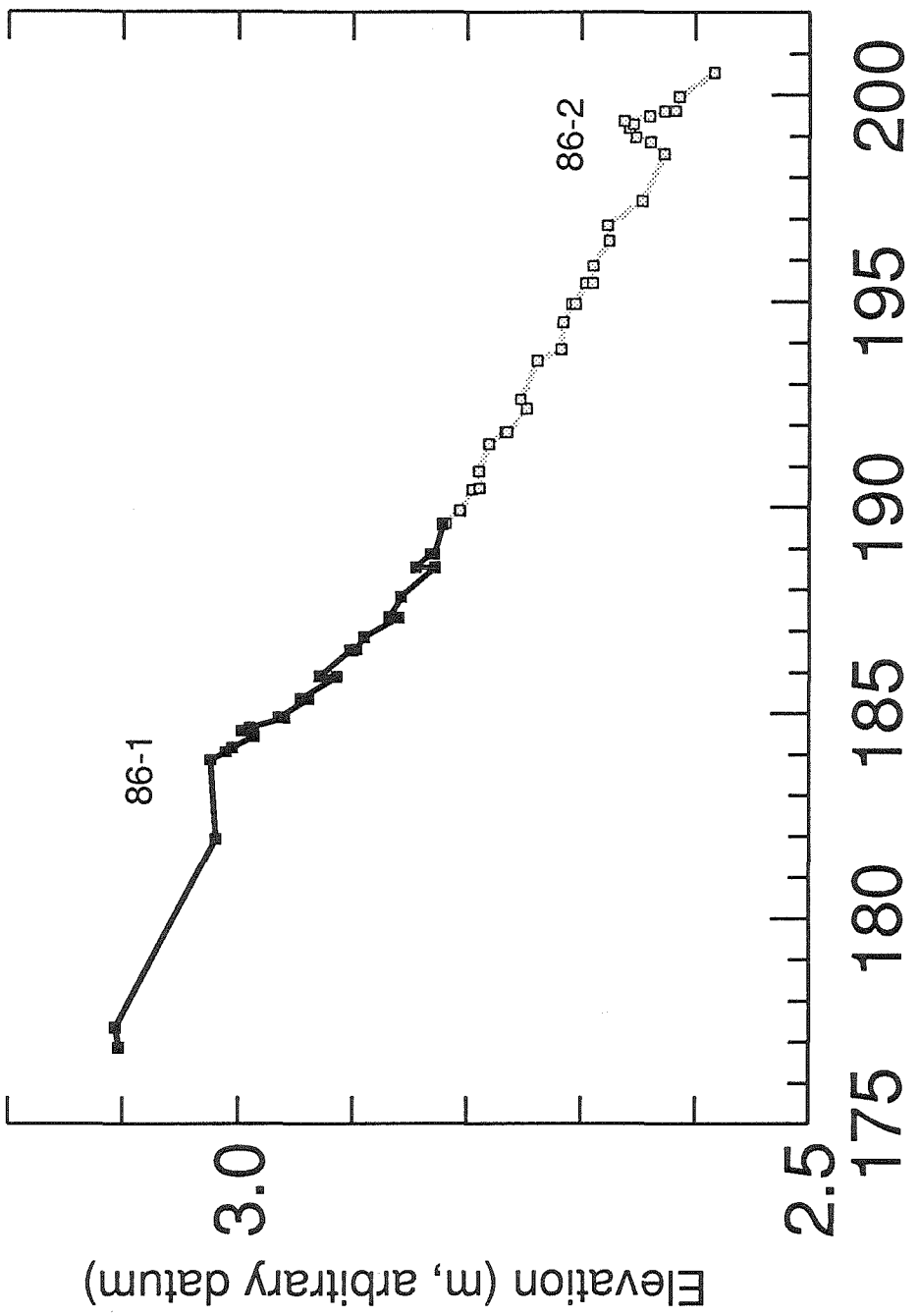


**Figure 2.8** 1986 Elevation of Station T relative to arbitrary datum (change in line shading indicates resetting of on ice benchmark).

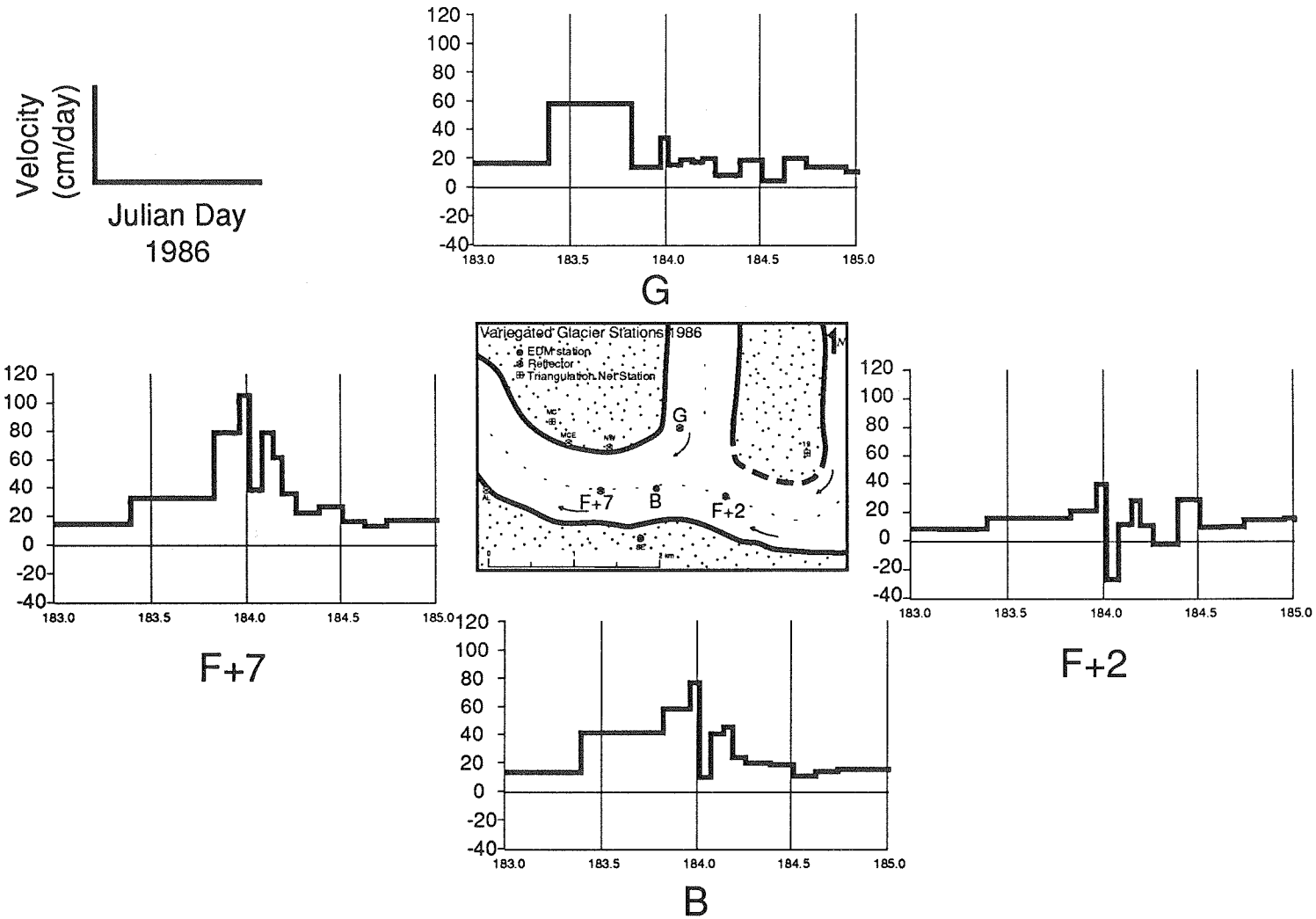


**Figure 2.9** Surface velocity records for mini-surge 86-1. Map in center shows locations of sites.

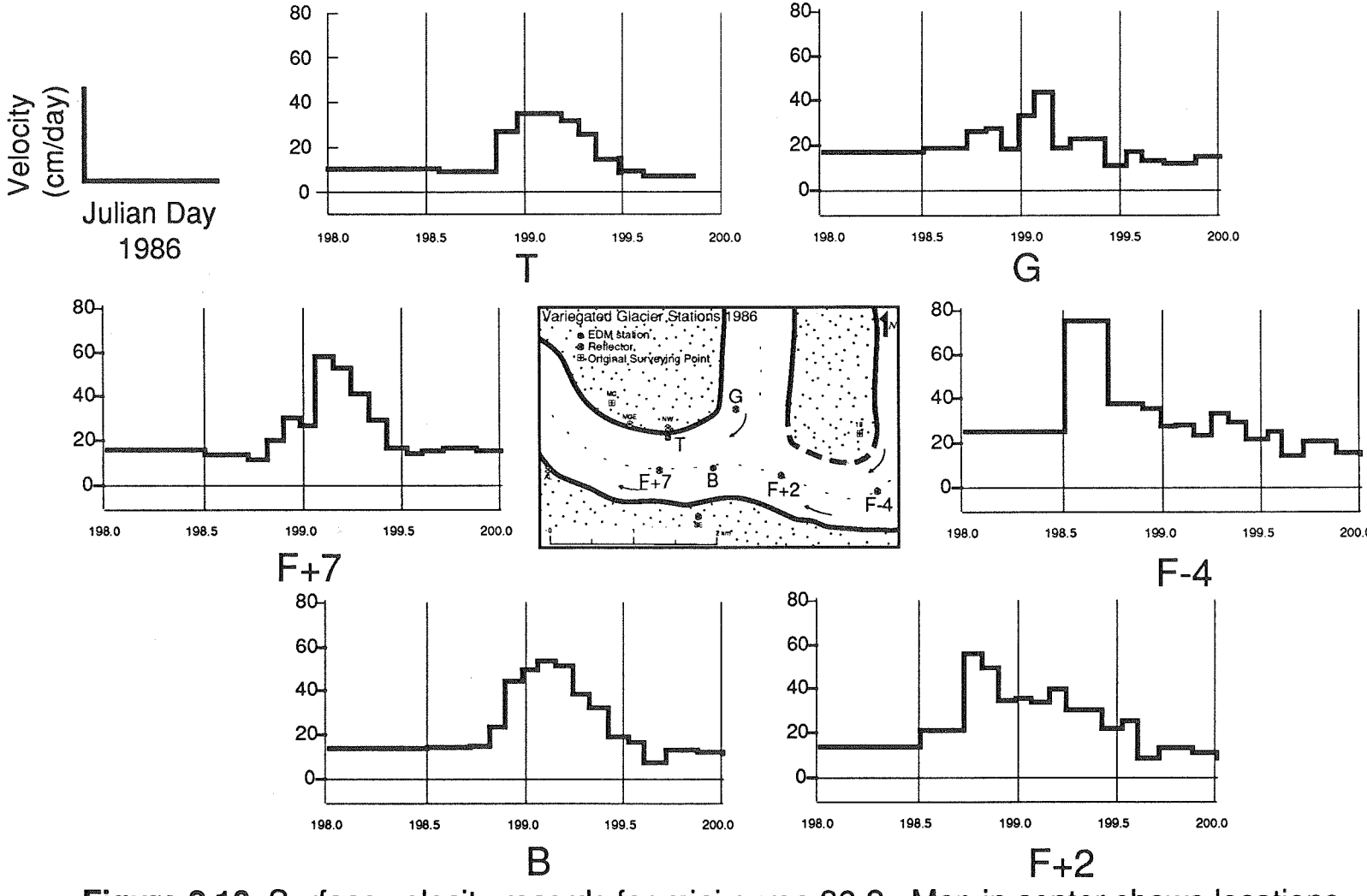


**Figure 2.10** Surface velocity records for mini-surge 86-2. Map in center shows locations of sites.

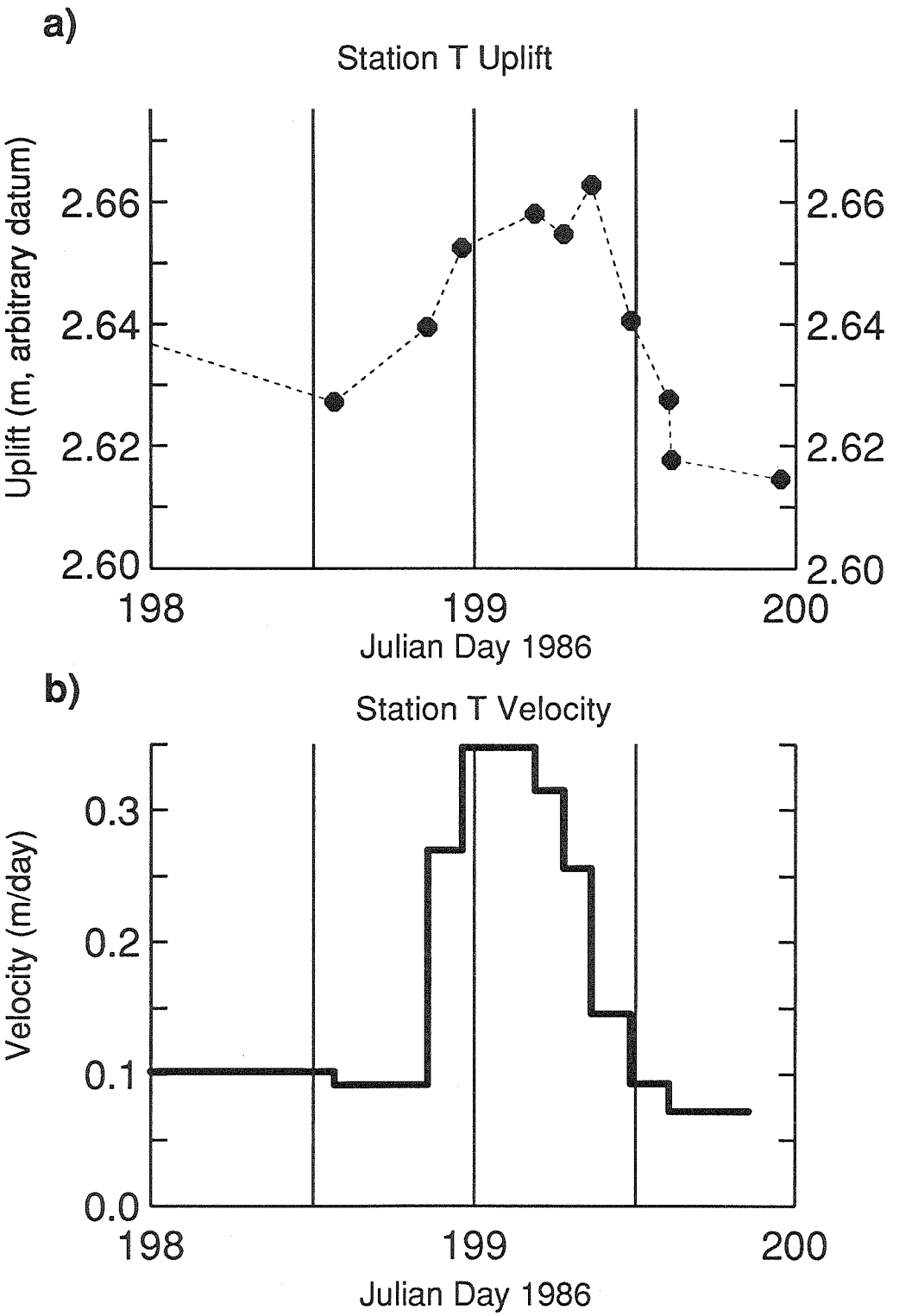


**Figure 2.11** Detailed record of mini-surge 86-2 at station T a) uplift relative to arbitrary datum b) velocity toward reflector MCE.

# Chapter 3

# Theory of Mini-Surge Wave Propagation

## Introduction

Mini-surges are detected as disturbances in the regular patterns of surface velocity, basal water pressure, and ice quake activity. As was noted in the last chapter, increased sliding velocity and surface uplift during a mini-surge suggest that a locally increased amount of water at the bed may be responsible for the disturbances. Any model of mini-surge behavior based on the presence of a pulse of water would require that the basal water system be capable of propagating this wave of increased water volume. Thus to understand a mini-surge, it is necessary to establish the requirements for the propagation of a wave of increased water volume in the basal water system.

Many geometries have been suggested for the distribution of water at the bed of a glacier. Weertman favored a "film" of water between the ice and underlying debris and bedrock [Weertman, 1972]. The thickness of this film was variable with location and time. Kamb [1987] and Walder [1986] discussed the complexities of systems of linked cavities which would form on the downglacier side of bed protuberances. Röthlisberger [1972] and Nye [1976] developed the physics behind an elegant system which involves tunnels melted into the ice by heat dissipated by the flowing water. Various modifications of these ideas, and models based on porous flow through the bed material, have also been proposed.

In most glaciers, including Variegated, water exits the terminus in one or more discrete streams which emerge from tunnels. Thus in the lower reach a tunnel system of some sort must exist. Experiments involving dye injections suggest that water transport under Variegated Glacier in the non-surging state is dominated by flow in a tunnel-like conduit [Brugman, 1986]. Brugman based this conclusion on observations of rapid transport time, little dispersion of the dye, and the fact that dye was only detected in one

outlet stream. For dye injected during the surge, she found much longer travel times, greater dispersion, and the presence of dye in several of the outlet streams. The results during the surge have been used to argue for a distributed flow system at the bed, such as a system of linked cavities [Brugman, 1986; Kamb et al., 1985]. Additional evidence for a distributed flow system includes measured uplift both during the surge and during mini-surges; this has been interpreted as being the result of cavities opening at the bed [Kamb and Engelhardt, 1987; Kamb et al., 1985]. Humphrey et al. [1986] have also argued for increased water access at the ice/rock interface during mini-surges, based on an accompanying turbidity pulse, as noted in the last section.

For Variegated Glacier it would appear, from the observations described above, that two different basal water systems can be in operation, dependent on the current state of the glacier. In the non-surging state there is good evidence for a tunnel system, as argued by Brugman. During a mini-surge, arguments based on measurements in the outflow stream favor a distributed flow system in the upper reach of the glacier and a tunnel in the reach unaffected by mini-surges [Humphrey et al., 1986]. During the surge, behavior clearly distinct from a tunnel system is seen, and a system of linked cavities is likely [Kamb, 1987].

The role of the basal water system in a mini-surge is defined by the observations of variation in water pressure and uplift. The mechanism behind the propagation of the pulse of water which accompanies the mini-surge is not immediately obvious from the observations.

Several short qualitative descriptions of a possible mechanism for water pulse propagation have been presented [Raymond and Malone, 1986; Humphrey et al., 1986; Kamb and Engelhardt, 1987; Iken and Bindschadler, 1986]. All of these descriptions have a common physical basis centered on an increase in the conductivity of the basal system due to the action of water pressure in opening cavities at the bed. The idea is put in semi-quantitative terms by Kamb and Engelhardt, who require an upglacier increase in

hydraulic conductivity for the wave to propagate. In these models the wave is started by the release of stored water into the basal water system at some upglacier point.

In the next two sections mathematical models are developed to investigate the propagation of water pulses in the basal water system. Two systems are investigated: the tunnel system of Röthlisberger and Nye, and a system based on a distributed hydraulic conductivity linked to water pressure, which is a representation of a conductivity based on cavitation.

## Tunnel System Response to a Mini-Surge Like Disturbance

Mini-surge disturbances are a relatively new topic in glacial hydrology. Their existence has only been documented on a few glaciers. When attempting to develop an understanding of mini-surge propagation, it would seem reasonable to start by investigating the behavior of the "standard" glacial hydrologic system, the tunnel system, when perturbed by an introduced pulse of extra water.

The ice tunnel model of glacial hydrology, as formulated by Röthlisberger [1972] and Nye [1976], does not have the ability to handle a rapidly varying water volume. A pulse of water pressure introduced into this system would propagate along the conduit at the speed of sound, which is much faster than the mini-surge propagation speeds. In this model, all water is contained in the conduit(s), and changes in the water volume of the system can only be produced by melting of the walls or enlargement of the tunnel by ice flow, which are relatively slow processes. To have pressure pulse propagation speeds of the observed magnitude, it is necessary to add to the standard tunnel model a storage capability for water that allows substantial changes in stored volume of water to occur relatively rapidly.

Such water storage is a natural component of the glacier hydrologic system, and has been proposed and discussed by a number of authors [Röthlisberger and Lang, 1987; Tangborn et al., 1975]. The water storage can be accommodated in intraglacial void

space that communicates via intraglacial conduits (such as moulins) to the tunnel(s), or it can be accommodated in basal cavities that typically form on the downglacier side of bed irregularities. The standard tunnel system is modified by adding the storage of water external to the main conduits, which is assumed to be an increasing function of the phreatic level in the glacier. This can be expressed in the simplest way as

$$V = w_e \nu h \tag{3.1}$$

where $V$ is the volume of water stored in the system per unit length of glacier, $w_e$ is the width over which the storage occurs, $\nu$ is the porosity, and $h$ is the height of the phreatic surface above the bed; as a measure of basal water pressure, $h=P_w/(\rho_w g)$, where $P_w$ is the water pressure, $\rho_w$ is the density of water, and $g$ is gravitational acceleration. Water storage was not included by Röthlisberger or Nye because it was not pertinent to the problems they were addressing with the tunnel model.

A tunnel system modified by the addition of storage , such as in Equation 3.1, has the ability to handle the input of a pulse of extra water, but it is not immediately clear how the system will respond to the presence of the extra water. The possibility of pulse propagation in a tunnel is here investigated numerically using Nye's [1976] equations for time dependent flow of water in an ice walled conduit, modified to include intraglacial water storage. The coordinate system for the model is illustrated in Figure 3.1. Definitions of symbols and typical values used are given in Appendix 3.

The tunnel system equations are based on the competition between radial inflow of ice, which acts to close a tunnel, and heat generated by water flow, which acts to enlarge it. Nye [1976, Equation 16] expressed this as

$$\frac{\partial S}{\partial t} = \frac{m}{\rho_i} - 2S\left(\frac{P_i - P_w}{nA}\right)^n \tag{3.2}$$

where $S$ is the cross-sectional area of the conduit, $t$ is time, $m$ is the mass rate of melting per unit length of conduit, $\rho_i$ is the density of ice, $P_i$ and $P_w$ are the overburden pressure of ice and the water pressure, respectively, and $n$ and $A$ are constants in Glen's flow law

[Nye, 1953]. The second term on the right hand side of Equation 3.2 expresses the area rate of closure due to ice flow for a conduit of circular cross-section in an infinite mass of ice. This term is only an approximation for a tunnel located at the bed, but it is plausible to assume that closure of such a conduit (which might be non-circular) would be proportional to a power of the pressure difference [Nye, 1976].

The continuity equation for water in this system is based on Nye [1976, Equation 17] modified by the addition of a storage term and a local input term, and by multiplying by a tortuosity factor:

$$\frac{\partial V}{\partial t} + \omega \frac{\partial S}{\partial t} = \omega \frac{m}{\rho_w} - \frac{\partial Q}{\partial x} + I \tag{3.3}$$

Here $V$ is the storage defined in Equation 3.1, $Q$ is the water flux, $x$ is the down glacier coordinate, $\omega$ is the tortuosity (ratio of conduit length to down glacier length), and $I$ is the local rate of water input over the width of the glacier (input due to surface melt and rain). The tortuosity $\omega$ can be used to represent the effect of a winding conduit; it is taken equal to 1 in the modeling here, but is included in Equation 3.3 for completeness.

Water flow is governed by the Gaucker-Manning-Strickler relation expressed in the manner of Nye [1976, Equation 18]:

$$\xi(\beta - \frac{\partial h}{\partial x}) = \frac{NQ^2}{S^{\frac{8}{3}}} \tag{3.4}$$

where $N = (4\pi)^{\frac{2}{3}} \rho_w g \kappa^2$ for a circular conduit and $\xi = \frac{\rho_w g}{\omega}$.

Here $\beta$ is the basal slope of the glacier and $\kappa$ is the Manning roughness coefficient. $\partial h/\partial x$-$\beta$ is the downglacier gradient in hydraulic head.

The mass of ice melted per unit time per unit length of glacier, assuming local heat transfer, (after Nye [1976], Equation 19]) is

$$m = \frac{1}{L} Q \xi [\beta - R_1 \frac{\partial h}{\partial x}] \tag{3.5}$$

$$R_1 = 0.684$$

where $L$ is the latent heat of fusion of ice, and $R_1$ is the fraction of the heat produced (on account of the gradient $\partial h/\partial x$) that is not used to maintain the water at the pressure melting temperature [Röthlisberger, 1972, Equation 4].

Equations 3.1-3.5 may be combined and solved for $\partial h/\partial t$ *and* $\partial S/\partial t$:

$$\frac{\partial h}{\partial t} = \frac{\omega}{w_e \nu}\left[\left(\frac{1}{\rho_w} - \frac{1}{\rho_i}\right)\frac{S^{\frac{4}{3}}\xi^{\frac{3}{2}}}{LN^{\frac{1}{2}}}\left(\beta - R_1\frac{\partial h}{\partial x}\right)\left(\beta - \frac{\partial h}{\partial x}\right)^{\frac{1}{2}} + 2S\left(\frac{P_i - P_w}{nV_i}\right)^n \right.$$
$$\left. - \frac{1}{\omega}\left(-\frac{S^{\frac{4}{3}}\xi^{\frac{1}{2}}}{2N^{\frac{1}{2}}}\left(\beta - \frac{\partial h}{\partial x}\right)^{-\frac{1}{2}}\frac{\partial^2 h}{\partial x^2} + \frac{4S^{\frac{1}{3}}\xi^{\frac{1}{2}}}{3N^{\frac{1}{2}}}\left(\beta - \frac{\partial h}{\partial x}\right)^{\frac{1}{2}}\frac{\partial S}{\partial x}\right) + \frac{1}{\omega}I\right] \tag{3.6}$$

$$\frac{\partial S}{\partial t} = \frac{S^{\frac{4}{3}}\xi^{\frac{3}{2}}}{\rho_i LN^{\frac{1}{2}}}\left(\beta - R_1\frac{\partial h}{\partial x}\right)\left(\beta - \frac{\partial h}{\partial x}\right)^{\frac{1}{2}} - 2S\left(\frac{P_i - P_w}{nV_i}\right)^n \tag{3.7}$$

Taking the input rate $I(x)$ and ice thickness $h_i(x)$ as known., these equations allow the evolution of the system in time to be followed numerically using a finite difference scheme, permitting the investigation of the response to a local increase in the rate of water input to the basal system. Note again that $P_w=\rho_w g h(x,t)$ and $P_i=\rho_i g h_i$.

The model glacier used in the calculation has a basal slope $\beta=0.1$, an ice thickness $h_{ice}$ of 400 m, a width $w_e$=1000 m and constant distributed input over its length equivalent to $I=0.05w_e$ m$^2$/d, representing the contribution from ablation (an average value of 5 cm/d). A value for the porosity $\nu$ of 0.001 is based on order of magnitude estimates from Humphrey et al. [1986, p. 205], $\nu \geq 0.0005$ (estimate to explain water storage during mini-surges), and from Columbia Glacier (Chapter 3), where diurnal changes in water level (due to surface melt fluctuation amplitude of ~14 cm/d) had an amplitude of 25 m in a borehole, giving $\nu \approx 0.001$. At the head of the glacier the basal flux is taken to be 0, so the tunnel cross-sectional area is 0 there as a result. The boundary condition at the terminus is a water height $h$ (or exit water pressure) of 0. The model glacier is chosen to be 40 km long so that the imposed disturbance will not reach the terminus during the simulation. This length is twice the actual length of Variegated

Glacier, but this does not significantly influence the results seen in the upper part of the glacier, as the pressure in this region is not significantly different from the pressure in the same region for a 20 km long model.

The starting profiles of water height $h(x, t=0)$ and tunnel area $S(x, t=0)$ are calculated for the steady state condition using the procedure described in Appendix 1. These profiles are represented in the finite difference scheme by their values on a longitudinal profile discretized at 50 m intervals. First and second derivatives are approximated by the standard finite difference technique:

$$\frac{\partial h_i}{\partial x} = \frac{h_{i+1} - h_{i-1}}{2(50\ \mathrm{m})} \tag{3.8}$$

$$\frac{\partial^2 h_i}{\partial x^2} = \frac{h_{i+1} + h_{i-1} - 2h_i}{(50\ \mathrm{m})^2} \tag{3.9}$$

where $i$ is the number of the grid point where the derivative is desired.

For each time step $h(x, t+\Delta t)$ and $S(x, t+\Delta t)$ are calculated from Equations. 3.6 and 3.7 using the relations:

$$h(x,t+\Delta t) = h(x,t) + \frac{\partial h(x,t)}{\partial t}\Delta t \tag{3.10}$$

$$S(x,t+\Delta t) = S(x,t) + \frac{\partial S(x,t)}{\partial t}\Delta t \tag{3.11}$$

The pulse of water in the basal water system is produced by adding an extra input of water to a small part of the grid at a known rate. The extra input $I$ is added as a Gaussian distribution in $x$, over a reach 37 grid points wide (1800 m). It is scaled to produce an extra input flux of 10 $m^3/s$ (about 2 times the initial flux carried in this reach). The extra input is distributed as a Gaussian to keep the water level curve smooth, promoting stability in the numerical calculation. The extra input starts at $t=0$.

A simulation based on this model is shown in Figure 3.2. The extra water input for this simulation was centered at $x=8.6$ km and lasted for 9.6 h. This location was

chosen because the background flux at this point is 5 $m^3/s$, which is the inferred flux in the reach of Variegated Glacier subject to mini-surges. In Figures 3.2 *a* and *b* the water height ($h$) and tunnel cross-sectional area ($S$) are plotted as a function of $x$ every 4.8 hours ($t$=0, 4.8 h, 9.6 h, ...). In Figure 3.2 *a* the times for the first three curves are labeled.

The vertical discontinuity which develops in $S$ at $x$=8.6 km (Figure 3.2 *b*) is a reflection of the dominance of increased melting (due to the change in the hydraulic gradient) over ice flow. The discontinuity develops because of the increased gradient on the downglacier side of the input and the reduced gradient on the upglacier side.

Figure 3.2 *c* displays the height of water $h$ verses time at ten points along the glacier, spaced every kilometer from $x$=13.6 km to $x$=22.6 km. These records are the model equivalents of hydrographs from boreholes located at these points. Figure 3.2 *d* gives the time history of $S$ from the same locations.

The disturbance introduced into this simulation clearly propagates downglacier. The speed of propagation of the wave "front" is about 200 m/h, which is somewhat slow for a mini-surge, a factor of 2 or 3 slower than the observed velocities for the front ("onset" of Kamb and Engelhardt). Propagating waves of basal water pressure on Findelengletscher had velocities of 90 - 180 m/hour [Iken and Bindschadler, 1986] which is closer to the model result. This simulation was repeated with smaller extra inputs (2 and 5 $m^3/s$); propagation velocities of about 140 and 160 m/h resulted. Rates of extra input greater than 10 $m^3/s$ required time steps which were too small to be practical for the SUN Sparcstation 1 used for the calculation. I conclude that the velocity of the front in a tunnel system is relatively insensitive to the rate of input of extra water that causes a perturbation to arise, and also to the size of the perturbation.

To compare the propagating disturbance in this simulation to the observations made during a mini-surge, compare Figure 3.2 *c* to the hydrographs recorded by Kamb and Engelhardt, two of which are shown in Figures 2.2 *c* and *f*. In Figure 2.2 *c* the majority of the water level rise occurs in 1 hour, while in Figure 2.2 *f* the rise occurs over

3 hours. These rapid onsets are characteristic of mini-surges in this reach and must be a manifestation of the workings of the propagation mechanism. Examination of rise times in Figure 3.2 *c* show that in the tunnel system simulation the rise in borehole water level would take about a day. The gentle rise of the water level was characteristic of all the tunnel simulations run; it is a result of the slow process of enlarging the conduit by melting. While the enlargement of a tunnel by melting can be catastrophic, as in the case of a jökulhlaup, the initial stages must be slow, for a conduit initially in steady state; the increased flux through the system, required for increased melting, takes time to develop.

Although the tunnel system with the addition of storage provides the ability to propagate a disturbance at approximately the observed speed, it fails to reproduce the rapid rise in water level that characterizes the arrival of a mini-surge. The propagating disturbance in the tunnel system increases in amplitude as it moves downglacier because of the drawdown of water after the disturbance passes. This change in size is the opposite of the behavior observed for mini surges, which decrease in amplitude downglacier. The tunnel system must not be the only path for water flow during a mini-surge.

However, the simulations suggest that any tunnel system present in the reach affected by a mini-surge will be modified by the passage of the steep pressure gradient and will be able to carry a larger flux after the event. This may be the explanation for the fact that the water level tends to drop substantially below the pre-event level after a disturbance has passed [Kamb and Engelhardt, 1987].

## Pressure Dependent Conductivity Mechanism

In the introduction to this chapter I briefly described the mechanism put forward qualitatively by several workers to explain the behavior of the basal water system during a mini-surge. The mechanism is based on cavitation at the bed brought on by the high water pressure of the mini-surge pulse. This cavitation causes an increase in the hydraulic conductivity of the basal water system, which results in propagation of the

water pulse through the system. I here develop a quantitative model of this mechanism, to see if it can explain the observations.

Cavitation is a complicated process which is dependent on basal water pressure, basal shear stress, bed roughness, and sliding velocity. Here I will make the assumption that the hydraulic conductivity of such a system is an increasing function of basal water pressure. This is based on the idea that higher water pressures should lead to larger cavities, and thus to an increased hydraulic conductivity.

A system based on pressure dependent conductivity can be formulated in a manner similar to that used for the tunnel system. The storage relation, Equation. 3.1, will be retained, with the same effective width and bulk porosity. In this system the flow of water is expressed

$$Q = k(\beta - \frac{\partial h}{\partial x})^{\gamma} \tag{3.12}$$

where $k$ is a conductivity parameter (a function of $h$) and $\gamma$ can be either 1 (laminar flow) or 1/2 (turbulent flow). In the calculations described below, flow is taken to be turbulent, as argued by Kamb [1987].

Storage and water flow are related by requiring continuity:

$$\frac{\partial V}{\partial t} = -\frac{\partial Q}{\partial x} \tag{3.13}$$

This system can be followed numerically in a manner similar to that used for the tunnel system in the previous section. The governing equation for the time integration, derived by combining Equations 3.1, 3.12, and 3.13, is

$$w_e \nu \frac{\partial h}{\partial t} = -\frac{\partial \left[ k(\beta - \frac{\partial h}{\partial x})^{\gamma} \right]}{\partial x} \tag{3.14a}$$

or, in expanded form:

$$w_e \nu \frac{\partial h}{\partial t} = -(\beta - \frac{\partial h}{\partial x})^{\gamma} \frac{\partial k}{\partial h} \frac{\partial h}{\partial x} + \gamma (\beta - \frac{\partial h}{\partial x})^{\gamma - 1} k \frac{\partial^2 h}{\partial x^2} \tag{3.14b}$$

Equation 3.14 *b* is similar to a linear combination of two familiar equations. The first is the simplest expression of a nondispersive, nondiffusive wave equation [Lick, 1990]

$$\frac{\partial h}{\partial t} = -c\frac{\partial h}{\partial x} \tag{3.15}$$

where $c$ is the wave velocity. A system governed by Equation 3.15 will propagate an initial curve $h(x)$ with unchanged shape at a velocity $c$ in the positive $x$ direction. The second equation is the one dimensional diffusion equation

$$\frac{\partial h}{\partial t} = d\frac{\partial^2 h}{\partial x^2} \tag{3.16}$$

where $d$ is the diffusivity. In a system governed by this equation, disturbances to linear trends are damped out with time, without propagation (which would be defined by a change in the "center of mass" of the disturbance). Equation 3.14 *b* does not have the constant coefficients of Equations 3.15 and 3.16, but the similarity suggests the potential for both propagation and damping of pulses of increased water volume. If the conductivity $k$ in Equation 3.14 *b* is a constant, $\partial k/\partial h = 0$ and the first term on the right disappears, leaving only the resemblance to the diffusion equation. This suggests that disturbances will not propagate in a system with constant conductivity, and will only dissipate with time.

The behavior of a system governed by Equation 3.14 is here investigated for various forms of the conductivity function $k(h)$. Simple forms of $k$ which are increasing functions of water pressure can be represented with the first few terms of a Taylor series expansion about $h_0$

$$k(h) = k_0(1 + \frac{(h-h_0)}{d_1} + \frac{(h-h_0)^2}{d_2^2} + \frac{(h-h_0)^3}{d_3^3}) \tag{3.17}$$

where $h_0$ is the pre-event water level, $k_0$ is the conductivity of the pre-existing system, and $d_1$, $d_2$, and $d_3$ are the reciprocal coefficients of the expansion which will be chosen as

reasonable "doubling heights," or rises which make the contribution from that term equal to the background conductivity $k_0$. This formulation allows the model to accommodate the existence of a pre-event flux which is maintained during the event. A physical description of one possible system would involve a pre-existing tunnel with fixed conductivity $k_0$ and a conductivity due to cavitation at the bed which increases with increasing water pressure.

Another form used for the conductivity relation is

$$k(h) = k_0 \frac{h_\infty - h_0}{h_\infty - h} \tag{3.18}$$

where $h_\infty$ is the "floatation level" or phreatic level at which there is unbounded increase in conductivity. Equation 3.18 is based on the physical interpretation that cavitation (and as a result, conductivity) is a non-linear process which has a "critical point" at which the process becomes unstable. Equation 3.18 has a Taylor series expansion in which $d_1=d_2=d_3=...$, so all terms make equal contributions to the increases in conductivity (as this was interpreted in the preceding discussion).

An idea of the role of non-linearity in the conductivity relation is provided by making runs of the model with different numbers of terms in Equation 3.17, with the same value used for all the $d_i$'s of the terms included for a particular run. A run using conductivity relation 3.18 represents the effect of including all orders in the expansion 3.17, and thus further extends the range of non-linearity investigated.

Derivatives and the forward calculation of $h$ for each time step are based on Equations 3.8, 3.9, 3.10, and 3.14 *b*. The background conductivity $k_0$ is chosen so that the pre-event water flux is 5 $m^3/s$. This background flux is $k_0\beta^{1/2}$, which, for $\beta=0.1$, gives $k_0=15.8$ $m^3/s$ (assuming $\partial h/\partial x=0$ in the initial state). The disturbance in each of the simulations was produced in the manner of the last section, with an extra flux of 20 $m^3$/sec added at $x=7.0$ km for the first 9.6 hours. For all of the simulations based on Equation 3.14, there is no distributed input $I$, so the background flux is independent of $x$.

This allows the background water level to be $x$ -independent. The starting water level $h_0$ is taken to be 210 m (a reasonable level for what is observed on Variegated Glacier in the mini-surge reach, where the ice is ~400 m thick), the glacier's length is 40 km, and a 50 m grid spacing is used. The boundary condition at both ends is constant flux, which is not violated during a run as long as the disturbance does not affect the water levels near the boundaries.

To produce disturbances with similar propagation velocities, an estimated velocity is calculated from a relation based on the similarity already noted between Equation 3.15 and the first term on the right of Equation 3.14 *b*. This similarly suggests

$$\frac{1}{w_e \nu}(\beta - \frac{\partial h}{\partial x})^{\frac{1}{2}} \frac{\Delta k}{\Delta h} \approx c \tag{3.19}$$

where $\Delta h$ is a change in water height between two positions on a wave and $\Delta k$ is the corresponding change in conductivity. Using a typical measured mini-surge wave velocity of 500 m/hour, a value for $\partial h/\partial x$ of -0.05 (estimated from earlier simulations), and a value for $w_e \nu$ of 1 m in Equation 3.19, the following constraint results:

$$\frac{\Delta k}{\Delta h} = 1300 \text{ m/h} \tag{3.20}$$

The value for the slope $\partial h/\partial x$ was estimated for a point on the front of the curve about 50 m above $h_0$, so $\Delta h$=50 m will be used in Equation 3.20 to calculate appropriate values for the constants in the conductivity relation, subject to the previously mentioned simplification that all of the terms included in Equation 3.17 for a given run have the same value for $d$.

This was done for the three runs shown in Figure 3.3 *b*, *c*, and *d*, which have highest-order dependences of $k$ on $h$ that are cubic, quadratic, and linear, respectively. The form of $k$ used is shown on the individual plots in the Figure, as is the value for the doubling height $d$. Equation 3.20 was also used to find the appropriate value for $h_\infty$ for the run shown in Figure 3.3 *a*, which uses conductivity relation 3.18.

All of the disturbances in Figure 3.3 propagate downglacier. It is clear that the pressure dependent conductivity mechanism is capable of producing the propagation of such a disturbance, as was expected from the similarity with Equation 3.15. The propagation velocities at a point $h$ = 250 m on the fronts of the disturbances are shown in Table 3.1 for the third, sixth, and ninth intervals in the Figure. The velocities of the curves in Figure 3.3 *a*, *b* and *c* all start out above 500 m/h, the value used in Equation 3.19, but quickly drop as the steepness of the front diminishes. By the end of the simulation the velocities are all in the 300 - 400 m/h range. The propagation velocity of the front in Figure 3.3 *d* is always less than 500 m/h because this disturbance does not generate a steep enough face.

**Table 3.1**

| | Velocity Over Interval (m/h) | | |
|---|---|---|---|
| Interval: | Third | Sixth | Ninth |
| Run: | | | |
| *a* | 715 | 385 | 300 |
| *b* | 600 | 390 | 370 |
| *c* | 520 | 440 | 385 |
| *d* | 470 | 430 | 390 |

The four runs shown in Figure 3.3 were chosen to illustrate the effect of non-linearity in the conductivity relation on the shape of the propagating disturbance. It is clear from the figure that increasing the order of the pressure dependence of the conductivity sharpens the wave front. This effect is also seen in the time sections for these runs shown in Figure 3.4. Only the higher-order dependences on pressure used in the runs in Figure 3.4 *a* and *b* generate rises as rapid as those observed during mini-surges. The linear case illustrated in Figure 3.3 *d* in some respects resembles the results from the tunnel model, with a somewhat symmetric propagating pulse generating a

gradual rise which takes more than half a day, although the behavior after the passage of the peak is not the same.

The disturbances in each of the four runs shown in Figure 3.3 decay as they propagate downglacier. The degradation is a drop in steepness of the front and a rounding of the corners at the toe and top of the front. These changes show up in the time sections (Figure 3.4) as differences in succeeding curves: slower rise times, rounder corners, and a lagging of the peak relative to the initial rise of the front. All of these features were seen in the borehole records of Kamb and Engelhardt (compare Figure 1.2 *c* and *f* with Figure 3.4 *a* or *b*).

## Constant Form Solutions

The first two curves in Figure 3.3 *a* and the second curve in 3.3 *b* look as if they have reached, or are reaching, a plateau above which they will not rise, even if the extra input were not cut off at 9.6 hours. The existence of this plateau suggests that the conductivity in the model has increased enough to handle the extra flux, and that a wave front with a constant form (compare the first two curves in Figure 3.3 *a*) will now move downglacier. The shape of this constant form wave front will be determined below.

The existence of a wave front of constant form can be determined mathematically by looking for solutions of Equation 3.14 of the form $h(\xi)$ where $\xi = x\text{-}ct$. This has been done by Kamb and Fahnestock [in preparation] for laminar flow ($\gamma$=1) formulations using each of the conductivity relations in Figure 3.3, with the result in each case being an implicit analytical expression for $h(\xi)$. It was found that the solution for a linear dependence of conductivity on pressure increases without limit as $\xi \rightarrow -\infty$; there is no plateau reached in this case.

I would like to find the constant form solutions for the turbulent flow ($\gamma$=1/2) formulations used for the simulations in Figure 3.3. Rather than using the mathematical approach of Kamb and Fahnestock, I will use a more physically based starting point here.

In a wave of unchanging form, the flux (above background) at each point in the wave must be able to move the volume of water per unit length (above the background volume) forward at the wave velocity $U$. This can be expressed mathematically as

$$\frac{Q(x)-Q_0}{V(x)-V_0}=U \tag{3.21}$$

where $Q_0$ and $V_0$ are the pre-event (background) flux and stored water volume, and $Q(x)$ and $V(x)$ are the flux and water volume at any point $x$ in the wave.

Combining Equations 3.1, 3.12, and 3.21, and solving (for a fixed value of $t$, reflecting the constant form (in time) of the wave) for $dh/dx$ results in

$$\frac{dh}{dx}=\beta-\left[\frac{Uw_e\nu(h-h_0)+Q_0}{k}\right]^{\frac{1}{\gamma}} \tag{3.22}$$

This is a separable equation in $h$ and $x$, most easily solved for $x$:

$$x=\int dx=\int \frac{k^{\frac{1}{\gamma}}dh}{\beta k^{\frac{1}{\gamma}}-\left[Uw_e\nu(h-h_0)+Q_0\right]^{\frac{1}{\gamma}}}+C_0 \tag{3.23}$$

where $C_0$ is a constant which shifts the position of the solution in $x$ (corresponding to different times). Equation 3.23 is the implicit equation for $h$ which was integrated analytically for $\gamma$=1 by Kamb and Fahnestock. I am concerned with calculating the shapes of the constant form solutions corresponding to the runs in Figure 3.3 (with $\gamma$=1/2), so I will use Equation 3.22 with an appropriate value of $U$ to find the shape of the curve $h(x)$ by numerical integration.

The value for $U$ can be found from the curves in Figure 3.3 *a* and *b* using Equation 3.21; the extra flux $Q$-$Q_0$ is 20 $m^3$/sec in the runs and the change in storage is $w_e\nu\Delta h$ where $\Delta h$ is the change in height from the background level to the plateau. The values for $U$ calculated in this manner, used in numerically integrating Equation 3.22, give the constant form solutions shown in Figure 3.5 *a* and *b*. For the runs in Figure 3.3 *c* and *d*, which did not reach a plateau before the extra input was shut off, the value for $U$

was found by experiment, re-integrating Equation 3.22 with different values of $U$ until a match of the height of the waves at a set distance from the front was found. These two curves are shown in Figure 3.5 *c* and *d*; *d* also shows all four solutions plotted together for comparison.

As was the case for the laminar flow solutions, the linear conductivity function (Figure 3.5 *d*) does not reach a plateau, and so does not have a solution which propagates with unchanging form and a bounded value of $h$. The other 3 plots in Figure 3.5 do show bounded constant form solutions which correspond to the early curves in Figure 3.3. The constant form solutions in Figure 3.5 should be compared with the second curve in each of the plots of Figure 3.3, which have shapes developed from 9.6 hours of extra flux. The match between the constant form wave fronts generated by the model and by the approach taken in this section show that the time integration scheme used for the modeling is accurate and generates the true solutions. The shapes of the fronts in the solutions, for different orders of conductivity dependence on pressure, re-enforce the role of non-linearity in generating a rapid rise during an event.

## Conclusions

The results of this modeling effort can be interpreted as supporting the qualitative models based on cavitation. The tunnel system was unable to produce the sharp rise times observed in mini-surges. The high order dependence of conductivity on pressure which is necessary to maintain a sharp propagating front in the pressure dependent conductivity models argues for cavitation in the sense that the opening of cavities (due to high water pressure) is not a process which would be best approximated as a linear function of water pressure. Cavities begin to open only after the pressure reaches a level sufficient to infiltrate on the downglacier side of bed obstacles. The pressure at which this happens depends on bed geometry and sliding velocity. As the water pressure increases toward floatation (or beyond floatation, as it does locally during mini-surges)

the regions of the bed that cavitate increase in size. Thus the conductivity response to water pressure, if it is due to cavitation and the interconnection of cavities at the bed, would be a highly non-linear process, best approximated by a relation like Equation 3.18.

The pressure dependent conductivity mechanism produces the main features observed during propagation of a water pressure wave during a mini-surge if the pressure dependence of the conductivity is non-linear. A non-linear response to conductivity has the desirable effect of producing a steep propagating wave front, but another effect the non-linearity has is to retain water in the tail of the disturbance. This retention of water is visible when the runs shown in Figure 3.3 are compared: *a*, *b*, and *c* have trailing edges which reach all the way back to the point of initiation, while the trailing edge of the disturbance in *d* follows the wave front downglacier. The tunnel model provides a more extreme version of the linear case; in this system, the enlarged conduit allows the water level to be drawn down after the passage of the front.

As was noted in the previous section, the water level does drop after the passage of a mini-surge (the records in Figure 1.2 do not extend far enough in time to show the drop), some times to a new low for the season. While a cavity system is required to produce the steep front in a mini-surge, a more "tunnel-like" behavior is desired after the passing of the disturbance. Two ways of allowing for this behavior suggest themselves. The first is to make the background conductivity ($k_0$) be due to the flow in a tunnel which can be modified by the pressure wave. The second method involves introducing a time dependent response in the conductivity relation, representing a lag in the opening and closing of cavities in response to pressure variations. The net result of either modification is to add a history dependence to the model. This will be pursued in future work.

Field observations during a mini-surge, at the resolution they have been made to date, hint at the variable nature of the process at different positions on the glacier. Pressure and velocity measurements more densely sampled in space may reveal a

complex variability which can be related to local properties such as surface and bed slopes and ice thickness.

It may be that the type of conductivity increase required for mini-surge propagation can only happen over a certain range of basal shear stress and bed roughness. This would limit mini-surge behavior to glaciers which had conditions falling inside this range; it is possible that these conditions could be exclusive to glaciers which surge.

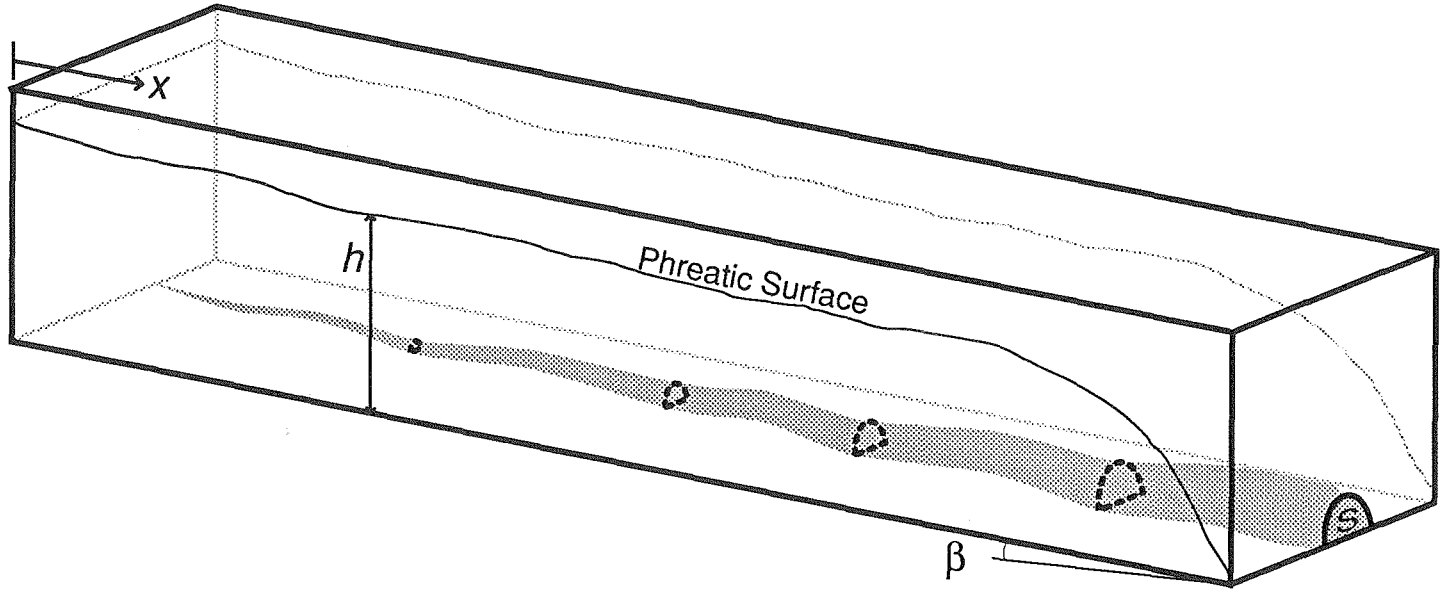


**Figure 3.1** Coordinate system used for tunnel and pressure dependent conductivity models. Both models are one dimensional; perspective is used to show surface area of tunnel cross-section for the tunnel model. In the pressure dependent conductivity model, the tunnel in this figure is replaced by a distributed flow system which has a pressure dependent hydraulic conductivity.

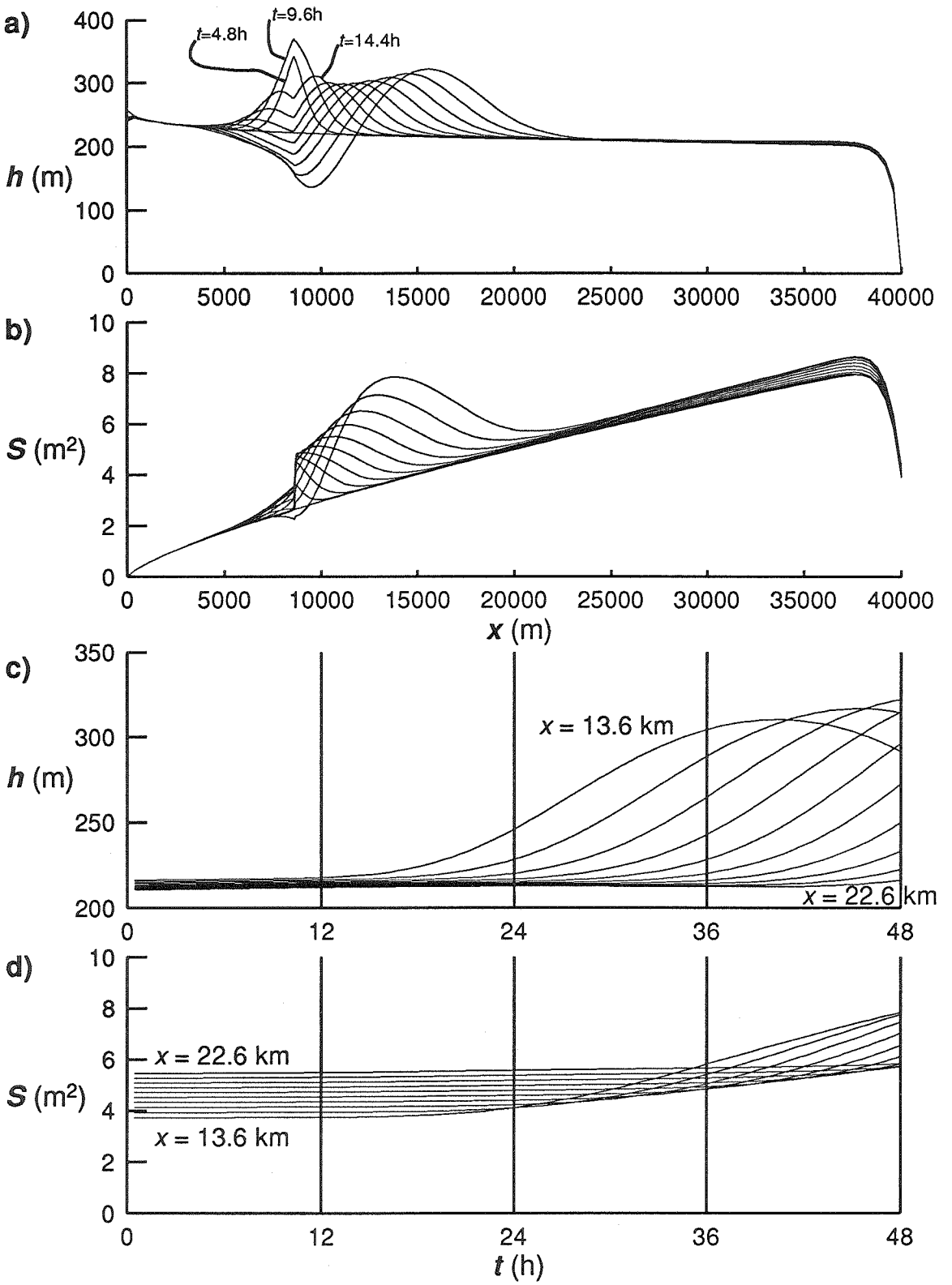


**Figure 3.2** Disturbance propagating in a tunnel. **a)** $h$ vs $x$, time interval between curves $\Delta t$=4.8 h. **b)** $S$ vs $x$, $\Delta t$=4.8 h. **c)** $h$ vs $t$ sampled every km from 13.6 km to 22.6 km. **d)** $S$ vs $t$ as in **c.**

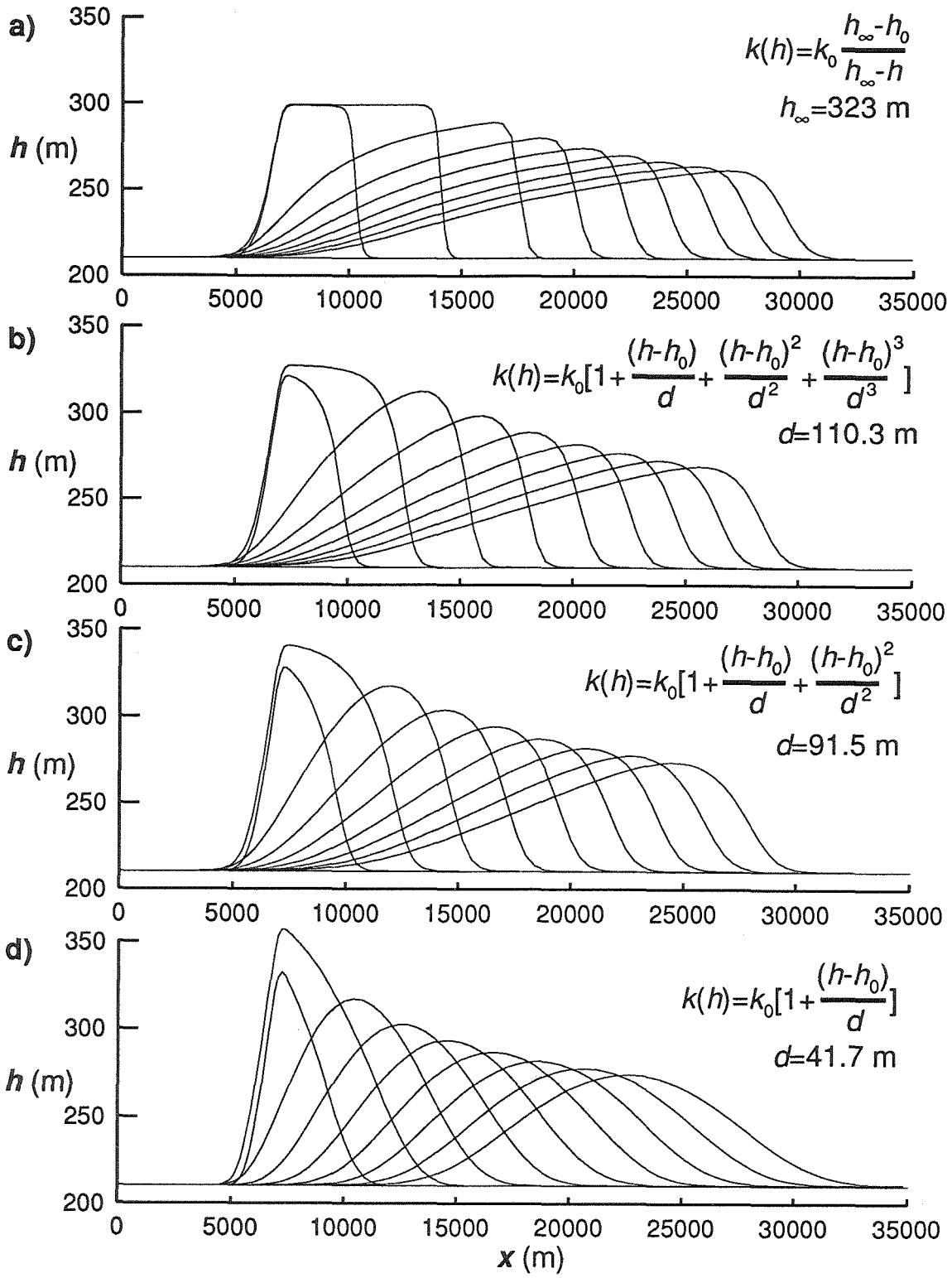


**Figure 3.3** Disturbances in pressure dependent conductivity model. Curves show water distribution every 4.8 hours. Conductivity functions are indicated for each graph.

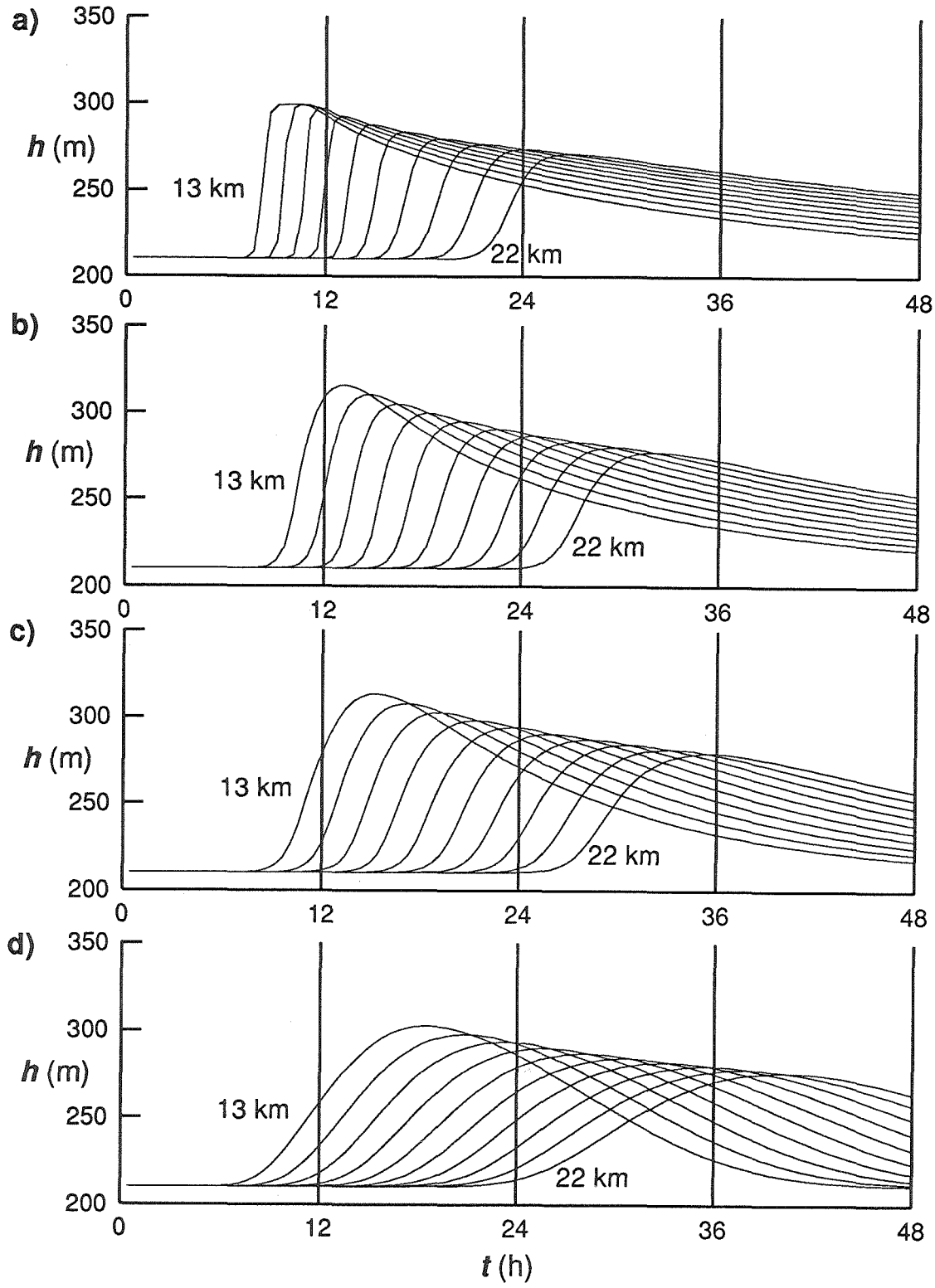


**Figure 3.4** Time sections ("borehole records") for four models shown in Figure 3.3. Sampling points for time sections are located at each km starting at $x$=13 km and extending to $x$=22 km.

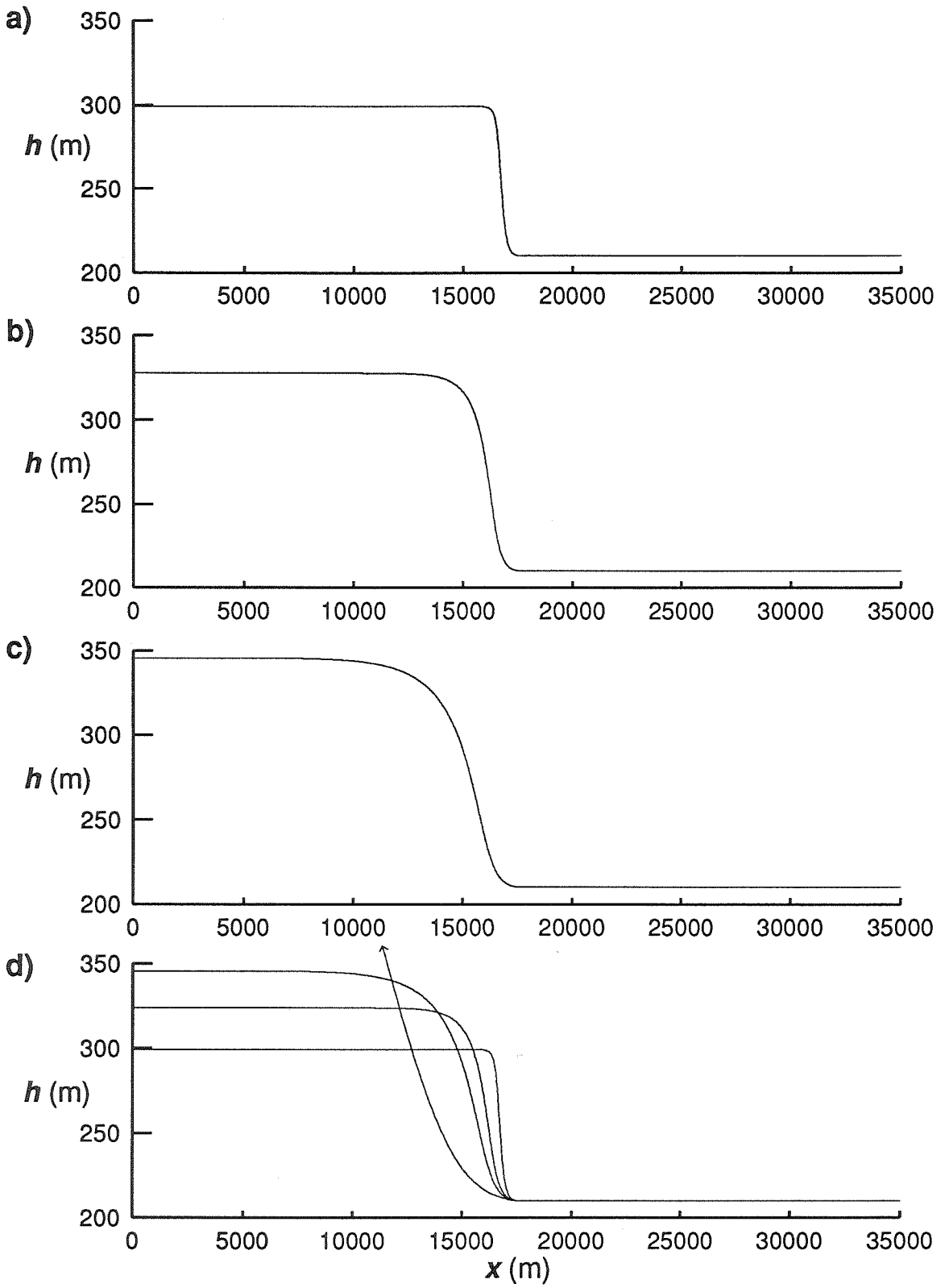


**Figure 3.5** Constant form solutions for simulations in Figure 3.3. The linear conductivity case in **d** increases without bound in direction of arrow. The curves in **a**, **b**, and **c** are repeated in **d** for comparison.

# Chapter 4

# Velocity Variations of Columbia Glacier

## Introduction

Columbia glacier is a large tidewater glacier in southern Alaska (Figure 1.1). It calves into Columbia Bay 10 km west of Valdez Arm, the fjord which provides the harbor for Valdez and the trans-Alaska pipeline terminal.

The glacier was 64 km long along its main branch in the summer of 1987 (Figure 4.1). In the 15 km long terminal reach which was the subject of this study, the width averages 5 km, the ice thickness ranges from 1000 m down to less than 300 m, and ice velocities are between 4 and 20 m/day across much of the glacier. The position of the terminus of the glacier remained stable on a moraine shoal and the north shore of Heather Island from the earliest records by Vancouver in 1794 until the beginning of a rapid retreat in the early 1980's.

The U.S. Geological Survey has conducted an ongoing set of observations of Columbia Glacier since 1977. The Survey began the Columbia project because of the dynamic behavior of the glacier and its proximity to the shipping channels used by oil tankers servicing the pipeline terminal. Early work on the glacier led to the prediction of an impending catastrophic retreat [Post, 1975]. This retreat began in about 1982, and has led to accelerated calving and increased ice-flow velocities in the terminal reach [Meier et al.,1986]. The retreat of the terminus away from Heather Island, off the moraine shoal, is shown by the successive terminus positions labeled with dates in Figure 4.2. These studies revealed an annual pattern of surface motion which is described in this except from Krimmel and Meier [1990]:

> "The velocity of Columbia Glacier varies seasonally. Throughout the upper part of the lower reach there are maxima occurring at approximately May 1 and minima in mid September each year, and these maxima and minima appear to be synchronous throughout

> much of the lower reach of the glacier. In addition, there is a pulse in velocity that occurs at the terminus late in the year that propagates about 5 km upglacier. This pulse in velocity is closely related to recession at the terminus."

Detailed Survey studies of surface velocity near the terminus of the glacier [Walters and Dunlap, 1987] revealed two interesting types of behavior. First, the glacier slowed during high tide and moved more rapidly as the tide ebbed. This effect was localized to the last few kilometers of the glacier, and was not seen 6 km upstream. Second, there was an increase in velocity following large rain storms. This latter behavior was a clear indication of hydrologic influence on sliding velocity. These observations led to an expansion of the work on the glacier to include borehole drilling and short interval monitoring of the velocity of points farther upglacier in an effort to improve understanding of the role of water in the dynamics of this glacier's behavior.

## 1987 Columbia Glacier Project

The 1987 Columbia Glacier Project, which produced most of the data discussed below, was a cooperative effort by groups from the Institute for Arctic and Alpine Research (INSTAAR, University of Colorado, Boulder), the U.S. Geological Survey Ice and Climate Project office (Tacoma, Washington), and the California Institute of Technology. The groups from INSTAAR and the USGS made detailed measurements of surface motion, ablation, meteorologic conditions, stream discharge, and the filling rate of an ice marginal lake. The group from Caltech drilled holes to the base of the ice to monitor water pressure variations and investigate basal conditions. A short summary of the observations made as part of this project follows. For a detailed description, see Meier et al. [1991].

## Surface Observations

### Surveying

The velocities of targets on the ice surface were measured from July 7 to August 31 (J. D. 188-243). The velocity of retro-reflectors at the drilling sites (Figure 4.2) were

determined from EDM surveys from Kadin repeated automatically every ten minutes, weather permitting. These velocity data, smoothed by a cubic spline with the error limit set to 0.009 m, is presented in Figure 4.3 *a* [Meier et al., 1991]. The velocities of markers at intermediate points on the ice surface were tracked by theodolite measurements made at less frequent intervals than the EDM measurements. These points are identified in Figure 4.2 as flags f2, f3 and fn3, and f4. All markers had velocities close to, but slightly slower than, the lower drill site.

**Surface Melt and Meteorology**

Ablation was measured 200 m out on the ice surface southeast of Kadin Ridge (site A on Figure 4.2). The ablation was recorded by a modified river stage recorder. The ablation rate is plotted in Figure 4.4 *b* [Meier et al., 1991]. The ablation record suffered from noise introduced by instrument failure and sensitivity to wind. The data show some correlation between ablation rate and air temperature, but fail to reflect the extra ablation associated with high winds.

Meteorological observations were recorded at Kadin and at Gate (Figure 4.2). Data from an anemometer, rain gage, and thermocouple were recorded on a Campbell Scientific CR10 data logger. The data obtained at Kadin are shown in Figures 4.4 *a* and *b* [Meier et al., 1991].

**Filling Rate of Kadin Lake**

The water level in ice-marginal Kadin Lake was recorded with a pressure transducer. The filling rate of the lake is shown in Figure 4.4 *c* [Meier et al., 1991]. The lake level did not drop during the season. Dan Stone has shown that the amount of water collected in the lake over the measurement period is equal to the amount produced from ablation and precipitation in the Kadin drainage basin, indicating that there was no input from the drainage system under Columbia Glacier [Stone, 1988]. In Figure 4.4 *c* the filling rate of the lake is given as the volume rate of water input.

### Stream Gaging

The discharge of the upper Number One River was recorded at Gate, where a stream gaging station was established. The data are shown in Figure 4.4 *c* [Meier et al., 1991]. The Number One River drains an eastern lobe of the glacier that separates from the main branch near Km 46-48 (Figures 4.1, 4.2). The main outflow stream from the glacier discharges directly into the ocean, and so cannot be gaged.

## Surface Observation Results

The velocity measurements show variation on three time scales. These variations are related to seasonal changes, occasional storms, and diurnal fluctuations.

There is a change in velocity from the early summer level of 8±0.5 m/day (lower drill site) and 4.5±0.3 m/day (upper drill site) to a lower later season level of 6.5±0.5 m/day (lower site) and 3.6±0.3 m/day (upper site). This drop occurred between day 208 and day 211.

Several velocity events occurred during the period of measurement. The velocity events, which stand out above the background velocity as increases in speed lasting several days, are all coincident with high rates of water input due to rainfall or high wind resulting in increased ablation. The velocity events are identified by number in Figure 4.3 *a*. The corresponding extra water inputs are seen in Figure 4.4 *c* as changes in the filling rate of Kadin Lake. The meteorological events that produced the extra water input are apparent in Figure 4.4 *a*.

The daily variation in velocity is undoubtedly related to the daily variation of water input due to ablation (Figure 4.4 *b*), which is reflected in the daily fluctuation of the Kadin Lake filling rate (Figure 4.4 *c*).

## Borehole Observations

The group from Caltech drilled to the bed of the glacier using a hot water drilling technique. The boreholes were located at two sites on the ice (Figure 4.2). The upper site

(designated site 52) was located between Km 51 and Km 52, just upglacier from the constriction in the glacier width between Kadin and Grand Central. The lower site (designated site 59) was located between Km 58 and Km 59 on the only sufficiently large flat topped serac which could be found below the constriction.

**Drilling**

Three boreholes were drilled at site 52. They are identified with the site number and a number representing the drilling order. The holes at this site averaged 965 m in depth and were located within 200 m of each other. In the second and third holes the water level, which remained high during drilling, dropped as the bed was approached. This drop, and the successful bottom sampling operations in holes 52-2 and 52-3, indicate that the holes reached the bed. Only borehole 52-3 remained connected to the basal water system for the remainder of the season, as evidenced by the variable water level in this hole. Boreholes 52-1 and 52-2 lost connection and filled with water within 1-2 weeks of drilling.

Two boreholes were drilled at site 59. The small size of the serac top which served as the drill site required that the holes be only 5 meters apart at the surface. Both of these holes reached the bed at a depth of 526 to 527 m and remained connected with the basal water system for the remaining period of the study as evidenced by continually fluctuating water levels. Turbid water flowed up the lower 200 m of borehole 59-2, exiting into an internal conduit [Humphrey et al., in preparation]. Successful sampling of bottom materials [Humphrey et al., in preparation] also indicated that this hole had reached the bed.

**Basal Conditions**

Basal conditions were investigated with sampling and penetrating equipment in holes 52-2, 52-3 and 59-2. The thickness of basal debris was at least 0.5 m at the bottom of hole 52-3 and about 0.1 m below hole 59-2 [Humphrey et al., in preparation]. Humphrey has calculated a maximum viscosity for the debris based on the amount of

bending in a drill stem which was stuck at the bed for three days in borehole 52-3 [Humphrey et al., in preparation].

**Basal Water Pressure**

Basal water pressure, as measured by the height of water in the boreholes, was recorded with pressure transducers in all holes. The record from hole 52-3 and a combination of the records from holes 59-1 and 59-2, plotted as distance to water level below the ice surface, are presented in Figure 4.3 *b*.

Before a pressure transducer was installed in a hole, water pressure was measured by hand, using a float on a string which was lowered over a measuring wheel. The float measurements, which were made during and immediately after drilling, are shown as the irregularly spaced points on the left side of Figure 4.3 *b*.

The level of the water in a borehole which is connected to the bed can be taken as a measure of the basal water pressure (basal water pressure=$\rho_w g h$, where $h$ is the height that water stands in the borehole). In Figure 4.3 *b* water levels near the surface represent higher basal water pressures than water levels at greater depths.

The basal water pressures measured at the two sites were high. This was expected from the high flow velocity: high velocities on Variegated Glacier during surge and during the passage of mini-surges are correlated with water pressures that are a large fraction of the overburden, or floatation, pressure. The water pressures measured on Columbia Glacier are somewhat less variable than the pressures measured during surge on Variegated Glacier [Kamb et al., 1985]. Records from both sites on Columbia Glacier show temporary excursions above floatation and drops to lower values, but the range of variation is within a few percent of the floatation pressure, except at site 59 after J.D. 234, when the pressure dropped 10 percent below the floatation pressure.

The floatation level is at a height $h_f = (\rho_i/\rho_w)h_i$ where $\rho_i$ is the column-mean ice density and $h_i$ is the ice thickness at the site. Accurate determination of the depth to the floatation level in a borehole is complicated by the difficulty of determining the average

elevation of the ice surface in the vicinity of the borehole due to the heavily crevassed nature of the glacier. Water levels near the floatation level will correspond to depths below the ice surface of $h_{ice}$-$h_f$, which has a value of 97 m for site 52 and 53 m for site 59 (assuming $\rho_i$=0.9).

Water was heard flowing into borehole 52-3. The water may have come from the perched water table held in water filled crevasses in a region which extended upglacier from site 52 several kilometers to the north and northeast. Water flow was also audible in the holes at site 59. The flow of water into these holes may have been responsible for keeping them open and connected during the period of measurement.

## Borehole Results

The value of the water level measurements as indicators of pressure in the basal water system is demonstrated in part by the records themselves. The record from hole 52-3 maintains a level of 95 ± 8 meters from the end of drilling on day 196 until the drop which followed velocity event 4 on day 218, except for the sharp excursion on day 208, which was related to velocity event 1. This twenty day long period of consistent water level, in spite of inflow into the hole near the surface, in spite of the numerous small variations in the level, and in spite of the fact that the base of the hole traveled over more than 80 meters of bed during this time, suggests that this water level was representative of the basal water pressure in this region.

The lowest water level in hole 52-1 was 20 m lower than the low levels observed simultaneously in hole 52-3 and may have represented the pressure in the system closer to a main drainage conduit. As with any borehole, the level in hole 52-3 may be only locally representative; it is possible that the level is somewhat higher than the level representing the average value for the area. If the inflow into the hole was nearly constant, as might be expected from a large water-filled crevasse system, then the water level in the hole would be elevated a set amount by any constant impedance between the

hole and the basal system, but the variations in water level would still be a reflection of changes in the pressure of the basal system [Engelhardt, 1978]. The high frequency variations in the record from hole 52-3 between days 209 and 229 may be in part due to variations in the impedance of the connection between the borehole and the basal system, due perhaps to the ice sliding over obstacles. A similar pattern of high frequency variation is not seen in the records from site 59, possibly because of a less restricted connection to the basal water system at this site or a lower flux of water into the hole from the surface.

Fluctuations in basal water pressure which last for several days or more appear to be the result of periods of elevated water input to the glacier. The response to an increase in input rate is a small rise in pressure followed by a larger drop in pressure as the input rate returns to a normal level. In some instances the pressure recovers to pre-event levels. This behavior is seen at both drill sites in response to the input related to velocity event 2, at site 52 in response to event 3, and at site 59 in response to event 4. Exceptions to this behavior are the response at both sites to event 1 and at site 59 to event 3, when no drop was seen, and the response at site 52 to event 4, when no rise was visible before the drop.

Only the first velocity event is accompanied by a strong rise in water pressure. This water pressure rise, which was only observed in borehole 52-3, occurs as a double peak 3-6 hours after the peak in velocity at this site (Figure 4.3 *a* and *b*). In general, large changes in water pressure do not accompany velocity events on Columbia Glacier. The lack of a strong correlation between water pressure and velocity may be the result of the consistently high water pressure, which is so close to the floatation level that only a small further increase in pressure is sufficient to have a marked influence on sliding velocity. As just mentioned above, there is a hint in the pressure records of a slight increase at the start of the velocity events, but it is difficult to quantify because of the amplitude of the shorter term variations in the record.

Diurnal fluctuations in the water pressure developed at both sites by the end of the season. At site 52 the variations were smooth and closely matched the sliding velocity variations, while at site 59 the diurnal peak was sharper and occurred about six hours before the daily peak in sliding velocity.

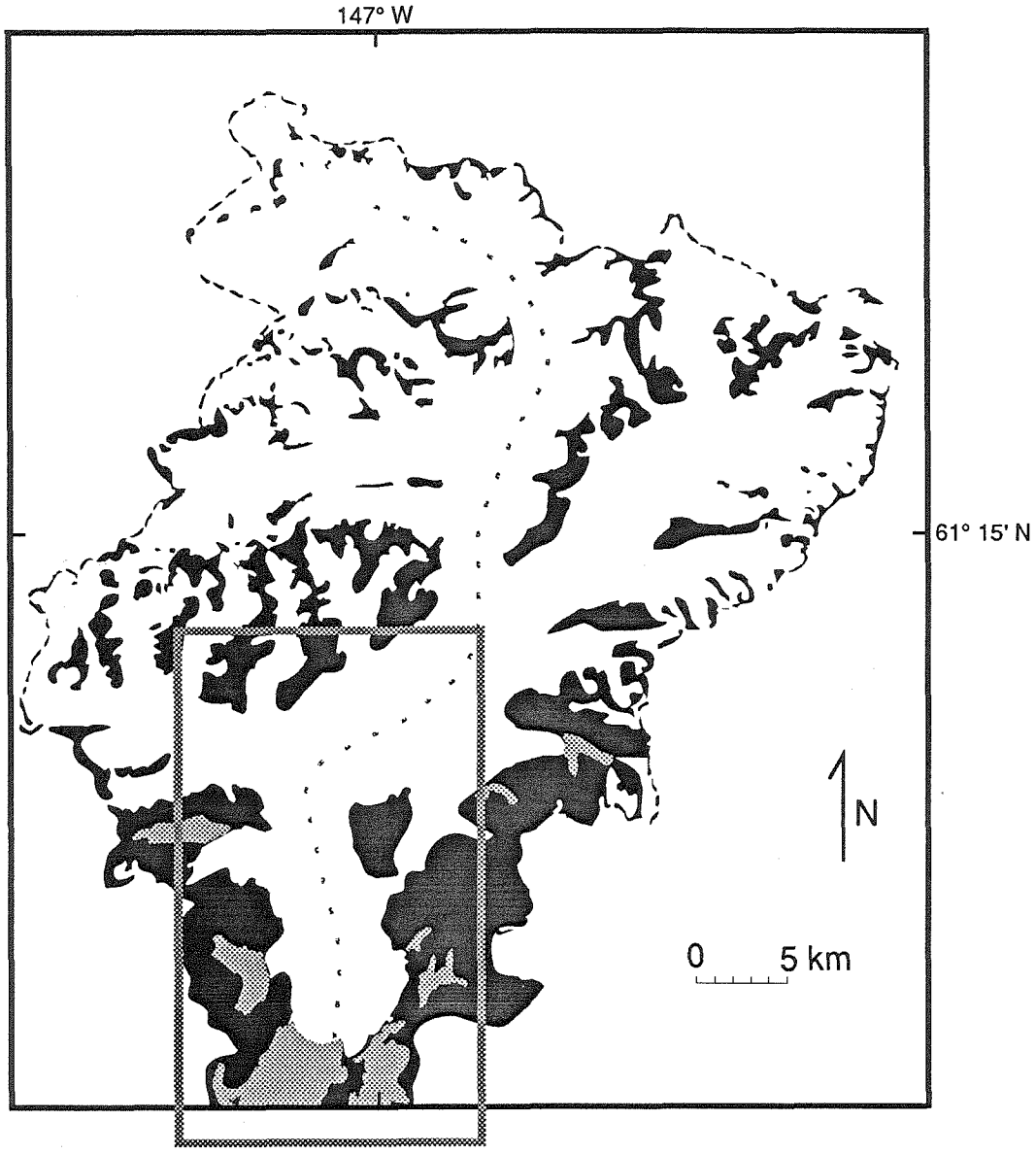


**Figure 4.1** Columbia Glacier and drainage basin (after Meier et al. 1985). Ice marginal lakes and ocean are in grey, bedrock in black. Dashed line is approximate centerline of main channel. Grey rectangle is region convered by Figure 4.2

**Figure 4.2** Map of Lower Columbia Glacier showing 1987 surveying and drilling sites (after Meier et al., 1985). Four dated terminus positions are shown. Crest of moraine shoal corresponds approximately to 1974 terminus. Centerline coordinate of main glacier in "Km" from head. Ice contours from 1974 (contour interval 50 m, 50 m contour not shown)

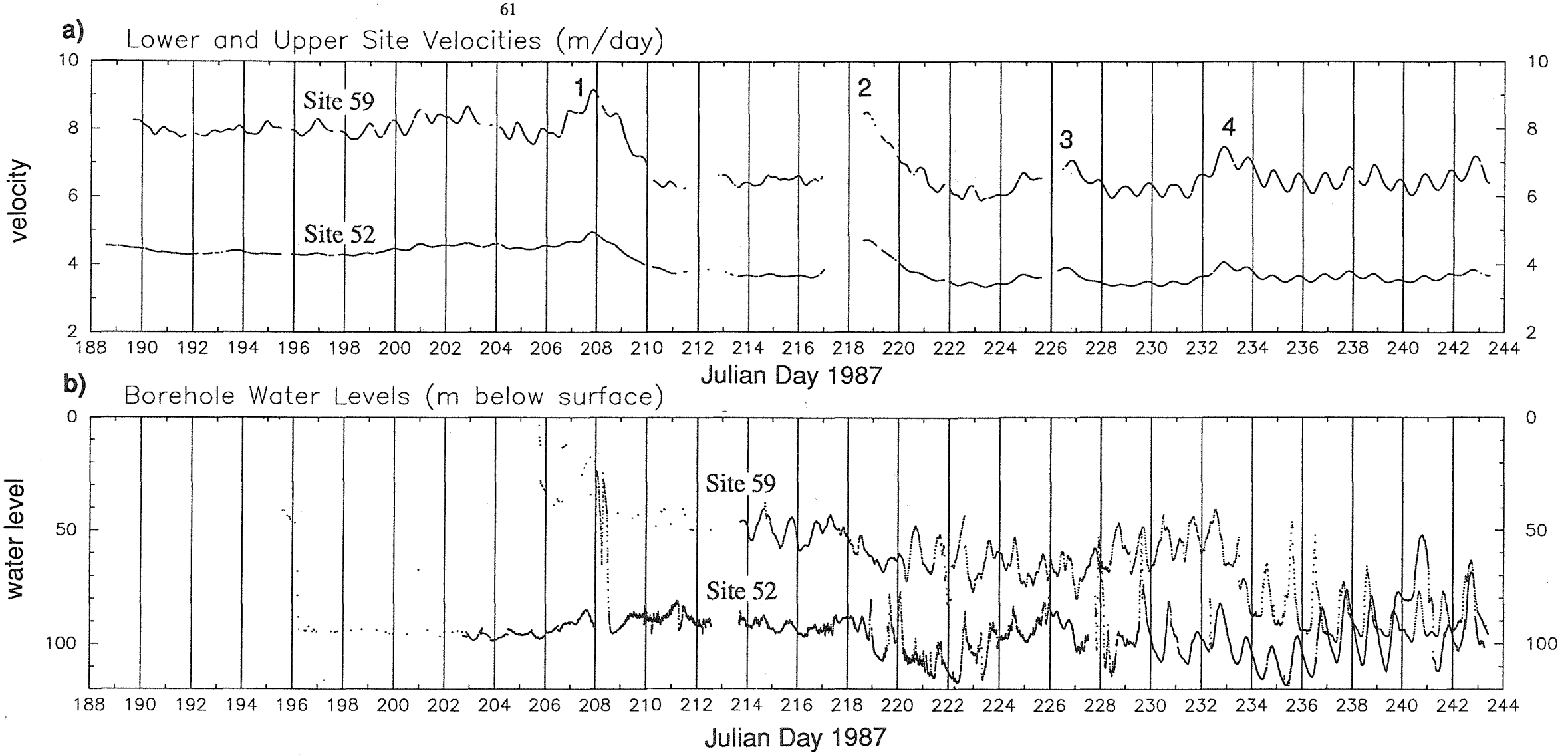


**Figure 4.3** Columbia Glacier surface velocity and basal water pressure, summer 1987. Velocity events designated by number. Velocity data kindly provided by Meier, INSTAAR.

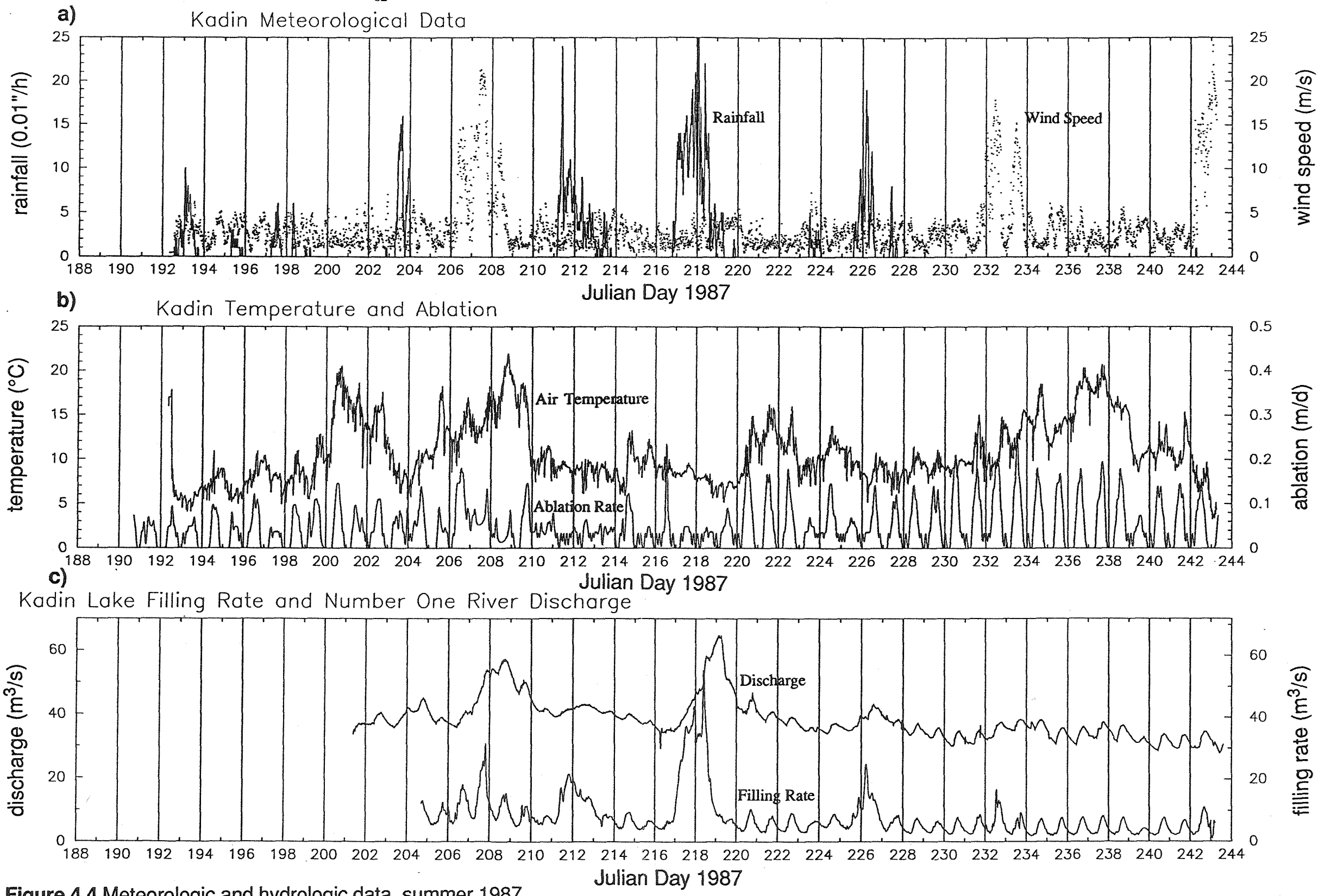


**Figure 4.4** Meteorologic and hydrologic data, summer 1987.
Data kindly provided by Mark Meier and coworkers, INSTAAR.

# Chapter 5

# The Role of Water in The Velocity Variations of Columbia Glacier

## Evolution of the Basal Water System

The data from the 1987 Columbia Glacier Project (Chapter 4) present a complicated picture of the behavior of a large tidewater glacier. The glacier responds to forcings which vary on time scales from one day to several months. The nature of these responses is highly varied and time dependent; the behavior of the glacier evolved during the period of the study. Major changes in behavior occurred at the same time as the increases in the water input rate associated with the velocity events.

It appears that several of these periods of elevated input rate altered the subsequent behavior of the hydrologic system of the glacier. The first period of elevated input (event 1, Figures 4.3 and 4.4) was followed by a drop in sliding velocity. The period of elevated input associated with event 4 was followed by a pronounced drop in water pressure at site 59 and a change in the character of the diurnal pressure oscillations at both sites. These changes in the behavior of the system were most likely the result of the increased water input; it may be that the increases in input rate are the major force behind changes in the basal system.

In the previous section I identified four velocity events in the records from the 1987 field season. It was demonstrated that these large speed ups did not, in general, have a coincident strong peak in water pressure. In the next section I investigate another possible role of water in the determination of sliding velocity.

## Changes in Water Storage

When the ice velocity is compared with the records for water input and discharge, it is apparent that although there is a strong correlation among all three, the input events typically occur slightly before the corresponding velocity peaks. A similar relation holds

between the velocity records and the discharge record of the Number One River, with the discharge peak following the peak in velocity. This timing suggests that it may be an increase in volume of retained water that is responsible for the increased velocity of the ice. This correspondence was also noted by Krimmel and Meier [1990].

In order to calculate changes in the volume of water stored in the glacier, we need to relate records of input and output to each other. The data contain two independent measures which can be used to estimate the rate of water input to the glacier, and one measure of output. The volume of stored water will be calculated in two ways, using an independent estimate of the water input to the glacier for each calculation.

Water input to the lower reach of the glacier has three sources. The first source is the daily ablation of firn and ice which is due to solar radiation and the air temperature. The other two sources are rain storms and periods of warm, ablating winds, which produced the pulses of extra water responsible for the velocity events. Both of these processes are seen in the meteorological records, but, as mentioned before, the increased ablation due to wind storms was not recorded properly by the ablatographs. One proxy record of the rate of water input to the glacier is the filling record for Kadin Lake. A second independent input record can be derived from the meteorological data.

As was mentioned in the last chapter, the discharge from the main glacier cannot be measured because the outlet is below sea level. This requires that the discharge of the Number One River be used as a proxy for the output.

### Estimated Storage Using Kadin Lake Filling Rate

For the first calculation of change in the volume of water stored in the glacier, the filling rate of Kadin Lake will be used as a proxy for the input of water to the glacier. The value of the lake as a recorder of melt water production and precipitation was established by Dan Stone [1988]. Using the surface area of the lake (5.4 $km^2$) and the area of the drainage basin (36 $km^2$) as determined by Stone, the lake filling rate may be expressed as an input flux per square meter of drainage area. This record is used as an estimate of the

rate of water input per square meter of the ice surface. In the following calculation, the Number One River discharge will be related to this input record. A diagrammatic illustration of the procedure followed in the calculation is shown in Figure 5.1.

Both input and output records contain a background component, but the sources of the backgrounds are different. The background component of the discharge is from points far enough upglacier that variations with time have been damped out, and also from the outflow of water from lakes in the drainage basin. In this calculation we are interested only in the output from the area of the glacier close enough to the outlet to contribute to the variable part of the discharge. While this area cannot be directly determined from the data, the effects of the upglacier flux on the calculation can be reduced by subtracting a constant flux (30.5 $m^3/s$, estimated from Figure 5.3) from the discharge. The constant part of the Kadin Lake filling rate, which could be attributed to a small amount of groundwater discharge or percolation through the firn, or other runoff delay is also removed.

The discharge is scaled to the input record by integral normalization over the period from J.D. 217.0 to J.D. 243.0. The normalization is done by determining, using numerical integration, the total volumes of water represented in the input and discharge records over this period, and then multiplying the discharge by the ratio of the input volume to the output volume. The time interval chosen for the normalization is a period which has approximately the same ice velocity at its beginning and end, and which starts immediately before input event 2 and ends eight days after event 4. This interval was chosen because the calculation is being done to determine if there is a storage volume effect on velocity, so any period likely to contain a net change in volume, as indicated by different velocities at the beginning and end, was avoided. Other intervals which meet this criterion could have been used.

The change with time of the volume of stored water is now calculated by numerical integration of the difference between the scaled input and output flux records

developed above. The resulting curve of change in storage volume is shown as the curve labeled "storage calculation 1" in Figure 5.4 and as the heavy solid curve in Figure 5.7 *c*.

The fluctuations in storage as calculated above have a marked resemblance to the large amplitude changes in the velocity records. Figure 5.7 *c* shows the synchronous nature of the variations in storage and velocity. The prominent features which match well are the large drop in velocity following event 1 and the peak and tail of event 2. There is only a weak signal in the storage curve for the speed-up in event 1. The general correspondence of storage volume and velocity over the 40 days of the record suggests that there is a consistent mechanism involved in the determination of sliding velocity and that its functional dependence on water volume is unaffected by the evolution in the basal system over the period of measurement.

**Estimated Storage Using Meteorological Inputs**

The calculation of stored water volume is here repeated with an independent input function derived from meteorological variables in order to check the result from the last section. The input from rain storms is taken directly from rain gage data, while ablation due to large wind storms is calculated from an estimation of boundary layer turbulent heat transfer. The heat transfer calculation is described in Appendix 2. A non-dimensionalized characteristic distance in this theory, the ratio of the height (above the ground surface) at which the wind speed and temperature measurements were made to a characteristic distance representing surface roughness, is poorly constrained, and so the calculated amount of ablation due to turbulent heat transfer is scaled by a constant. The value of the constant is chosen so that the amount of water input during event 4 exceeds the volume of the extra discharge during this event. This choice is made for the following reason. The storage calculation in the last section showed a drop in storage following event 1. This drop is the result of the difference between the amount of ablation in the Kadin Basin from the wind storm and the size of the discharge flux. If the Kadin Lake record under-represented the amount of ablation due to wind, this could be

responsible for the drop in the storage curve. The scaling used in the present calculation is intended to prevent an under-estimation of the ablation due to the wind storms, providing a check on the validity of the drop shown in the first calculation.

The second storage calculation is diagramed in Figure 5.2. A constant background is subtracted from the Gate discharge record, as in the first calculation. The rain and wind ablation input record has a background value of 0, so no modification is necessary. The discharge is normalized to the input record and the volume of water stored is calculated as before. This calculation is called "storage calculation 2 *a*" and its result is shown in Figure 5.4 as the curve labelled with this name.

The curves from storage calculations 1 and 2 *a* are compared in Figure 5.4. Curve 2 *a* drops constantly over the interval J.D. 204-225, except for peaks associated with the events. The curve from calculation 1 drops after the first event, but then levels off. The discrepancy between these two curves can be understood by comparing the input records for the two calculations; these records are shown in Figure 5.5 The Kadin Lake filling record (Figure 5.5 *a*) has a background level of ~0.01 m/d on J.D. 205; the background drops to 0.005 m/d by J.D. 227 and then remains constant. The drop in background input rate probably reflects the gradual disappearance of snow from the hillsides in the lake's drainage basin. The Gate discharge record shows a similar drop in background level over the period of measurement (Figure 5.3). In calculation 1, the drops in the backgrounds of the input and discharge records compensate each other; in calculation 2 *a*, with the lack of a background in the input record, the extra discharge in the first half of the Gate record results in the downward trend in the storage curve.

The second storage calculation is repeated here as calculation 2 *b*, using a discharge record that has had the tapered background removed (Figure 5.3). The linear trend of the background was chosen to match the low discharge values before the first three velocity events and to match the average discharge near the end of the record. The

result from this calculation is shown in Figure 5.4 (curve labelled "storage calculation 2 *b*") and in Figure 5.7 *c* (dashed curve) in comparison with the site 52 velocity record.

The drop in water volume following event 1 is present in the results from the second calculation, even though the amount of ablation by wind more than balanced the discharge during event 4. Based on the argument given above, this supports the existence of the drop after event 1 as an actual feature of the storage.

## Interpretation of Calculated Storage

The correspondence of the results of the calculations 1 and 2 *b* is good; the match in timing and magnitude of the drop after event 1 and the excursion related to event 2 can be seen in detail in Figure 5.7 *c*. The scale of water volume (relative to an arbitrary datum) in this figure came from the scaling of the filling rate of Kadin Lake to the area of the Kadin drainage basin, for calculation 1, and from the rain gage data, for calculation 2. The normalizations of output to input carried out in the calculations did not effect the scaling of the input functions.

The value of the storage curves, Kadin Lake filling rate, and Number One River discharge as predictors of velocity can be assessed by comparing the three plots in Figure 5.7. In each of these plots the velocity of site 52 is included for reference. As was mentioned at the start of this section, the discharge, lake filling rate, and velocity are all correlated, but they are out of phase with one another. The storage curves are in phase with the velocity curve.

The value of the storage volume curve as a predictor of velocity is graphically demonstrated in the cross-correlation diagram in Figure 5.6. The curves in this figure are the correlation coefficients at different phase shifts for the pairs of records shown in Figure 5.7. Before the cross-correlation calculation a 24 hour moving average was applied to the velocity, lake filling rate, and discharge records to remove the diurnal signal, which would otherwise produce a double peak with a total width of one day,

making the phase shifts associated with speed-up events harder to see. While the peak correlation coefficients for discharge and velocity and for Kadin filling rate and velocity are strong (0.75 for discharge and 0.68 for input), the peak correlations between these pairs are for time shifts of half a day forward and half a day backward, respectively. The correlation between storage volume and velocity is stronger (0.92 for calculation 1, 0.94 for calculation 2 *b*) and the peaks in correlation are at time shifts near 0, representing variations that are essentially in phase.

The large variations in sliding velocity thus appear to be a direct result of changes in the volume of water retained under the ice. The direct relation between sliding velocity and the volume of water at the bed is explained in a qualitative sense below.

As was already noted, the pressure records from Columbia Glacier do not show large fluctuations in association with the velocity events. It has also noted that the pressures are constantly near floatation; at this level large changes may not be required to modify the velocity. From these observations and the calculated stored water volume of this section, the following picture of the roles of water pressure and water volume can be suggested:

As the rate of water input from the surface begins to increase, a slight rise in pressure causes the enlargement of cavities, increasing the volume of water held in the basal system. These cavities remain enlarged until the drainage system which transports water to the terminus begins to adjust to the new water input rate, at which time the extra water starts to drain and the cavities begin to reduce in size. If the modification to the drainage system is substantial, the local water pressure may fall below pre-event levels as the water is drained, and may remain low for a few days until the flux through the drainage system drops back to pre-event levels. In this discussion the opening of new cavities is not considered because the high sliding speed and high water pressure would seem to make the prior existence of numerous cavities likely.

The way a velocity variation results from an increase in the volume of cavities (and thus a decrease in the area of contact between the ice and the bed) is that the glacier slides faster so that the resistance generated by flow of ice around the remaining undrowned bed roughness elements remains equal to the gravitationally imposed basal shear stress. In this model, the slowdown which followed event 1 is the result of a loss of water from the basal system, causing a rougher bed and larger area of ice/bed contact, producing a lower velocity. The volume involved in this loss represents ~0.1 m loss of cavity height averaged over the width of the glacier, according to the 0.1 m decrease in water storage indicated in Figure 5.7 *c*.

## Comparison With Other Observations and Theories

Several authors have suggested a causal link between increased cavity size and higher sliding velocity. Weertman and Lliboutry were the first to propose theoretical models of sliding involving cavitation [Weertman, 1979; Lliboutry, 1968]. Iken [1981] modeled the effect of water pressure and cavitation on sliding velocity. Mayo [1986 presentation at Chapman conference on fast glacier flow, Whistler, B. C.] proposed for the variation of velocity on Columbia Glacier due to rainfall input an explanation which attributed the increase in speed to cavitation produced by high water pressures brought about by the increase in local input rate. At the time the basal water pressure had not been measured. He also attributed the slowdown over the summer to the opening of a drainage system causing water in cavities at the bed to drain.

The storage of water in glaciers has been proposed to explain field observations by several workers. For the drainage basin of South Cascade Glacier, Tangborn et al. [1975] attributed a discrepancy between the estimated input volume (melt plus rainwater) and the integrated discharge to the release of water stored in the glacier. In this case no reference was made to increased sliding velocity due to the stored water, and no surface

uplift was detected by surveying (which is curious, as the volume of stored water corresponded to 1.4 meters of water distributed evenly under the ice).

As was mentioned in Chapter 2, Iken et al. [1983] attributed the uplift of Unteraargletscher at the beginning of the melt season to the opening of water filled cavities at the bed. The maximum measured uplift was 0.6 m, and was associated with an increase in velocity from 5 cm/d to 15 cm/d.

Kamb et al. [1985] attribute the surge of Variegated Glacier to the retention of water in the basal water system; several slowdowns during the surge corresponded to floods at the terminus. As was mentioned in Chapter 1, Humphrey et al. [1986] suggested the possibility of an increased stored water volume during mini-surges; this is also indicated by surface uplift ([Kamb and Engelhardt, 1987] and Chapter 3), and was associated with high sliding velocities. A connection between retained water and high sliding velocity was thus indicated for both the surge and mini-surges of Variegated Glacier, but in these cases a large increase in water pressure accompanied the events, which was not the case on Columbia Glacier.

The Columbia Glacier data and the calculated storage curves demonstrate a relation between water storage and sliding velocity in a closely sampled time series over a 40 day interval. This demonstration provides a new constraint for models of basal sliding in fast moving glaciers.

## A Model Of the Basal Water System of Columbia Glacier

The storage arguments of the last section suggest the existence of a network of cavities under Columbia Glacier. The extensive surface crevassing and lack of substantial amounts of surface water below the ice fall at Km 54 suggests that water collects locally and reaches the bed locally in this region. The flux of water reaching the bed in a small area would not be sufficient to maintain a tunnel large enough to survive

the constant advection over a rough bed. The water reaching the bed locally must enter the cavity system, if small tunnels are not in existence.

In spite of the evidence for a cavity system, there are arguments against such a system being the only path for water flow under the glacier. The large discharge from the glacier, the localized upwelling frequently seen at the terminus, and the pattern of seasonal variation in velocity all suggest that the main water path along the glacier is a tunnel system as explained below.

Kamb [1987] and Walder [1986] have each argued that in a system of linked cavities the hydraulic gradient is an increasing function of the flux. A tunnel system is much more efficient at carrying a large flux; the hydraulic gradient of a tunnel in steady state is proportional to $Q^{-2/11}$ [Röthlisberger, 1972]. From this standpoint, the large discharge from Columbia Glacier during the melt season (>100 $m^3$/sec) would best be handled by a tunnel system.

Aerial photography and observation [USGS] of the terminus of the glacier frequently indicates the presence of a zone of upwelling in the water in front of the ice cliff. This region is clear of brash ice and the upwelling water is turbid (charged with glacial flour). The upwelling changes position along the front and is not always present, but it does indicate that flow is at times localized as it exits the glacier.

The pattern of seasonal variation in velocity over all but the last five kilometers of the glacier is in a general sense negatively correlated with discharge. The ice moves fastest during late winter and early melt season, and slows over the summer [Krimmel and Meier, 1990]. If velocity were determined by water pressure, this pattern of variation would argue for the controlling influence of a tunnel system, which in steady state has an inverse relationship between flux and water pressure [Röthlisberger, 1972]. A system of linked cavities would have to enlarge to increase the discharge, but according to the last section this would lead to higher velocities, and thus a positive correlation between velocity and discharge.

These features all argue for the existence of a tunnel system.

A straightforward way of incorporating the need for both cavity-system-like behavior and tunnel-system-like behavior in a basal water system is to have a hybrid system composed of coexisting sets of linked cavities and tunnels. I will consider the basic form of a hybrid cavity/tunnel system below.

**The Cavity/Tunnel System**

Cavities, which form on the downstream side of bed roughness features, carry the distributed input once it reaches the bed. Tunnels of a size comparable to the cavities, carrying the local input, would be destroyed by advection over the rough bed, as was mentioned earlier. The only tunnels which could survive in this system would have to be large enough to avoid this fate.

Water flow in the cavity system would be controlled by the local hydraulic gradient. In a basal water system composed of either cavities or tunnels the longitudinal hydraulic gradient is approximately parallel to the surface slope of the ice for all but a few kilometers near the terminus. In a cavity/tunnel system, tunnels would be at a lower pressure than the linked cavities in the regions between the tunnels. The transverse hydraulic gradient in the inter-tunnel region would be much steeper than the longitudinal gradient, which is tied to surface slope as mentioned above. The dominant direction of water flow in the cavities would be toward the nearest tunnel.

Bindschadler [1983] calculated transverse profiles of hydraulic head based on small tunnels carrying a local transverse flux to a main tunnel in the center of a glacier occupying a parabolic channel. In his Figure 5 [Bindschadler, 1983] the hydraulic head rises rapidly away from the central tunnel, becoming nearly parallel with the surface within the first 100 meters. The dependence of the slope of the phreatic surface in the transverse ($y$) direction can be written (after Röthlisberger [1972, Equation. 11]):

$$\frac{\partial h}{\partial y} \propto Q^{-\frac{2}{11}} P_e^{\frac{24}{11}} \tag{5.1}$$

This assumes a horizontal bed and ice surface and $n$=3.

Thus the surface rises rapidly near the tunnel, where $P_e$ is largest, and flattens out as $P_e$ approaches 0 (floatation).

A sketch of the hydraulic head distribution in a cross-section of a cavity/tunnel system is shown in Figure 5.8. In this sketch the rapid rise of the phreatic surface near the tunnel is shown. It does not have the same form as that calculated by Bindschadler, because a cavity system has a different $Q$-$P_e$-$\partial h/\partial y$ relation than a tunnel system. An approximation to the behavior of the hydraulic head in a cavity system can be made from Kamb [1987], assuming a system with a constant discharge, sliding velocity, and an even distribution of orifices of the same size connecting larger cavities. The equivalent relation to Equation 5.1, from Kamb, [1987, Equation 18] (for a step orifice) is

$$\frac{\partial h}{\partial y} \propto Q^2 P_e \tag{5.2}$$

Here the dependence on effective pressure is not as strong as in Equation 1, but the effect of effective pressure is to make the gradient large near the central tunnel, dropping to 0 as the floatation level is approached. In Equation 5.2 the hydraulic gradient depends on the square of the flux. The flux in a system with distributed input will increase as the tunnel is approached, requiring the hydraulic gradient to be steepest at the tunnel. Thus the phreatic surface will rise steeply near the tunnel, rapidly approaching a level of high pressure and becoming parallel with the ice surface, as illustrated in Figure 5.8. The strong gradient near the tunnel is essential to the model, as it represents the cavity system providing a resistance to the flow of water into the tunnel system. If there were no resistance to flow in the cavity system the bed would be at the pressure of the tunnel system at steady state, which is much lower than the pressures required to maintain the high velocity and the large distributed cavity system. The resistance to flow in the cavity system provides a limit on the rate of water input to the tunnel, allowing the two systems to coexist.

One interesting aspect of the cavity/tunnel system is that a large fraction of the bed is covered by the cavity system, and the influence of tunnels on the pressures in this system is restricted to a local region near the tunnel. This makes it reasonable to expect that most boreholes drilled in random locations will sample the high water pressures of the cavity system. The consistently high water pressures found in the boreholes on Columbia may have been representative of the pressure distribution, in a statistical sense.

## Velocity Variations and the Cavity/Tunnel System

### *Seasonal Fluctuations in Velocity*

The cavity/tunnel system produces seasonal fluctuations in velocity in response to the seasonal changes in discharge. As already stated, the seasonal fluctuations are suggestive of an inverse relation between water pressure and discharge. This behavior is characteristic of the tunnel system. Schematic representations of the pressure distribution in a cross-section of the glacier in both winter and summer are shown in Figure 5.8.

### *Reaction of the Cavity/Tunnel System to Storm Input*

The reaction of the cavity/tunnel system to extra water input from a storm or increased ablation involves a rapid expansion of the cavities in response to an increase in pressure in the conduits which carry the distributed input to the bed, and a slow enlargement of the tunnel system, which has been thrown out of balance by the pressure increase in the cavity system. As the tunnel enlarges in response to the increased pressure, the pressure is lowered and the cavities shrink. The variation in cavity size (storage volume) leads to the observed velocity variation.

The tunnel will not respond to the increased input of water until the water pressure in the cavity system near the tunnel rises. The water pressure near the tunnel rises as the volume of water in the cavity system increases. The response of a tunnel to a distributed increase in water input will be investigated numerically in the next section.

## The Response of a Tunnel to an Increase in Distributed Input

The response of a tunnel system to an increase in distributed input, as would be expected from a rainstorm, is not the same as the response seen in the water pulse propagation problem in Chapter 3. In the case considered in Chapter 3, the localized increase in water input changed the hydraulic gradient in the system, as well as raising the pressure. The change in hydraulic gradient led to a local increase in flux and melting, and to propagation of the water pulse. In the present case, with an increase in distributed input, the phreatic surface will rise uniformly over most of the glacier, changing the hydraulic gradient significantly only near the terminus. The response of the tunnel system upglacier from the terminus is dependent on the increased water pressure slowing ice flow closure of the tunnel, allowing what had been the steady state melting rate to begin enlarging the tunnel.

### Tunnel Model Response

The response of a tunnel in a cavity/tunnel system to an increase in distributed input is investigated numerically with the techniques described in Chapter 3 (Equations 3.1 - 3.11). In order to simulate the effect of water storage in a cavity system, the model uses the storage function

$$V = \frac{w_e \nu}{h_\infty - h} \tag{5.3}$$

This relation is similar to the conductivity relation Equation 3.18; both equations are intended to approximate the effect of the expansion of cavities as the floatation level is approached.

In the simulation described here, $h_i$=700 m, $w_e$=5 km, $\beta$=0.02, and the distributed input $I$=0.15 m/d for the first two days, dropping to 0.05 m/d for the remainder of the run. The initial distribution of $h$ and $S$ are calculated using the technique of Appendix 1, for $I$=0.05 m/d. The response of a tunnel to the increase in pressure caused by this two day

long increase in input rate is illustrated by a model run shown in Figures 5.9 and 5.10. Figure 5.9 shows the daily value of $h$ at 12 points on the glacier over the 20 day run and Figure 5.10 gives the value of $S$ at the same points.

In this run it takes about 5 days after the end of the elevated input before water pressures drop below pre-event levels and another 10 days before they recover. The tunnel cross-sectional area ($S$) enlarges and then drops below pre-event levels, recovering toward the end of the run.

This model is a simple approximation of a cavity/tunnel system. The actual effect of water storage in the cavity part of the system and the hydraulic interaction of the cavities and the tunnel must be more complicated than is implied by Equation 5.3. The rate of response of the tunnel system depends on the rate of pressure change at the tunnel, which is dependent on the volume of water stored relative to the pressure change. The detailed timing and behavior in this simulation can only be as good a representation as Equation 5.3 is of the true water storage relation. The run is used here to demonstrate that the tunnel in such a system will react, on a time scale of days, to an increase in water input rate.

The oscillation in $h$ shown in Figure 5.9, which appears to be growing with time for the curves in the reach from Km 50 to the terminus (Km 60), is not increasing as rapidly with time for the curves at Km 30 and Km 40. The increase in the amplitude with time at the downglacier points is due to the rapid flow of the extra water (from the raised input) out of the upper glacier, due to the initial enlargement of the tunnel (this effect is similar to the drawdown of water in the tail of the propagating disturbance in Figure 3.2 *a* that leads to the increasing amplitude at points downglacier). The rate that the water is replenished is slower after the end of the extra input, so the oscillation which is set up in this system will change if the system is followed further in time. The effect of the second cycle of increase in $h$ on the upglacier part of the tunnel is not as pronounced as the initial enlargement caused by the increased input; this may reflect a damping of the oscillation.

## Variation of $P_e$ in a Tidewater Glacier and Related Calving Behavior

Bindschadler [1983] used a tunnel model to calculate longitudinal water pressure distributions in several glaciers. For Columbia Glacier, he used a distributed input and longitudinal surface and bed profiles for the calculation, which integrated the pressure from the terminus in the manner of Röthlisberger. His results suggested very low effective pressures in the lower reach which he believed were responsible for the rapid sliding in this reach.

In this section I will investigate the influence of seasonal variations in the longitudinal pressure distribution on sliding velocity. The motivation for this investigation is based on a simple consequence of the inverse velocity-pressure relation of a steady state tunnel system.

The pressure in a tunnel in a tidewater glacier is fixed at sea level at the terminus; upglacier it will by inversely related to the flux. A sketch of the summer and winter pressure distributions is shown in Figure 5.11. If the sliding velocity is controlled by pressure, the difference in velocity between the terminus and a point upglacier will be larger in the summer than in the winter. This sliding velocity distribution will cause higher rates of extension (and thinning) during the summer. As the ice is thinned, the effective pressure at the bed is reduced, resulting in more rapid sliding and increasing the rate of thinning. This situation may be responsible for the pulse of velocity and calving at the end of the melt season.

To place this idea in more quantitative terms, I will model the effect of the effective pressure distribution on basal sliding, taking into account the role of longitudinal gradients in sliding velocity in producing extension and thinning of the ice. In this model a glacier with a given initial ice profile is followed as it slides over the bed and is thickened or thinned by gradients in the sliding velocity. The model is cast in simple terms in order to emphasize the role of the distribution of effective pressure:

ablation and shear flow of the ice are neglected and the ice is required to obey continuity, which determines the changes in ice thickness due to extension or compression imposed by basal sliding over a bed which is horizontal.

For each time step the technique described in Appendix 1 is used to calculate the water pressure distribution using the current ice thickness distribution and the appropriate flux for either summer of winter. The pressure and ice thickness are used to calculate the sliding velocity, which is then used to determine the amount of translation and deformation of the ice that will take place during that time step.

This model uses a sliding law with a linear dependence on basal shear stress ($\tau_b$) and an inverse relation to $P_e$:

$$v_s = \frac{c\,\tau_b}{P_e + P_0} = \frac{-ch_i \dfrac{\partial h_i}{\partial x}}{\dfrac{\rho_w}{\rho_i}(h_\infty - h) + \dfrac{P_0}{\rho_i g}} \tag{5.4}$$

In this relation $v_s$ is the sliding velocity, $P_0$ is a factor which allows for a (constant) drag due to lateral shear (preventing an unrestrained increase in velocity as $P_e \rightarrow 0$), and $c$ is a constant with dimensions of velocity. $c$ is chosen to produce realistic sliding speeds; in this run $c$ = 2 m/day. Equation 5.4 incorporates the contributions which may change during a simulation (ice thickness, surface slope, and effective pressure) in a simple fashion. Many sliding laws have been proposed in the literature; in general they have functional dependences similar to Equation 5.4, most taking $\tau_b$ to a power between 1 and 3 and $P_e$ to a power between -1 and -3 [eg. Kamb, 1987; Bindschadler, 1983; Budd et al., 1979]. The $P_0$ term is unique to the formulation used here. We are interested in variations in the sliding velocity brought about by an imposed longitudinal variation of $P_e$ (due to the seasonal input flux); the use of a simple form for the sliding relation will allow the results to be interpreted easily.

For this model only the last 14 km immediately above the terminus is considered. The bed is horizontal and the ice thins linearly from 540 m at Km 50 to 380 m at Km 64

(the terminus) (the Km coordinate system is used to provide a comparison with Columbia Glacier). The ice thickness is represented on a grid initially spaced at 50 meters in the longitudinal direction. The deforming ice is followed by the grid, with sliding causing translation of the grid and gradients in sliding velocity changing the ice thickness at the grid points. The water depth at the terminus is 300 m. For calculation of rate of water input, the glacier is taken to be 5 km wide.

Two simulations, each representing 80 days, are shown in Figures 5.12 and 5.13. The winter simulation (Figures 5.12 *b* and 5.13) uses a distributed input of 0.0005 m/day, intended to represent the water input to the bed during the winter. In this run the glacier advances steadily, the ice thickness at each location increasing because of the movement of the longitudinally tapered glacier. The velocity varies over the glacier, being lowest at the terminus and increasing with the increasing ice thickness upglacier. With this velocity distribution, the model glacier advances and thickens in the terminal reach.

The summer simulation, shown in Figures 5.12 *a* and 5.13, uses an input of 0.05 m/day, which is characteristic of the melt season. The starting ice profile is the same as that used for the winter run. In the melt season simulation, the effective pressure decreases as the terminus is approached. This effect causes the velocity to be highest at the terminus and to drop upglacier, creating a region of extension over the last 5 km of the glacier. The extension in this region causes thinning of the ice over the 80 days of the simulation, leading to a "pulse" of high velocity and rapid thinning toward the end of that period. The thinning is responsible for lowering the effective pressure in this reach, and the effective pressure dominates the sliding velocity relation, leading to the high velocity. The timing of this event in the model is dependent on the choice of a sliding law and the initial conditions, but the region of the glacier over which this extension takes place is determined by the pressure distribution dictated by the tunnel system, the discharge, and the pressure boundary condition imposed by sea level.

This pulse of thinning and increased velocity at the terminus should be compared with the short description of the observed behavior of Columbia Glacier quoted from Krimmel and Meier on the first page of Chapter 4. The pulse produced by the model is similar to the pulse of velocity they observe, in both location and magnitude, and it also starts at the terminus and spreads upglacier. It is easy to relate the pulse produced by the model to an increased calving rate if the ice is required to calve as it approaches floatation. Sikonia [1982] proposed an empirically derived calving relation which has the calving rate proportional to $P_e^{-2}$.

The pulse of thinning which the model predicts can be looked for in profiles of Columbia Glacier. Five of these profiles, made from aerial photographs [Krimmel, unpublished data], are shown in Figure 5.14. These profiles are not systematically spaced in time (the times of the photo flights are given in the figure). The drop in surface elevation of the ice over the last 4 to 5 kilometers between the flights on 9/10/86 and 1/26/87 is interpreted here to be the result of a pulse similar to the one produced by the model. The pulses of velocity and calving observed on Columbia Glacier generally occurred in October and November [Krimmel, personal communication].

The model demonstrates a condition which allows the thinning rate of the ice to be influenced by the discharge of water from the glacier. In general, this influence results in a lowering of velocity upglacier from the terminus (as discharge increases), while the velocity near the terminus responds to a pressure condition that is fixed to sea level, and so does not drop. The control of extension (and thinning) near the terminus of the glacier may be the reason that calving and discharge are related (Sikonia [1982] calculated a correlation coefficient of 0.8 between calving and discharge records).

Work on Columbia between 1975 and 1983 revealed an association between the formation of embayments in the terminus of the glacier and the location of the outlet stream. The active calving in an embayment was located at the position of outflow from underneath the glacier; when the outflow stream moved to another part of the

embayment, the calving stopped at the initial location and started at the new stream location [Meier et al, 1977]. The relation between the location of calving along the terminal ice cliff and the location of the outlet stream may be understood in similar terms: at the ice face the velocity is high but upstream along the tunnel the pressure is low, resulting in a low sliding velocity; the result is a pattern of extension, thinning and calving that is similar to the one described above but is laterally localized near the tunnel.

The tie between discharge and extension does not provide a model of the process responsible for the actual calving of ice from the glacier, but it does provide a clear step toward calving, as a result of thinning of the ice. In this sense, the model may be said to address the issue of the determination of calving rates. The development of a calving law, which would account for the influence of tidal forcings as the ice approached floatation, as well as for the influence of the ice cliff, is beyond the scope of the work presented here. It is clear from the success of the simple model, however, that a calving law will have to incorporate the influence of longitudinal velocity gradients imposed on the ice by the basal water pressure distribution if it is to reproduce the variation in calving rate during the summer.

The simple combination of a sliding law, a longitudinal distribution of basal water pressure appropriate to the season under consideration, and deformation of the ice by the gradients in sliding velocity results in a model which reproduces many of the characteristics of the summer cycle of velocity and calving (with the addition of a calving relation) on lower Columbia Glacier. The ability of this model to generate a winter advance and a late summer pulse of velocity and implied pulse of calving suggests that the model contains the essence of the controlling mechanism for variations in the terminal reach of the glacier. This model has application to other tidewater glaciers, and may, in a refined state, be used to enhance predictions of calving rates and timing of the advance or retreat of these glaciers.

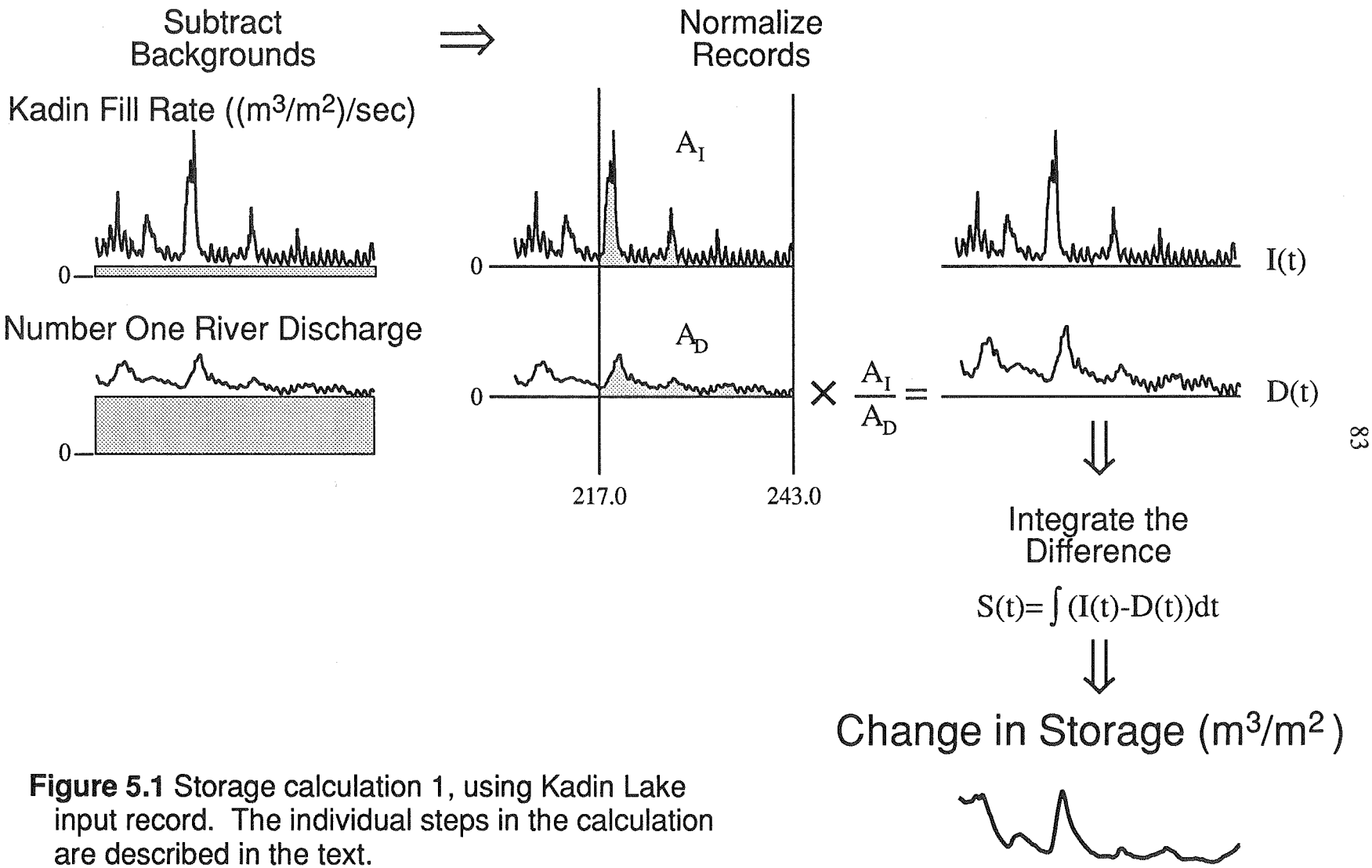


**Figure 5.1** Storage calculation 1, using Kadin Lake input record. The individual steps in the calculation are described in the text.

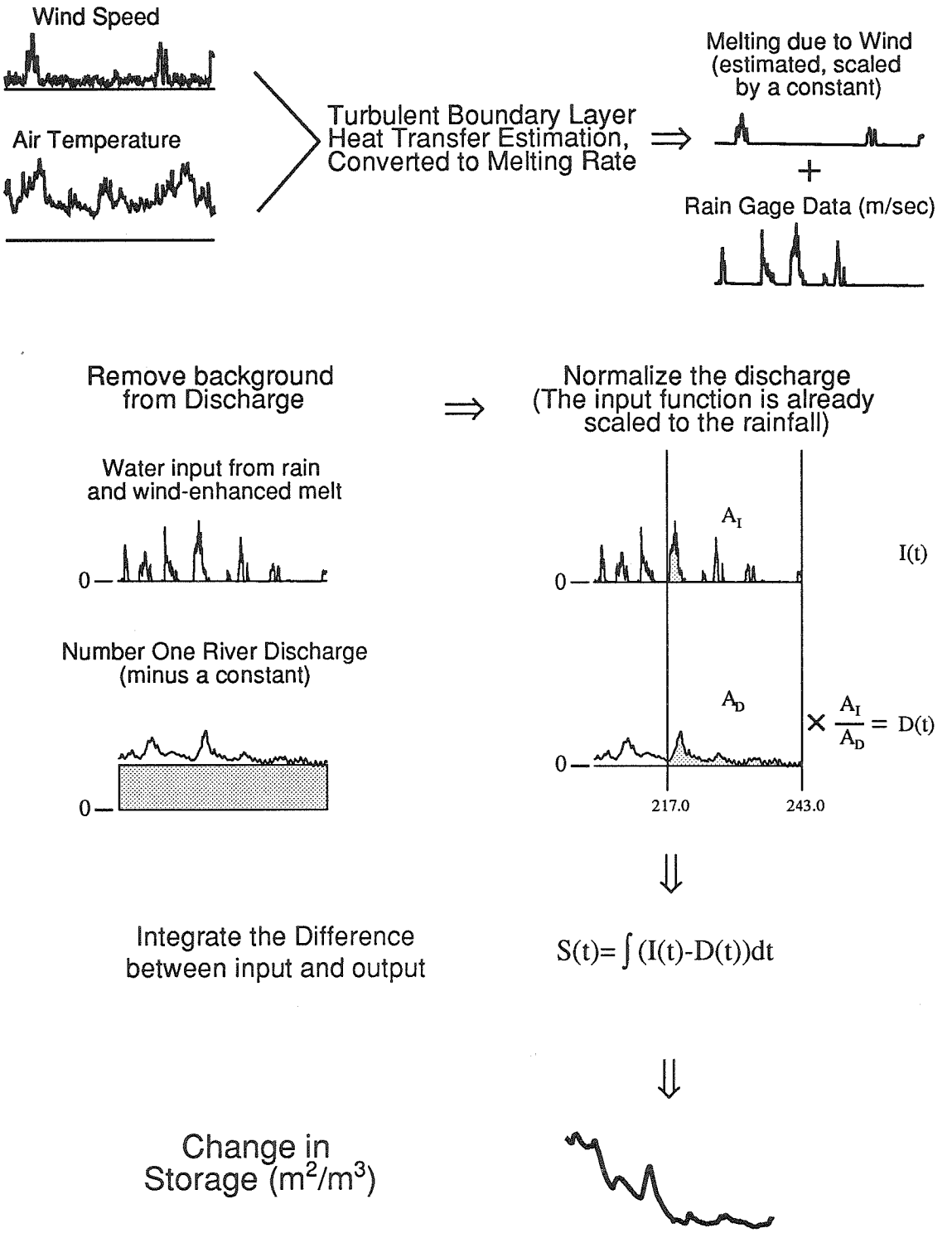


**Figure 5.2** Storage calculation 2, using meteorological input. The individual steps in the calculation are described in the text and in Appendix 2.

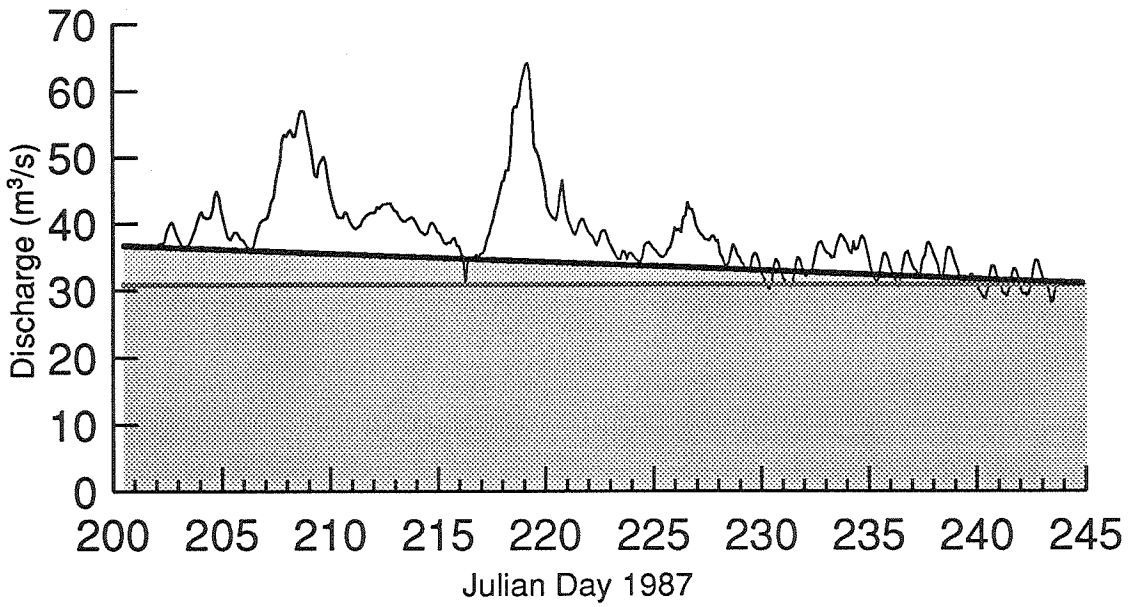


**Figure 5.3** Background removed from Gate discharge. Grey line is the constant background used in calculations 1 and 2 *a*. Black line is tapered background used in calculation 2 *b*.

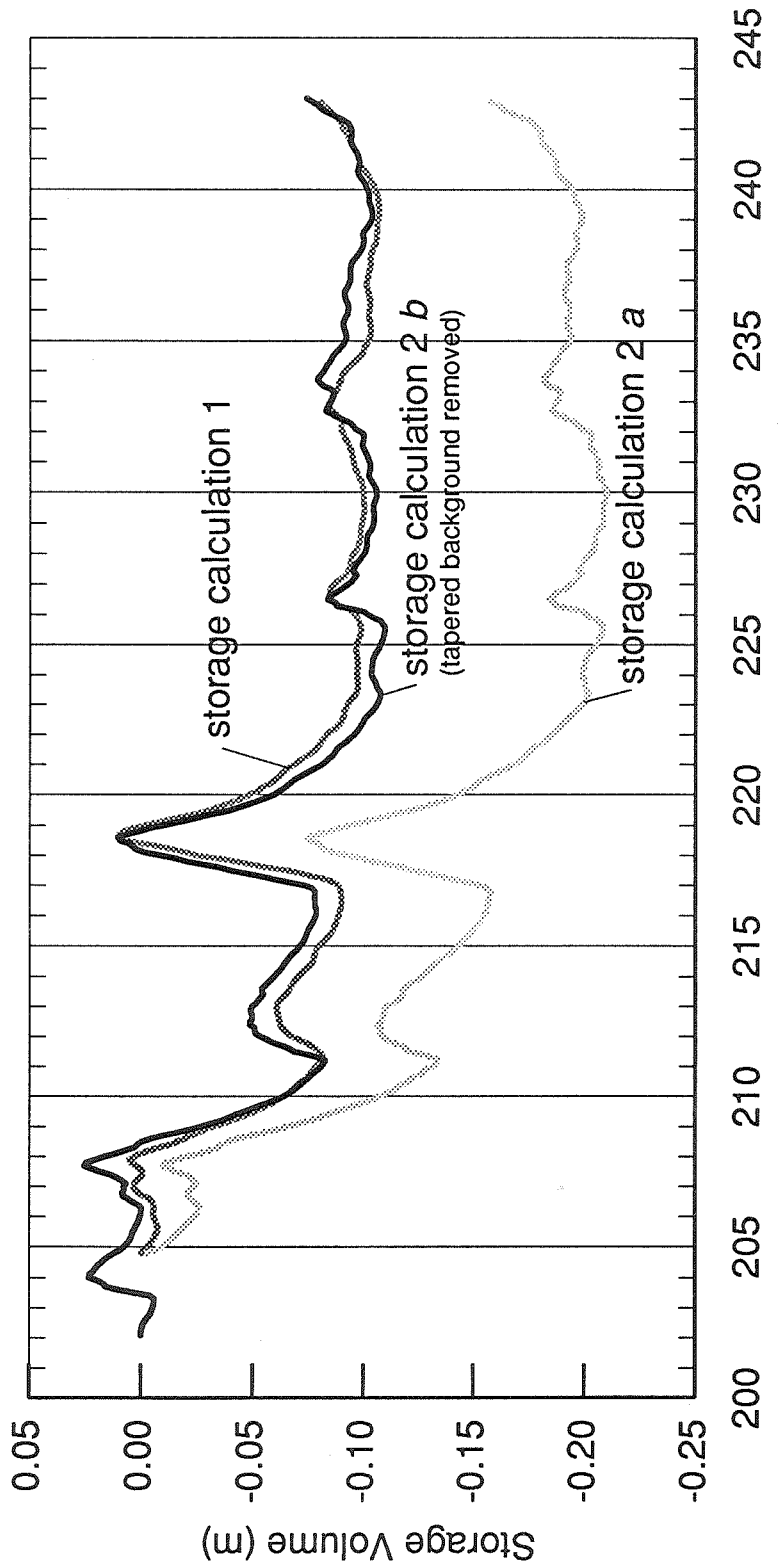


**Figure 5.4** Comparison of calculated storage volumes from storage calculations 1, 2 *a*, and 2 *b*.

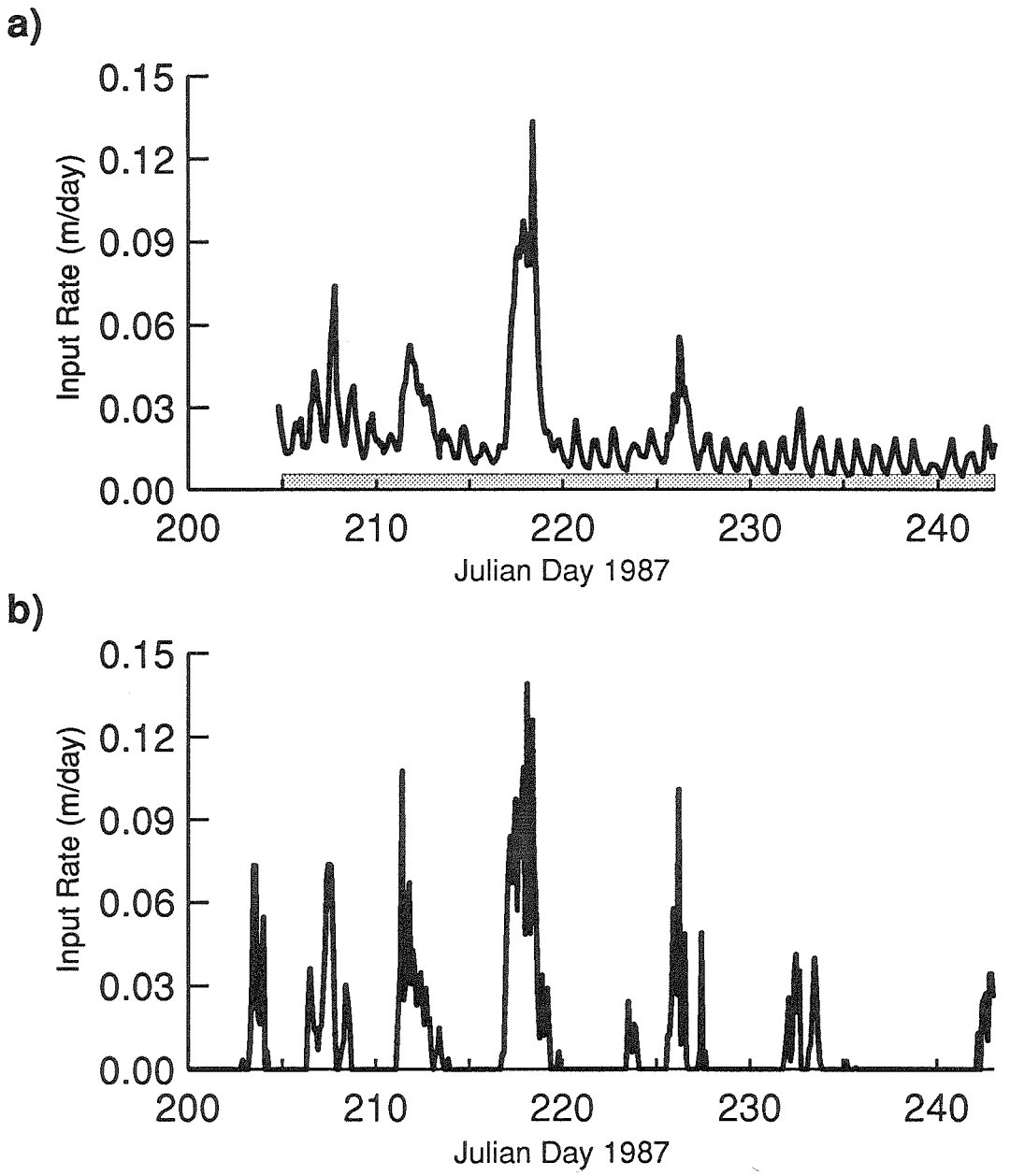


**Figure 5.5** Input curves for storage calculations. **a)** Filling rate of Kadin Lake, expressed as input rate per $m^2$ to basin. For storage calculation 1, the shaded background is subtracted. **b)** Input curve for storage calculations 2 *a* and *b*. Input rate is rainfall + calculated ablation from wind storms (Appendix 2).

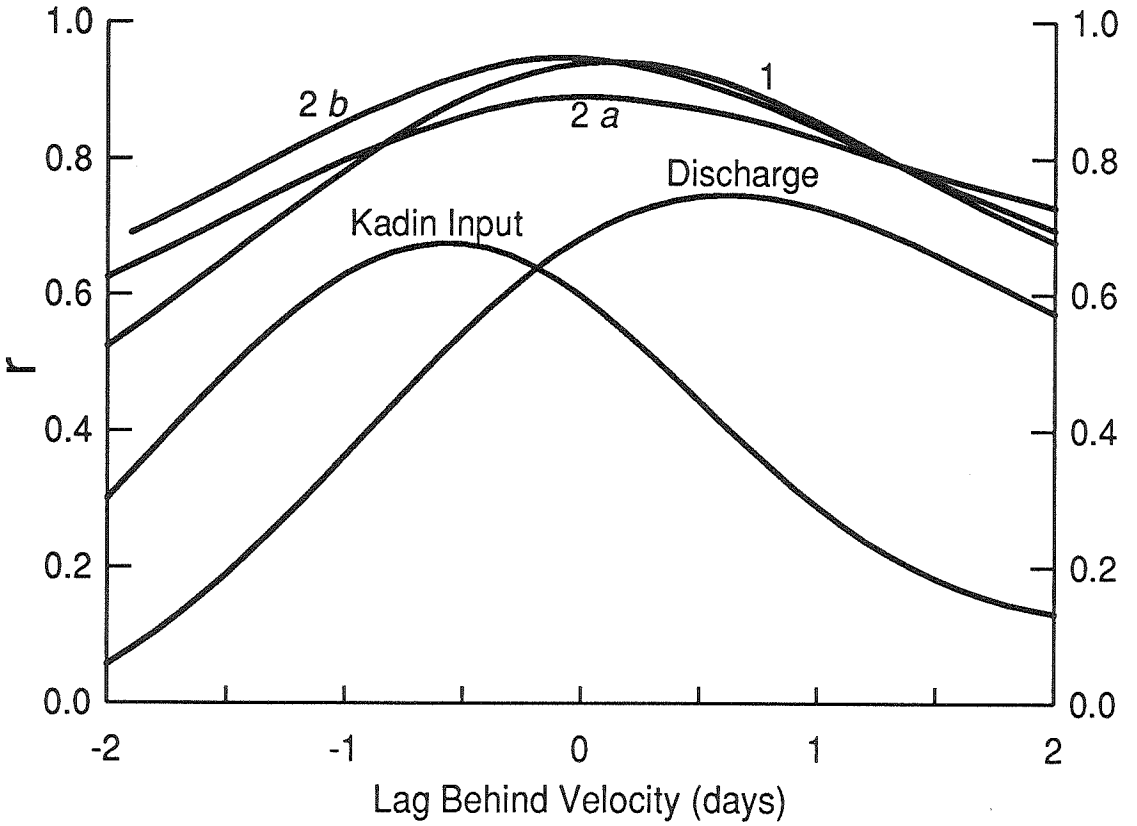


**Figure 5.6** Cross-Correlation of 24 Hour Average Velocity and: calculated storage (indicated by calculation number), Kadin Lake input rate, and Number One River Discharge.

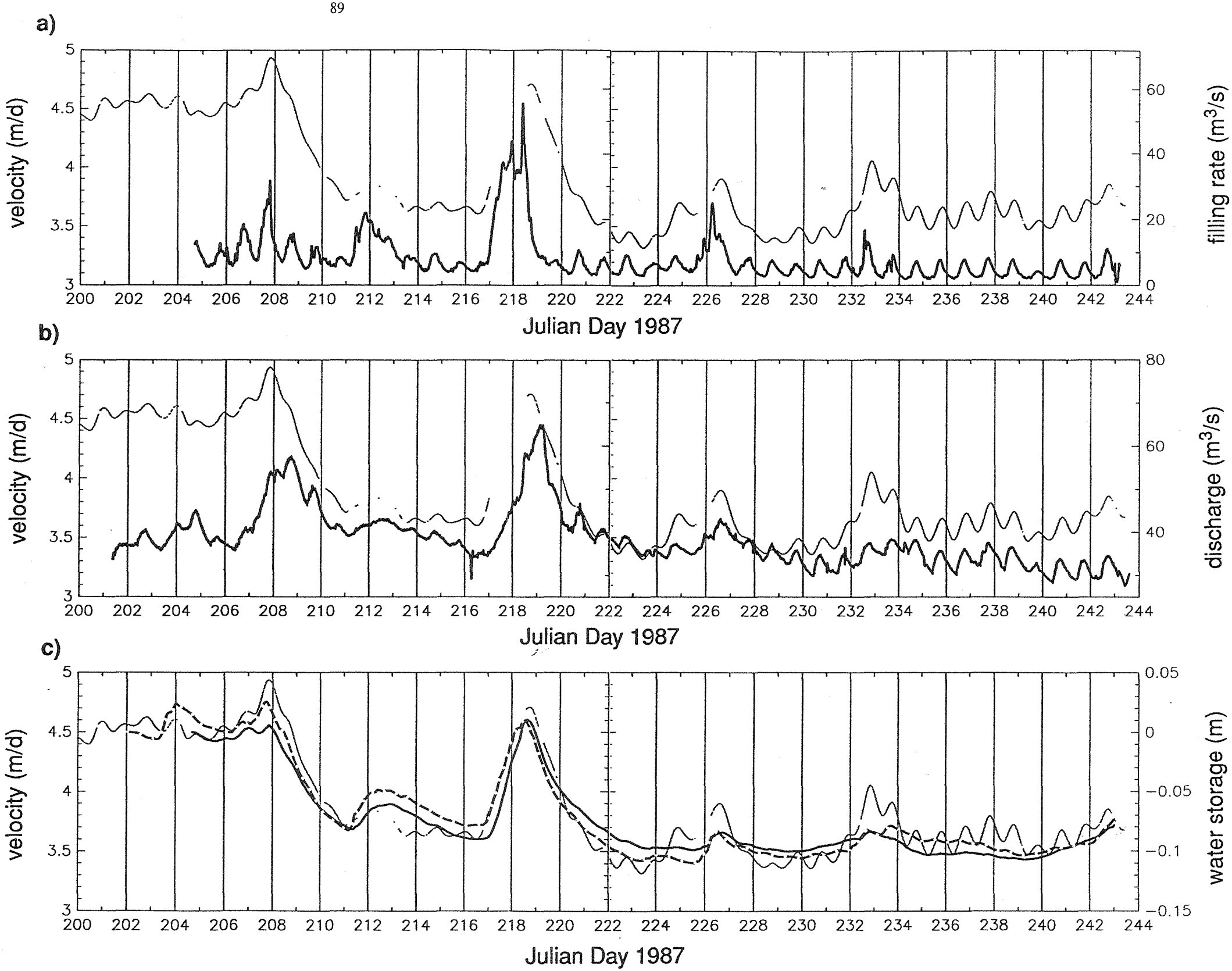


**Figure 5.7** Comparisons of site 52 velocity and a) Kadin Lake filling rate, b) Number One River discharge, c) water storage curves 1 (solid line) and 2 *b* (dashed line).

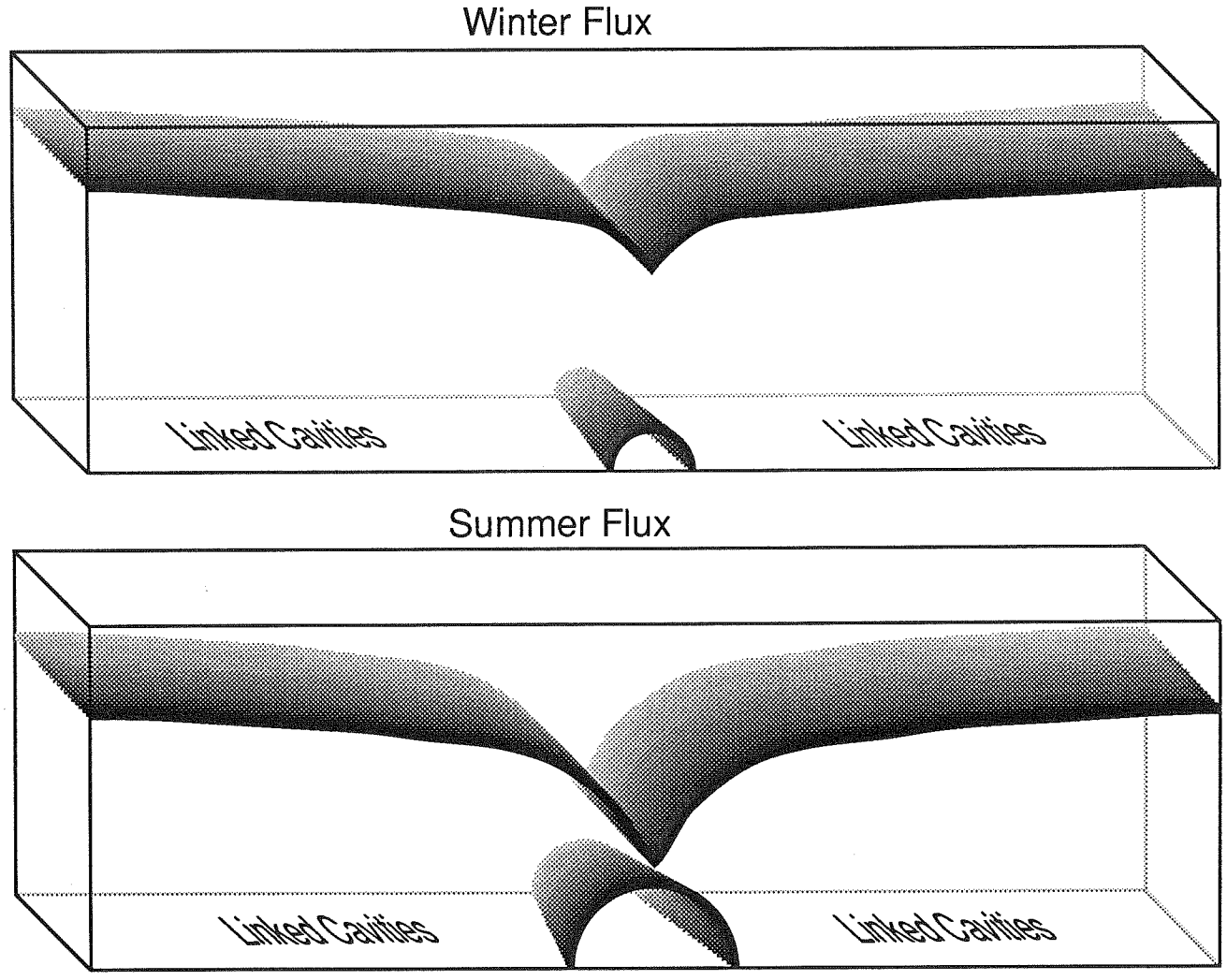


**Figure 5.8** Cross-sections of glacier showing phreatic surface changes due to flux.

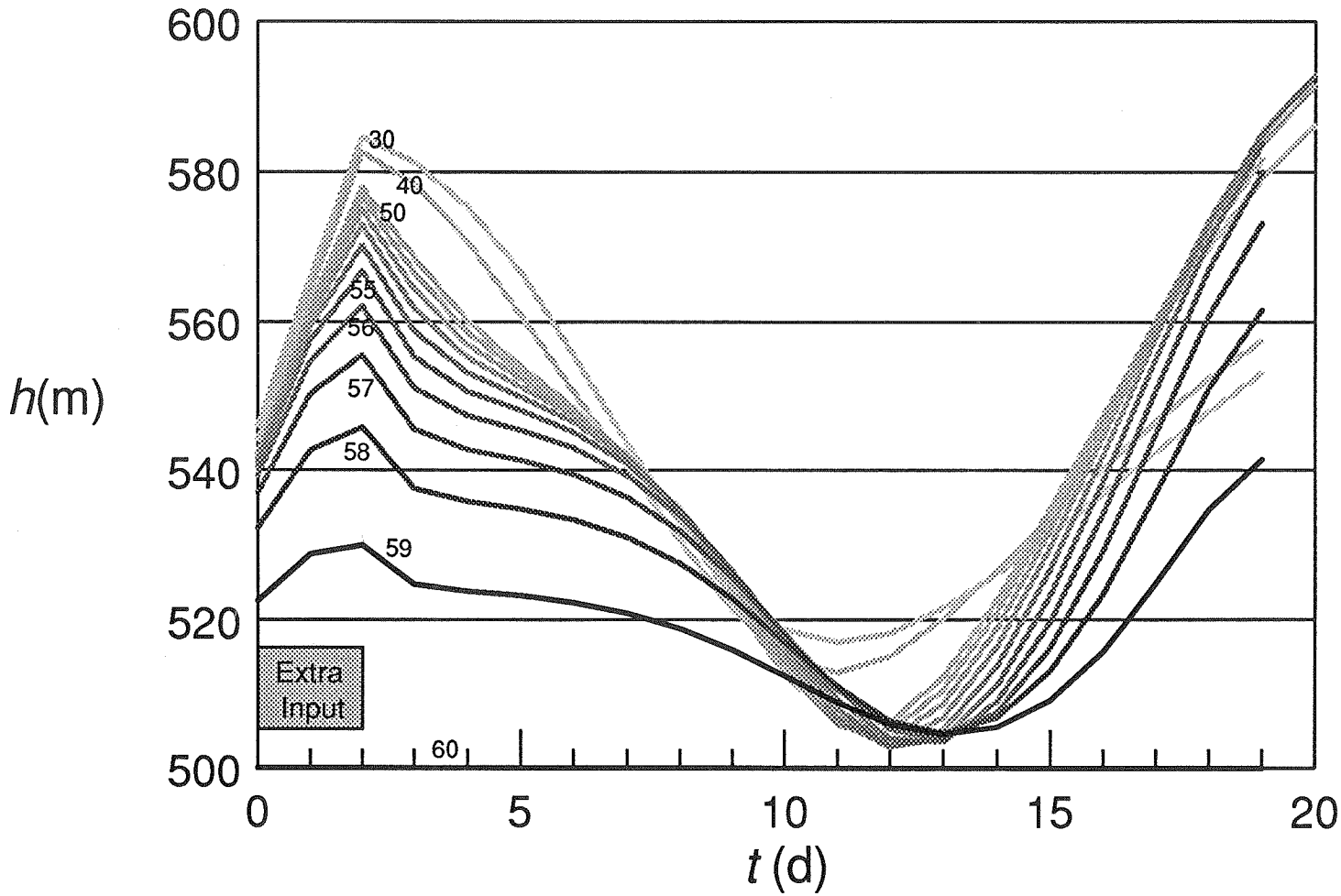


**Figure 5.9** Tunnel model: response of *h* to increase in distributed input (daily values). Numbers on curves are km from head of glacier; terminus is at 60 km. Box shows duration of extra input (details in text).

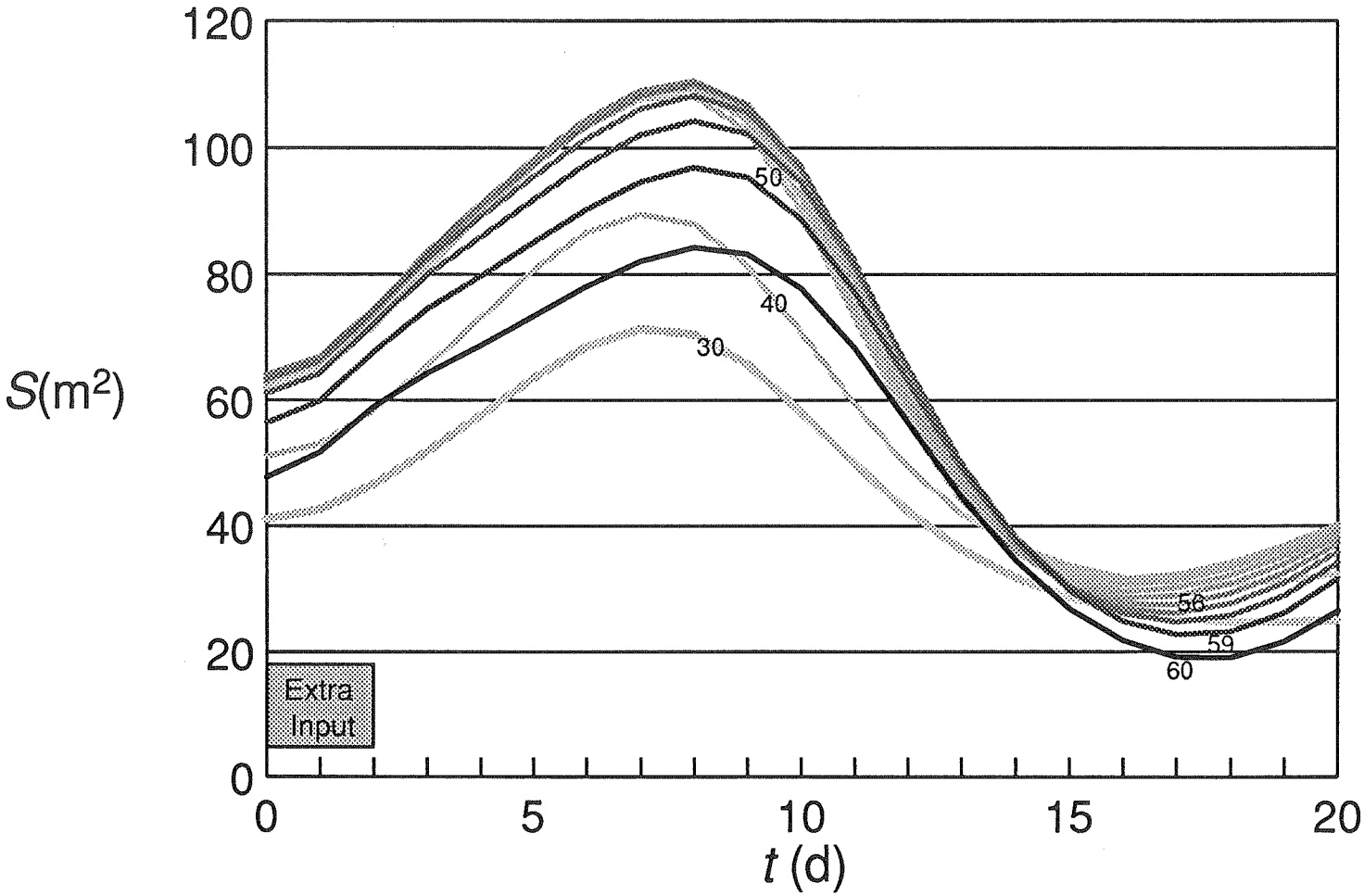


**Figure 5.10** Tunnel model: response of *S* to increase in distributed input (daily values). Numbers on curves are km from head of glacier; terminus is at 60 km. Box shows duration of extra input (details in text).

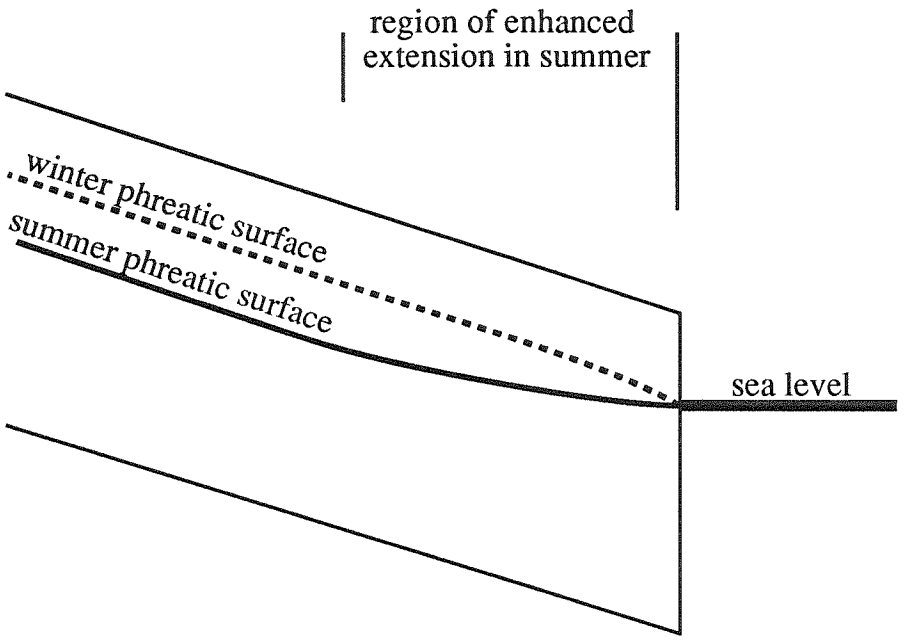


**Figure 5.11** Schematic diagram of summer and winter phreatic surfaces. Region of increased extension and thinning in summer indicated.

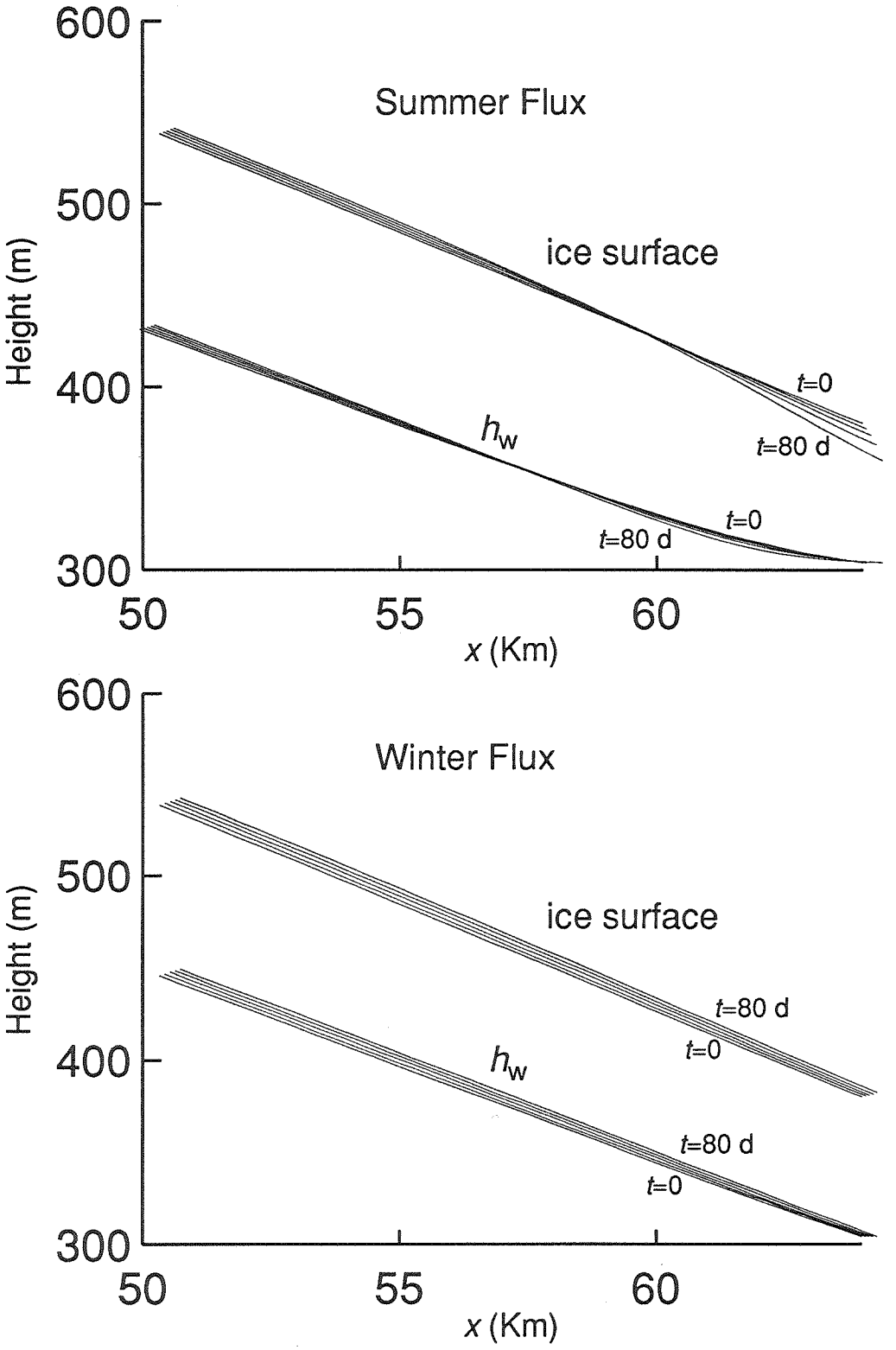


**Figure 5.12** Model results for 80 day simulations at **a)** summer (0.05 m/day surface melt) and **b)** winter (0.0005 m/day equivalent surface melt) inputs.

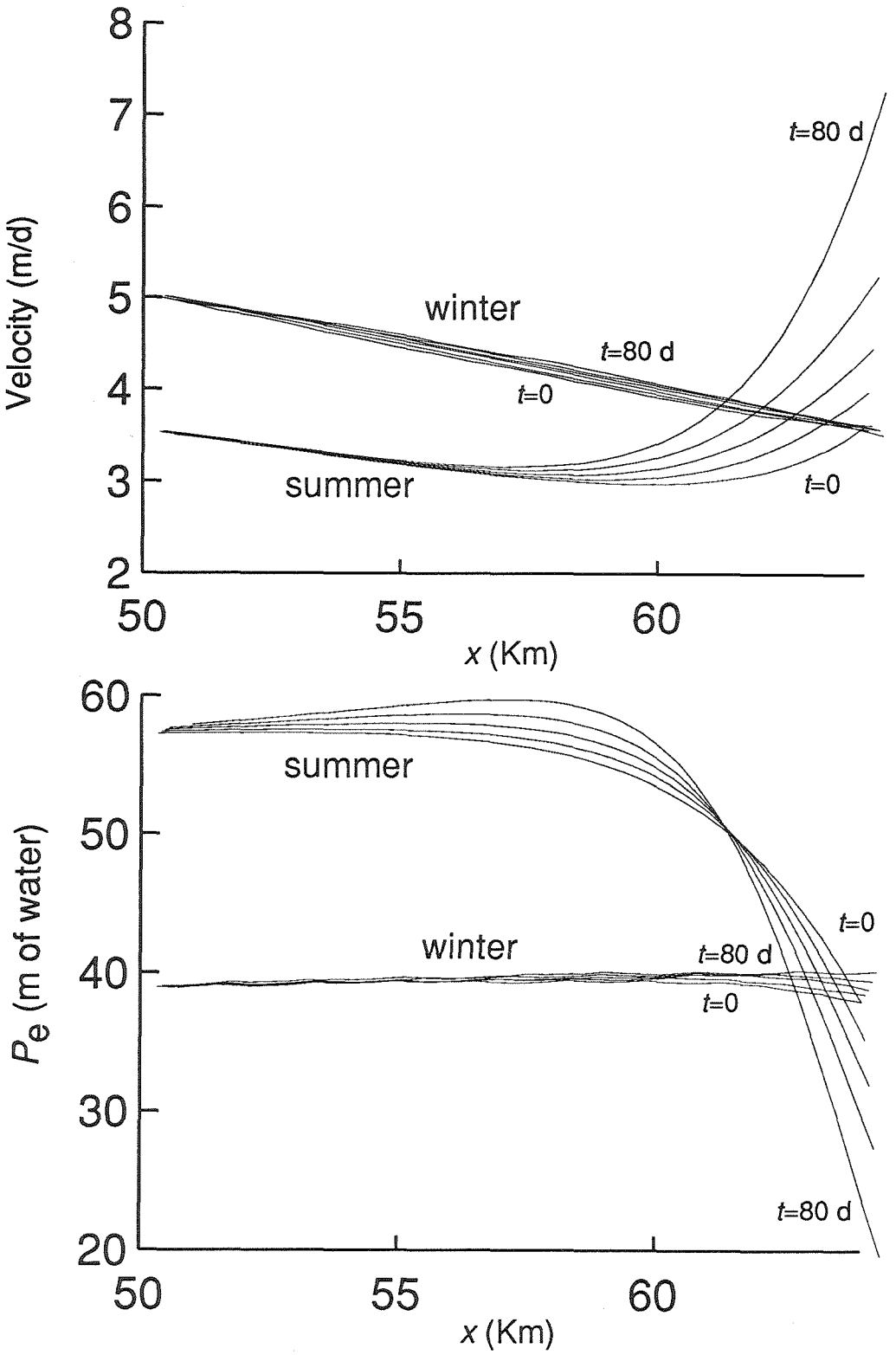


**Figure 5.13** Model results for 80 day simulations with summer and winter inputs as in Figure 5.12. **a)** velocity **b)** $P_e$.

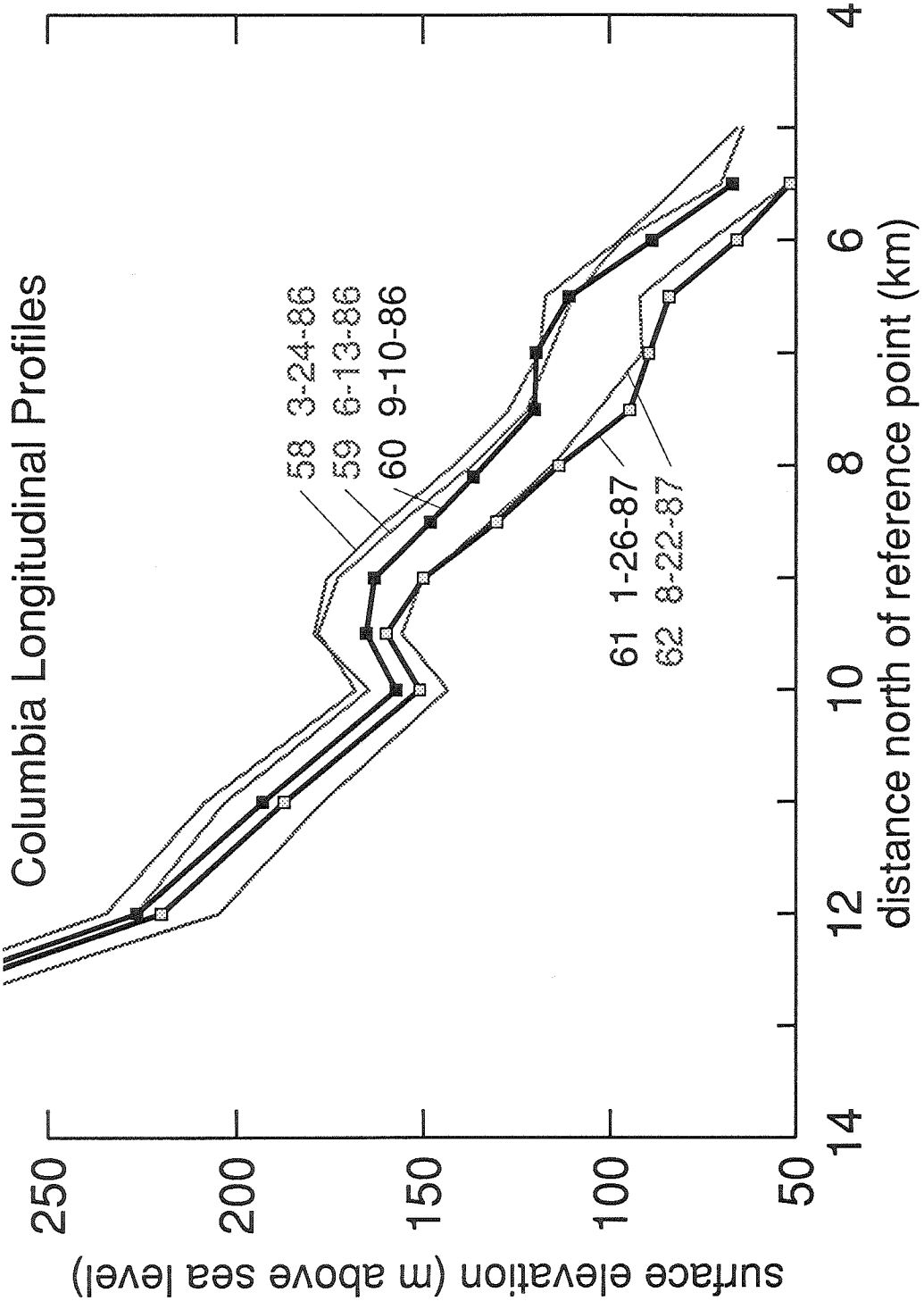


**Figure 5.14** Surface elevation along a flow line for five air photo flights. Flight numbers and dates indicated. (Data provided by Robert Krimmel, USGS)

# Chapter 6

## Conclusions and Future Work

The results from this thesis suggest that the role played by water in the production of velocity variations in glaciers can, in a few cases, be understood in fairly simple terms. While the processes investigated here are not now fully understood, the initial success of the techniques indicate that future work in similar directions will be productive.

The mini-surges of Variegated Glacier tell us something about conditions in the drainage system in the upper glacier during the early months of the melt season. The propagating behavior of these disturbances is not the result of water movement through a tunnel system, although any tunnel present in the reach will be modified by the passing of the event. The results from modeling the propagation of a pulse of water indicate that a system which increases its conductivity in response to increasing water pressure, in a manner that might be expected of a system of basal cavities, could explain the observed behavior. Further work on these disturbances should include more detailed observation of the source region and its behavior during mini-surge initiation, to understand how the water pressure builds prior to the onset of propagation. In addition, systematic monitoring of other glaciers, in an effort to determine how common this type of behavior is, would help in developing an understanding of what characterizes a glacier, or a particular reach of a glacier, that exhibits this behavior.

I have been able to explain a few of the major variations in velocity on Columbia Glacier in relatively simple terms based on hydrologic processes, as summarized below. Tests of these ideas against existing data indicate that they appear to be reasonable representations of the processes responsible for this glacier's flow behavior.

The strong correlation between stored water volume and glacier velocity shown from the storage calculation provides a straightforward indication of the dominant role of

water in the motion of Columbia glacier. This result represents a new constraint for models of rapid basal sliding.

The hybrid cavity/tunnel system proposed for Columbia Glacier allows for the explanation of velocity events in terms of increased water storage and also provides a way of explaining the aspects of the glacier's behavior that are suggestive of a tunnel system. A tunnel calculation to be used to model the effects of longitudinal variations in velocity on acceleration of the terminus and calving behavior. The re-advance of the glacier during the winter and early melt season may be reproducible by this model, but there is little to constrain the existence of a tunnel system under the glacier during this time of year. The possibility that the rapid sliding motion would wipe out the small tunnels in existence at this time suggests that the basal system could be forced into an all cavity system until the next melt season. Future observational work could address this possibility by monitoring the transition from summer to winter conditions using a field program similar to that used in 1987. The question of the transition into a winter regime could also be addressed by modeling the response of a tunnel system to a representative drop in distributed input rate.

The previously determined correlation between discharge and calving rate is here explained as being a result of longitudinal variation in velocity caused by the effective pressure distribution imposed by a tunnel system. This same idea applied locally near the terminus may explain observations that relate active calving at the face to the location of the outflow stream.

Thus the varied flow behavior of Columbia Glacier appears to be largely the result of the behavior of the subglacial drainage system.

An investigation of the behavior of tidewater glaciers which could detect the consequences of longitudinal variations would need to use data gathered from frequent (bi-weekly) photo flights and digital image analysis techniques to produce data sets of the velocity variations in the lower reaches of several tidewater glaciers over an annual cycle.

This data would allow the applicability of the models in this thesis to be tested, and would, without doubt, provide an additional perspective on the problem of fast glacier flow.

# Appendix 1

## Calculation of Steady-State Configuration of a Tunnel System

The steady state longitudinal distribution of water pressure and tunnel cross-sectional area at the bed of a glacier can be estimated from a tunnel calculation similar to the one made by Röthlisberger [1972]. The calculation carried out here differs from Röthlisberger's by the addition of a distributed input of water and by the resulting longitudinal variation of water flux. I use the modified form of Nye's dynamic tunnel equations, described in Chapter 2. Starting with these equations will allow the role of the distributed input to be defined and will also allow a simplifying assumption made about continuity to be made explicit. The results of this calculation will be used to discuss pressure distributions which are imposed by winter or summer water fluxes.

The relevant equations are Equations 2.2, 2.3, 2.4, and 2.5. The coordinate system is defined in Figure 2.1.

The assumption of a steady state implies

$$\frac{\partial S}{\partial t} = \frac{\partial h}{\partial t} = 0 \tag{A1.1}$$

The input and flux gradient terms in the continuity equation (Equation 2.3) are taken to be much larger than the melting term:

$$\frac{m}{\rho_w} << -\frac{1}{\omega}\frac{\partial Q}{\partial x}, \qquad \frac{m}{\rho_w} << \frac{1}{\omega} I \tag{A1.2}$$

The water from the ice melted at the tunnel wall is neglected. This was done implicitly by Röthlisberger, whose use of continuity in his formulation involved the specification that $Q$=constant.

Using Equations A1.1 and A1.2 to simplify Equation 2.3 results in

$$I = \frac{\partial Q}{\partial x} \tag{A1.3}$$

Equation A1.3, when integrated, gives

$$Q = Ix \tag{A1.4}$$

which is simply the result of a distributed input in a steady state, in which the water produced by melting is neglected. The constant of integration in Equation A1.4 is 0 as the flux at the head of the glacier, at $x = 0$, is 0.

The assumption expressed in Equation A1.2 can be checked. Over much of the glacier the phreatic surface will be approximately parallel to the ice surface, so $\partial h/\partial x \approx 0$. Equation 2.5 simplifies to

$$m = \frac{Q\xi\beta}{L} \tag{A1.5}$$

If $Q$ is taken from Equation A1.4 and $m$ from A1.5, A1.2 reduces to

$$x << \frac{L}{g\beta} \tag{A1.6}$$

For Variegated Glacier $\beta \approx 0.1$, making A1.6

$$x << 335 \text{ km} \tag{A1.7}$$

For Columbia Glacier $\beta \approx 0.02$, giving the requirement:

$$x << 1675 \text{ km} \tag{A1.8}$$

Variegated and Columbia have lengths of 20 km and 60 km, respectively, so Equations A1.7 and A1.8 are satisfied.

In the discussion to follow, the model glacier has a constant slope, $\beta$, as well as a constant rate of surface input, $I$.

In order to calculate the longitudinal distribution of water pressure in a tunnel, we begin at the terminus, where the water pressure is fixed either by atmospheric pressure or, in the case of a tidewater glacier, by the water depth. Because the length of the glacier is known and the input rate $I$ is fixed, the flux of water at the terminus can be calculated using Equation A1.4. A relation can be found that determines the cross-sectional area of

the conduit ($S$) that would be required by the steady state condition, given the water pressure and flux. We can then use $Q$ and the $S$ so determined to find $h/\partial x$ from Equation 3.4. This gradient multiplied by an increment of distance gives the change in water height one step up the glacier. This new water height is then used in the same iterative process to find $S$ and $\partial h/\partial x$ at the next point up glacier.

The relation used to calculate the size of tunnel required to maintain a steady state for a given ice thickness, flux and water height is derived as follows:

From the water flow equation (Equation 2.4):

$$\frac{\partial h}{\partial x} = \beta - \frac{NQ^2}{\xi S^{\frac{8}{3}}} \tag{A1.9}$$

Substituting Equation A1.9 into Equation 2.5:

$$m = \frac{Q\alpha}{L}[\beta - R_1(\beta - \frac{NQ^2}{\xi S^{\frac{8}{3}}})] \tag{A1.10}$$

This melting must be balanced by flow closure of the tunnel. Combining Equations 2.2, A1.1, and A1.10:

$$2\rho_i S\left(\frac{P_i - P_w}{nV_i}\right)^n = \frac{Q\xi}{L}[\beta - R_1(\beta - \frac{NQ^2}{\xi S^{\frac{8}{3}}})] \tag{A1.11}$$

This is the required relation when $P_w$ is replaced by $\rho_w g h$ and $Q$ is replaced by $Ix$. This relation can be easily solved numerically to find the steady state tunnel size for a given flux, water height and ice thickness at a given point $x$.

The stepwise calculation of the pressure distribution begins at $h_0$ = (outlet pressure)/$\rho_w g$. $S$ is determined from Equation A1.11, $\partial h/\partial x$ from Equation A1.9, and then $h$ at a distance $\Delta x$ upglacier from

$$h(x_0 - \Delta x) = h_0 - \frac{\partial h(x_0)}{\partial x}\Delta x \tag{A1.12}$$

This process can be continued upglacier to obtain the basal water pressure distribution in the tunnel.

# Appendix 2

## Surface Melting Rate Estimation Based On Turbulent Boundary Layer Heat Transfer

The estimation of surface melting rate due to heat transfer in a turbulent boundary layer of air is based on Monin-Obukhov similarity theory [Arya, 1988, Chapter 11]. The theory provides a method of estimating the amount of sensible heat transfer through the turbulent boundary layer, given the values of some constants and the air temperature and wind velocity at a height $z$ above the surface.

The sensible heat flux is formulated

$$H_0(C_H(Ri_B(\Delta T,U),\frac{z}{z_0}),U,\Delta T) \qquad \text{(A2.1)}$$

where the parentheses in Equation A2.1 express functional dependence. $H_0$ is the sensible heat flux, $C_H$ is the heat transfer coefficient, $Ri_B$ is the bulk Richardson number, $\Delta T$ is the difference in air temperature between the height $z$ the surface, $U$ is the average wind velocity at the height $z$ and $z_0$ is a length scale that represents surface roughness. Figure A2.1 *a* shows the value of the melting rate $m_r$ calculated by the procedure described in the next paragraph. The points in this figure are the results of the calculation; the lines are provided to connect points with the same parameter values.

Calculation of the points in Figure A2.1 was done by first calculating a value for $Ri_B$ :

$$Ri_B = \frac{g}{T_0}\frac{z\Delta T}{U^2} \qquad \text{(A2.2)}$$

where $g$ is gravitational acceleration, $T_0$ is a the air temperature in the reference state, $z$ is taken to be 10 meters, and $\Delta T$ and $U$ are indicated on the graph. Using this value for $Ri_B$ and the ratios for $z/z_0$ indicated in Figure A2.1, $C_H$ was estimated from Arya [1988,

Figure 11.6 *b*]. This estimated value for the heat transfer coefficient was then put into the equation

$$H_0 = \rho c_p C_H U \Delta T \qquad \text{(A2.3)}$$

which is taken from Arya [1988, Equation 11.15]. In this equation, ρ is the density of air and $c_p$ is the specific heat of air at a constant pressure. The surface melting rate $m_r$ is simply this heat flux divided by the latent heat of fusion for ice:

$$m_r = \frac{H_0}{L} \qquad \text{(A2.4)}$$

From the points in Figure A2.1 *b* the amount of melting is estimated by using the linear regressions shown in this figure to determine the amount of melting for a given wind velocity at two temperatures, and then estimating the melting at the actual temperature by linear interpolation between these two points.

The ratio $z/z_0$ is not well constrained. This is in part because the appropriate value for the surface roughness is not known, and in part because the point where the wind velocity and temperature data were taken (on a ridge near Kadin) was not ideal (the theory assumes that the boundary is flat). Because of this, the melting rates which are estimated from Figure A2.1 *b* and the measured wind velocity and air temperature at Kadin are only approximate. I have treated these rates as being correct in a relative sense (the rate at one set of conditions being in the proper ratio to the rate at another set of conditions), and have scaled the results by a constant in order to obtain the values used in Chapter 3.

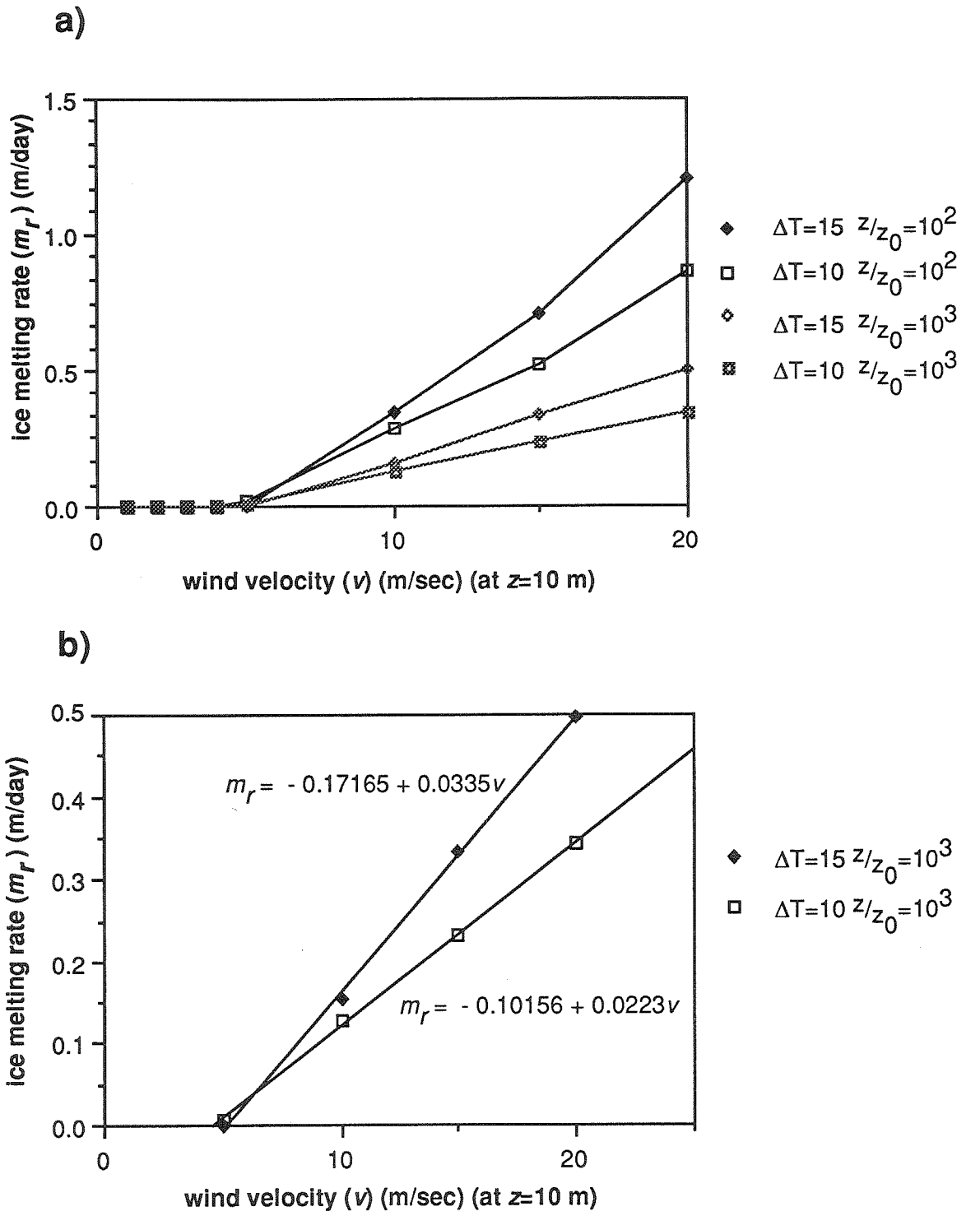


**Figure A2.1** Ice melting rate estimates from Monin-Obukhov similarity theory. **a)** Points calculated, lines for reference **b)** Linear fits to the curves from **a** used in estimation (see text).

## Appendix 3

## List of Symbols (with values used)

| Symbol | Name | Units or value used |
|---|---|---|
| $\beta$ | basal slope | 0.1 (typical of Variegated Glacier)<br>0.02 (typical of lower Columbia Glacier) |
| $\kappa$ | Manning roughness | 0.1 for ice walled conduit<br>[Nye, 1976, p. 194] |
| $\nu$ | bulk porosity | 0.001<br>(see text) |
| $\rho_i$ | density of ice | 900 kg/m$^3$ |
| $\rho_w$ | density of water | 1000 kg/m$^3$ |
| $\tau_b$ | basal shear stress | Pa |
| $\omega$ | tortuosity | 1.0 (no effect) |
| $A$ | ice viscosity parameter | 3.1 $10^7$ Pa s$^{1/3}$<br>1.0 bar y$^{1/3}$<br>$n$=3<br>[Nye, 1953, Equation 9] |
| $h$ | water height above bed | m |
| $h_i$ | ice thickness | m |
| $h_0$ | pre-event or reference water height above bed | m |
| $h_\infty$ | floatation water height or water height for unconstrained increase of conductivity or sliding velocity | m |
| $k$ | pressure dependent conductivity | m$^3$/s |
| $k_0$ | background conductivity (constant) | m$^3$/s |
| $L$ | latent heat of fusion of ice | 3.35 $10^5$ J/kg |
| $m$ | mass rate of melting | kg/s |

| | | |
|---|---|---|
| $P_e$ | effective pressure | (= $P_i$ - $P_w$) Pa |
| $P_i$ | overburden pressure of ice | Pa |
| $P_w$ | basal water pressure | (= $\rho_w g h$) Pa |
| $Q$ | water flux | $m^3/s$ |
| $R_1$ | fraction of generated heat not required to keep water at pressure melting point | 0.684 [Röthlisberger, 1972, Equation 18] |
| $S$ | tunnel cross-sectional area | $m^2$ |
| $V$ | volume of storage per unit length | $m^2$ |
| $v_s$ | sliding velocity | m/d |
| $w_e$ | effective width | 1000 m for Variegated Glacier<br>5000 m for Columbia Glacier |
| $x$ | downglacier coordinate | m |
| $y$ | cross-glacier coordinate | m |

## Bibliography

Arya, S. P., *Introduction to micrometeorology*, Academic Press, Inc., New York, 1988.

Bindschadler, R. A., The importance of pressurized subglacial water in separation and sliding at the glacier bed, *Journal of Glaciology*, *29*, 3-19, 1983.

Budd, W. F., P. L. Keage, and N. A. Blundy, Empirical studies of ice sliding , *Journal of Glaciology*, *23*, 157-170, 1979.

Brugman, M. M., Water flow at the base of a surging glacier, Ph.D. thesis, California Institute of Technology, 1986.

Engelhardt, H., Water in glaciers: Observations and theory of water levels in boreholes, *Zeitschrift fur Gletscherkunde und Glazialgeologie*, *14*, 35-60, 1978.

Engelhardt, H., N. Humphrey, B. Kamb, and M. Fahnestock, Physical conditions at the base of a fast moving Antarctic ice stream, *Science*, *248*, 57-59, 1990.

Hodge, S. M., Variations in the sliding of a temperate glacier, *Journal of Glaciology*, *13*, 349-369, 1974.

Humphrey, N., C. Raymond, and W. Harrison, Discharge of turbid water during mini-surges of Variegated Glacier, Alaska, U.S.A., *Journal of Glaciology*, *32*, 195-207, 1986.

Humphrey, N. F., B. Kamb, M. Fahnestock, and H. Engelhardt, Physical characteristics of the bed of the Lower Columbia Glacier, Alaska, *Journal of Geophysical Research*, submitted.

Iken, A., The effect of subglacial water pressure on the sliding velocity of a glacier in an idealized numerical model, *Journal of Glaciology*, *27*, 407-421, 1981.

Iken, A., H. Röthlisberger, A. Flotron, and W. Haeberli, The uplift of Unteraargletscher at the beginning of the melt season -- a consequence of water storage at the bed?, *Journal of Glaciology*, *29*, 28-47, 1983.

Iken, A., and R. A. Bindschadler, Combined measurements of subglacial water pressure and surface velocity of Findelengletscher, Switzerland: Conclusions about drainage system and sliding mechanism, *Journal of Glaciology*, *32*, 101-119, 1986.

Kamb, B., C. F. Raymond, W. D. Harrison, H. Engelhardt, K. A. Echelmeyer, N. Humphrey, M. M. Brugman, and T. Pfeffer, Glacier surge mechanism: 1982-1983 surge of Variegated Glacier, Alaska, *Science*, *227*, 469-479, 1985.

Kamb, B., Glacier surge mechanism based on linked cavity configuration of the basal water conduit system, *J. Geophys. Research*, *92*, 9083-9100, 1987.

Kamb, B., and H. Engelhardt, Waves of accelerated motion in a glacier approaching surge: The mini-surges of Variegated Glacier, Alaska, U.S.A., *Journal of Glaciology*, *33*, 27-46, 1987.

Kamb, B. and M. Fahnestock, Theory for propagation of mini-surge waves in Glaciers (in preparation).

Krimmel, R., and M. Meier, IGC Field Trip T301: Glaciers and Glaciology of Alaska, in *Glacial Geology and Geomorphology of North America, 28th International Geological Congress Field Trip Series*, vol. 1, pp. T301:1-61, American Geophysical Union, Washington, D.C., 1990.

Krimmel, R. M., and B. H. Vaughn, Columbia Glacier, Alaska: changes in velocity 1977-1986, *J. Geophys. Research, 92*, 8961-8968, 1987.

Lick, W., wave propagation, in *Handbook of applied mathematics: selected results and methods*, Second edition, edited by C. E. Pearson, pp. 815-877, Van Nostrand Reinhold, New York, 1990.

Lliboutry, L., General theory of subglacial cavitation and sliding of temperate glaciers, *Journal of Glaciology, 7*, 21-58, 1968.

Meier, M. F., A. Post, C. S. Brown, D. Frank, S. M. Hodge, L. R. Mayo, L. A. Rasmussen, E. A. Senear, W. G. Sikonia, D. C. Trabant, and R. D. Watts, Columbia Glacier progress report - December 1977, U.S. Geological Survey, Open File Report 78-264, March 1978.

Meier, M. F., and A. Post, Fast tidewater glaciers, *J. Geophys. Research, 92*, 9051-9058, 1987.

Meier, M. F., B. Kamb, W. W. Dunlap, H. Engelhardt, M. Fahnestock, N. Humphrey, R. M. Krimmel, S. Lindstrom, D. Stone, and R. A. Walters, Mechanical and hydrological basis for the rapid motion of a large tidewater glacier: 1. observations (in preparation), 1991.

Nye, J. F., The flow law of ice from measurements in glacier tunnels, laboratory experiments and the Jungfraufirn borehole experiment, *Proc. Roy. Soc. London Ser. A, 219*, 477-489, 1953.

Nye, J. F., Water flow in glaciers: jökulhlaups, tunnels and veins, *Journal of Glaciology, 17*, 181-207, 1976.

Paterson, W. S. B., *The Physics of Glaciers*, Pergamon Press, Oxford a. o., 1981.

Post, A., Distribution of surging glaciers in western North America, *Journal of Glaciology, 8*, 229-240, 1969.

Post, A., Preliminary hydrography and historic terminus changes of Columbia Glacier, Alaska, Hydrologic Investigations Atlas HA-559, U.S. Geological Survey, Reston, Va., 1975.

Raymond, C. F., and S. Malone, Propagating strain anomalies during minisurges of Variegated Glacier, Alaska, U.S.A., *Journal of Glaciology, 32*, 178-191, 1986.

Röthlisberger, H., and H. Lang, Glacial Hydrology, in *Glacio-fluvial sediment transfer: an alpine perspective*, edited by A. M. Gurnell and M. J. Clark, pp. 207-274, John Wiley & Sons, Chichester, 1987.

Röthlisberger, H., Water pressure in intra- and subglacial channels, *Journal of Glaciology, 11*, 177-203, 1972.

Sikonia, W. G., Finite element glacier dynamics model applied to Columbia Glacier, Alaska, *U.S. Geol. Surv. Prof. Pap.,1258-B*, 1982.

Stone, D., An investigation of the integrity of the Kadin Lake Ice Dam, senior honors thesis, University of Colorado, 1988.

Tangborn, W. V., R. M. Krimmel, and M. F. Meier, A comparison of glacier mass balance by glaciological, hydrological and mapping methods, South Cascade Glacier, Washington, in *Snow and Ice-Symposium-Neiges et Glaces (Proceedings of the Moscow Symposium, August 1971)*, pp. 185-196, IAHS-AISH Publ. No. 104, 1975.

Walder, J. S., Hydraulics of subglacial cavities, *Journal of Glaciology, 32*, 439-445, 1986.

Walters, R. A., and W. W. Dunlap, Analysis of time series of glacier speed: Columbia Glacier, Alaska, *J. Geophys. Research, 92*, 8969-8975, 1987.

Weertman, J., General theory of water flow at the base of a glacier or ice sheet, *Rev. Geophys. Space Physics, 10*, 287-333, 1972.

Weertman, J., The unsolved general glacier sliding problem, *Journal of Glaciology, 23*, 97-115, 1979.